



Adaptation and Evaluation of bedload transport models for mountain streams



Master's Thesis

for the Master's Program **Kulturtechnik und Wasserwirtschaft** at the
University of Natural Resources and Life Sciences, Vienna

by

Thomas Weninger

Matr.Nr. 0840770

Supervision:

Univ.Prof. Dr. DI Johannes Hübl

Institute of Mountain Risk Engineering, BOKU, Vienna

Dr. DI Dieter Rickenmann

Swiss Federal Institute for Forest, Snow and Landscape Research, Birmensdorf, CH

April 2015

Abstract

The aim of this study was to examine the variability in bedload transport for the special case of steep mountain streams where measured bedload transport rates vary over up to four orders of magnitude for a given discharge. The data basis for the analyses were time series of transport rates and discharge which were recorded continuously at geophone stations in two glacier fed alpine streams since spring 2008. As a first step, a detailed check for plausibility of the measured data revealed interesting insights about implausible measurements and resulted in the exclusion of more than half of the data, most of them related to low flow periods. The remaining data pairs were used to calculate the critical bed shear stress by use of the exponential bedload transport equation of Cheng (2002). The behavior of this threshold was described statistically and its variability was reproduced in order to implement a stochastic sub-step to a modern deterministic bedload transport model. Therefore, several simple approaches, preferably causing little computation effort, were tested, the goodness of the results was estimated and future applicability discussed. It was shown that some of the developed methods are applicable and potentially appropriate to improve bedload transport calculation procedures, although considerable deviations still remain.

Zusammenfassung

Als Geschiebe werden Feststoffe bezeichnet, die in wasserführenden Gerinnen an der Sohle gleitend, rollend oder springend transportiert werden. Die Transportrate ist prinzipiell von der fließenden Wassermenge abhängig, trotzdem variiert sie bei gegebenem Durchfluss über bis zu drei Größenordnungen. Etablierte Methoden, mit denen versucht wird, den Geschiebetransport quantitativ zu berechnen und vorherzusagen, basieren meist auf der Annahme, dass ab dem Übertreten eines bestimmten Grenzzustandes der Transport beginnt. Dieser Grenzzustand wird deterministisch in Form einer Sohlschubspannung oder eines Durchflusses definiert und fließt als Konstante in die verwendeten Formelapparate ein, wodurch die natürliche Variabilität nicht zufriedenstellend reproduziert werden kann.

Im Zuge dieser Arbeit wurde versucht, einfache Ansätze für stochastische Rechenschritte zu entwickeln, deren Implementierung zu einer Verbesserung der Resultate von Geschiebetransportsimulationen speziell bei Wildbächen führt. Die Analysen wurden basierend auf indirekten Messungen der Geschiebetransportraten in zwei

Gletscherwildbächen in Tirol durchgeführt. Mittels sogenannten Geophonen wurden diese Raten seit dem Frühjahr 2008 kontinuierlich gemessen und mit einem Mess-, beziehungsweise Integrationsintervall von 15 Minuten aufgezeichnet. Die Geophone messen den Teil der Bewegungsenergie, der vom bewegten Geschiebe auf sohlgleich eingebaute Stahlplatten übertragen wird. In der Folge wird aus den Messwerten über empirische, in Kalibrationsmessungen ermittelte Funktionen die transportierte Masse errechnet.

Eine vorangestellte Plausibilitätsanalyse führte zum Ausschluss von mehr als der Hälfte der Daten, zum größten Teil aus Niederwasserperioden, aufgrund von noch nicht erklärbaren Phänomenen im Messsystem. Aus den verbleibenden, plausiblen Messungen von Geschiebetransportrate und Durchfluss kann die Grenz- oder kritische Sohlschubspannung errechnet werden. Dazu wurde die exponentielle Transportformel nach Cheng (2002) verwendet, die auch Ergebnisse liefert, wenn die aktuelle Sohlschubspannung unter der kritischen liegt. Damit kann, laut jüngeren Untersuchungen, die Realität besser abgebildet werden als mittels älterer Ansätze. In der Folge wurde versucht, die Information über den rechnerischen Grenzwert mit einfachen stochastischen Methoden nachzubilden. Die Ergebnisse zeigen, dass einige der gewählten Ansätze grundsätzlich praktikabel sind, der Rechenaufwand begrenzt gehalten wird und potenziell bessere Simulationsresultate erzielt werden können. Dennoch bleiben beträchtliche Abweichungen bestehen, und die Praxistauglichkeit muss noch weiter geprüft werden.

Declaration

Hereby I declare that I have written this thesis by my own. Furthermore, I confirm that no other sources have been used than those specified in the thesis itself. This thesis, in same or similar form, has not been available to any audit authority yet.

Vienna, April 2015

.....

Contents

1	Introduction.....	1
1.1	Motivation and background.....	1
1.2	Goals of the thesis.....	2
2	Literature review.....	2
2.1	Bedload transport.....	2
2.2	Flow velocity and flow resistance.....	4
2.3	Bedload transport equations.....	7
2.4	Variability of bedload transport.....	9
2.5	The modeling tool sedFlow.....	11
3	Data.....	13
3.1	Study area.....	13
3.2	Field measurements.....	15
3.3	Continuous bedload transport measurements.....	17
4	Methods.....	20
4.1	Plausibility check.....	20
4.2	Search for patterns in critical shear stress.....	24
4.2.1	Determination of θ_c and basic concept.....	24
4.2.2	Temporal variability of θ_c	25
4.2.3	Hysteresis and further relations.....	26
4.2.4	Selected regressions with θ_c	27
4.2.5	Stochastical considerations.....	29
4.3	Punctual bedload simulations for the control sections.....	32
4.4	Bedload simulations with sedFlow.....	34
4.5	Model skill estimation.....	35
5	Results.....	36
5.1	Punctual bedload simulations.....	36
5.2	sedFlow simulations.....	39
6	Discussion.....	40
7	Conclusions.....	42
8	Acknowledgements.....	43
9	Literature.....	44
	Appendix A.....	49
	Appendix B.....	59

1 Introduction

1.1 Motivation and background

Bedload is “the part of the total stream load that is moved on or immediately above the stream bed, [...] transported by traction or saltation along the bottom; the part of the load that is not continuously in suspension or solution” (Jackson, 1997). In the densely populated alps, bedload transport issues influence human lives in many ways. Hence, some broadly noticed consequences are the forming of entire alpine landscapes, damages during flood events or lessened capacity of retention structures. In Switzerland, for example, an estimated sum of up to 5.1 billion CHF financial damage was caused specifically by bedload transport from 1972 to 2011. This is approximately one third of the total damage caused by floods and landslides (Badoux et al., 2014).

Following such motivations, intensive research to understand bedload transport in steep mountain streams has been carried out at the Swiss Federal Institute for Forest, Snow and Landscape Research (WSL) for decades. Recently, a major outcome was the development of an indirect measurement system for bedload transport, the so-called Swiss Plate Geophone (Rickenmann et al., 2014). The basis for this thesis are data from two geophone stations which were installed in alpine streams by the Tyrolean hydropower company TIWAG in cooperation with the WSL. The measurements started in 2008 and as their temporal resolution is relatively high, this is a unique opportunity to investigate bedload transport patterns based on a large dataset.

Besides, there have been attempts to calculate bedload transport rates for several centuries all over the world. Especially in steep streams, the results are still considerably uncertain what is mainly caused by the large variety in the hydrological characteristics of such alpine catchments. The ongoing progress in computing power facilitates detailed simulations with the purpose to answer specific research questions. At WSL, one research focus lies on the estimation of future trends in bedload transport with special regards to climate change. Therefore, the simulation model sedFlow was developed which includes state-of-the-art bedload transport calculation procedures for steep mountain streams and enables fast computation of long-term simulations.

1.2 Goals of the thesis

As fundamental basis, there is the collection of most up-to-date bedload transport simulation methods on the one hand and on the other hand a large data set delivered by the geophones which can be used to apply and evaluate the former. Furthermore, it is known that the initiation of bedload particles motion is highly volatile, whether temporal or spatial (Einstein, 1936). Accounting for a wide range of physical phenomena in simulations would lead to complex calculation procedures, extensive determination of input data and long computation times. Hence, it might ease model appliance and improve results if the unpredictable and immeasurable subprocesses are generalized and expressed by means of stochastics. Meanwhile, literature presents several attempts to include stochastic elements in bedload transport (see 2.3). Most of them use rather complex algorithms entailing long computation time or were developed for larger lowland rivers.

The result of this work should be a sound suggestion about how to include a stochastic module in the established bedload calculation procedure which delivers significantly better results than non-stochastic simulations and ensures limited computation times. Therefore, some successive work-flow steps will be necessary. First of all, the data need to be analyzed for plausibility. If it is usable, the main research will be about finding patterns which may be described statistically and reproduced subsequently. The determination of an algorithm and its implementation in sedFlow might follow. Finally, evaluating the simulated results using statistical methods should lead to a statement whether the implementation is possible and reasonable.

2 Literature review

2.1 Bedload transport

In many parts of the world, bedload transport was observed since the beginning of human water use some millennia ago. First very basic research was documented by the ancient Greeks, namely Aristotle and Archimedes, who discovered dynamic principles of movement in a medium and hydrostatics (Viollet, 2012). Accordingly, bedload transport occurs whenever the eroding forces applied to the bed by flowing water exceed the forces which stabilize the bed sediments. Thus, whether a sediment particle is transported depends on its size, shape, weight, orientation in the bed and on the instantaneous flow conditions in the stream (Rickenmann, 2013). Generally, motion of solids in water may

take place in different manners. Sediment grains can float on the water surface, drift suspended in the water body or move along the bed jumping, rolling or sliding (Hassanzadeh, 2012).

A big part of bedload transport research is concentrated on the physics of bed erosion. Actually, complex interactions of many processes happen in the bed of a natural channel. The most basic equilibrium theory includes gravity, respectively the weight of the sediment particle, and the hydrostatic pressure onto the grain as stabilizing forces. On the eroding side, they are opposed by flow pressure of water, buoyancy and the component of weight parallel to the bed slope. However, this simplification would be valid only for laminar flow of a Newtonian fluid and if the sediment particles are entirely exposed to the flow. In real streams, additional hardly detectable forces influence bedload mobilization and motion crucially (Hassanzadeh, 2012). As a physical generalization, the total pressure acting on the bed surface is termed as bed shear stress τ and can be calculated with equation 2.1.

$$\tau = \rho g h S \quad (2.1)$$

Symbols are used as follows:

ρ ... density of the fluid [M / L^{-3}]

g ... gravitational acceleration [$L T^{-2}$], approximately constant: $g = 9.81 \text{ m s}^{-2}$

h ... flow height [L]

S ... bed slope [-]

More precisely, natural channel beds are made up of inhomogeneous mixtures of sediment particles, unless they are rocky beds which are not considered here. Grain size, density, shape or sedimentation structure differ in small, but also larger scales along the stream. Such irregularities in the river bed are obstacles for the flowing water and induce turbulent flow. Consequently, turbulence causes pressure forces in all directions which underlie very rapid changes in strength and direction (Einstein, 1950). So far, it is hardly possible to quantify these forces. Within the turbulences, however, energy is transformed from kinetic water flow energy to other forms like heat or sound, mainly through friction in the bed. This process needs to be considered in attempts to calculate flow velocity (Rickenmann, 2013).

Furthermore, a high variance in the local bedload grain size influences sediment mobilization when small particles hide downstream of bigger ones (Hassanzadeh, 2012).

In this case, situations may occur when the smaller grains should move, according to simple models, but the actual energy acting on them is still too small. As a consequence of all this, only parts of the bed particles are in motion over a large range of discharges what complicates predictions (Cheng, 2002). In some channels, cohesive forces stabilize the bed additionally. Besides, the transporting fluid might change its properties like viscosity, suspended load, or temperature over time or space (Einstein, 1950; Hassanzadeh, 2012; Rickenmann, 2013). All these circumstances complicate a detailed and precise insight into sediment transport in river beds. Moreover, also site-specific characteristics like lateral erosion, vegetation effects and many others have to be considered to achieve a holistic view.

In recent scientific studies, there is a sharp separation between the work on bedload and suspended sediment transport processes due to differences in measurement systems and experimental design. Concerning bedload transport, the main research interest is the initiation of transport which is the key to further issues like total bedload transport and also stream morphology. Therefore, many studies were done in laboratory flumes during the last century. Early and famous experiments were carried out and analyzed by Einstein (1950) and Meyer-Peter & Müller (1949), who surveyed bedload transport in channel beds with nearly uniform grain sizes. Until nowadays, numerous further flume experiments delivered data, also for nonuniform bedload material and steep slopes (e.g. Smart & Jäggi, 1983; Bathurst et al., 1987; Rickenmann, 1990). By means of these data, the researchers tried to find significant relationships, mostly between sediment transport rate and discharge, or shear stress respectively. Commonly, a subsequent goal was to develop a mathematical procedure for the computation of bedload transport rates also in natural channels without the need for additional field measurements.

2.2 Flow velocity and flow resistance

Friction between flowing water and the solid channel bed lessens the flow velocity and the eroding forces. More precisely, two different types of bed resistance, or roughness respectively, determine the extent of flow energy losses: the grain resistance and the form resistance. The former causes friction losses on every single grain and is usually expressed by a characteristic grain size while the latter is defined as the resistance of larger and more stable structure elements in a stream bed like steps or rocks. Hence, the

form roughness needs to be considered separately, especially in steep mountain streams where it is responsible for a great part of the energy losses (Rickenmann, 2013).

Generally, a precise estimation of the flow velocity is crucial for comprehending bedload transport. Therefore, many detailed and mathematically complex approaches were developed throughout the last centuries (e.g. from Euler, Bernoulli, Darcy & Weißbach, de Saint-Venant; see in Bollrich et al., 2013). Some of these enable to describe water movement in up to three dimensions. In this thesis, however, the intention is to work with calculation procedures which are simple enough to do 1-D-simulations quickly and with low hardware requirements. For such purposes, the flow parameters are averaged over channel width and depth.

Therefore used simplified formulas are mostly based on equation 2.2, the classical flow formula after Brahms & de Chézy (Bollrich et al., 2013):

$$\bar{v} = C \sqrt{R S} \quad (2.2),$$

wherein \bar{v} = average reach velocity [$L T^{-1}$] and R = hydraulic radius (flow area A [L^2] divided by wetted perimeter I_w [L]). The Chézy coefficient C is a parameter which generally accounts for flow resistance. Since its publication, researchers intensively tried to adapt the formula to describe real flow processes. Thus, C is often related to measurable values like a characteristic grain size, certain empiric parameters or the ratio between hydraulic radius R and a characteristic roughness dimension. The equations of Strickler (1923) or Rickenmann (1996) are examples therefore. As a simplification, the hydraulic radius R is very often approximated by the flow height h .

Ferguson (2007) transformed discharge and average flow velocity to dimensionless equivalents and developed a variable-power resistance equation. The mathematical design of Ferguson's equations allows for grain resistance as well as for form resistance. Especially for steep shallow flows, this approach delivers better results in comparison to former fixed power law equations of the Brahms & de Chézy-type. Subsequently, Rickenmann and Recking (2011) compared different flow resistance approaches using a large dataset. They suggested to use Ferguson's formulas because of the good results for small relative flow depths and additionally modified the dimensionless variables further in order to propose a slightly more general calculation procedure which is given in equations 2.3 and 2.4.

$$q^{**} = \frac{q}{\sqrt{g S D_{84}^3}} \quad (2.3)$$

$$\bar{v} = 1.443 \sqrt{g S D_{84}} q^{** 0.6} \left[1 + \left(\frac{q^{**}}{43.78} \right)^{0.8214} \right]^{-0.2435} \quad (2.4)$$

Symbols are used as follows:

q^{**} ... dimensionless unit discharge

q ... unit discharge [$L^3 T^{-1} L^{-1}$]

D_x ... characteristic grain diameter [L], here $D_{84} \Rightarrow$ 84 volumetric percent of bedload are finer than D_{84}

Aberle and Smart (2003) pointed out that the input parameters as described above do not allow for the spatial arrangement of roughness elements which is crucial for the hydraulic behavior. Trying to obtain a more universally suitable prediction, they suggested to use a measure for the variability of bed elevation instead. Subsequently, Yochum et al. (2012) used a large dataset to compare flow resistance prediction methods including the above mentioned of Rickenmann (1994), Ferguson (2007) and Aberle & Smart (2003). They obtained best results using a so called relative bedform submergence R/σ_z or h/σ_z and suggested the use of either this value or the above-mentioned dimensionless unit discharge q^{**} in velocity calculations. Here, σ_z is the standard deviation of the bed elevation differences in a certain spatial range, e.g. a profile of a channel reach, and represents a roughness parameter which accounts for variable structure of the stream channel (see also in 3.1).

In this thesis, the approach of Rickenmann & Recking (2011) and an equation of Yochum et al. (2012), as given in the equations 2.5a and b, are used. The reasons for this choice were good results in earlier applications, simplicity and also promising possibilities for further research.

$$\bar{v} = 0.59 q^{*0.53} \sqrt{g \sigma_z} \quad (2.5a)$$

with $q^* = \frac{q}{\sqrt{g \sigma_z^3}} \quad (2.5b)$

2.3 Bedload transport equations

Especially for engineering applications, quantitatively and qualitatively sound bedload transport calculations are often useful. In order to provide appropriate instruments therefore, different calculation methods have been developed which are mainly based on one out of two different approaches, the deterministic and the stochastic.

Meyer-Peter and Müller (1949) published a strictly deterministic method, hereinafter called MPM. It is based on the concept of Shields (1936), who introduced dimensionless shear stress and critical shear stress. The latter is defined as the shear stress acting on a bed particle when it starts to move.

$$\Phi_b = a_1 (\theta' - \theta_c)^{b_1} \quad (2.6a)$$

$$\text{with} \quad \theta' = \left(\frac{k_{St}}{k_s} \right)^{1.5} \theta \quad (2.6b)$$

Equation 2.6a gives the MPM-approach in a simplified form, equation 2.6b reduces the shear stress accounting for form roughness. Symbols are used as follows:

Φ_b ... dimensionless transport rate (Einstein, 1950), [-], can be interpreted as transport intensity, index b for bedload

θ_c ... dimensionless critical shear stress as threshold at the initiation of motion [-]

a_1, b_1 ... empirical parameters [-]

$(k_{St}/k_s)^{1.5}$ correction for form roughness, see eq. 2.11 and 2.12 [-]

θ ... dimensionless shear stress (Shields, 1936) [-]

$$\theta = \frac{\tau}{\left(\frac{\rho_s}{\rho} - 1 \right) g D_x} \quad (2.7)$$

ρ_s/ρ ... density solid [M L⁻³] / density fluid [M / L⁻³]

θ' ... dimensionless shear stress, reduced due to form roughness (eq. 2.6b, 2.12)

Dimensional bedload transport rates are calculated with equation 2.8.

$$q_b = \Phi_b \sqrt{\left(\frac{\rho_s}{\rho} - 1 \right) g D_x^3} \quad (2.8)$$

q_b ... specific bedload transport rate [$M^3 T^{-1} M^{-1}$],

The critical shear stress θ_c may be either estimated with empirical equations (Lamb et al., 2008; Recking, 2013) or back-calculated from flume experiments or field measurements (e.g. Bunte et al. 2013). The former express θ_c as a function of the stream's friction slope. The equation of Lamb et al. (2.9) is also implemented as a default method in sedFlow.

$$\theta_c = 0.15 S^{0.25} \quad (2.9)$$

The above-mentioned equations build the backbone procedure of most deterministic bedload calculations. Accordingly, many researchers modified this approach, often based on the analysis of additional data (e.g. Rickenmann (1991) or Smart & Jäggi (1983) for mountain streams). Rickenmann (2001) developed equation 2.10 especially for steep slopes. Therein, also a reduction of the slope S is suggested to account for form resistance in steep mountain streams with large inhomogeneities in the bed (Eq. 2.11). The reduced slope S_{red} after Rickenmann & Recking (2011) substitutes bed slope S in equation 2.1, subsequently reduces the dimensionless shear stress θ from equation 2.7 and the dimensionless bedload transport rate after equation 2.10. Hence, the use of S_{red} also compensates the form roughness factor $(k_{St}/k_s)^{1.5}$ in equation 2.6b (see eq. 2.12).

$$\Phi_b = 3.1 \left(\frac{d_{90}}{d_{30}} \right)^{0.2} \sqrt{\theta'} (\theta' - \theta_c) Fr \frac{1}{\sqrt{\frac{\rho_s}{\rho} - 1}} \quad (2.10)$$

$$S_{red} = S \left(\frac{\bar{v}(\text{from Eq.2.4})}{v_0(q)} \right)^{1.5^{1.5}} = S \left(\frac{\bar{v}}{3.074 \sqrt{(g S D_{84})} q^{**0.4}} \right) \quad (2.11)$$

$$\theta' = \theta \frac{S_{red}}{S} \quad (2.12)$$

Besides, Wilcock and Crowe (2003) developed a different approach where they classify the bedload in several grain size classes which is called fractional computation. The transport rates are calculated for each class what enables simulating the development of the grain size distribution in the bed and in the transported material.

With all these methods it is hardly possible to get good results when flow conditions are near the critical state of incipient motion (Kleinhans & van Rijn, 2002). As a result of the previously described complex circumstances in channel beds, sediment transport does not start at a certain moment. Even at low discharges it is never equal to zero, indeed, the probability of motion becomes very small (Cheng, 2002). For this reason, Cheng transformed the MPM-equation to an exponential form which also accounts for flow stages when $\theta \leq \theta_c$ (Eq. 2.13). In all calculations here, the reduced dimensionless shear stress, θ' according to equation 2.12, was used in equation 2.13 and the factor a_1 was kept constant with a value of 5, as it was suggested for the MPM-equation in Wong & Parker (2006) and Hunziker & Jäggi (2002).

$$\Phi_b = a_1 \theta^{1.5} e^{\left(\frac{-\theta_c}{\theta^{1.5}}\right)} \quad (2.13)$$

The other key approach was developed by Einstein (1950). He tried to calculate bedload transport by applying an interaction of several stochastic functions, namely for the probability of a particle being moved, being redeposited and the travel distance. More recently, researchers tried to implement such stochastic modules to originally deterministic calculation methods. Kleinhans and van Rijn (2002) adjusted their own and the MPM-equation for fractional computation. To cope with the stochastic nature of bed shear stress due to turbulences, they assessed a probability distribution function for the bed shear stress τ , namely a normal distribution.

Additionally, Duan and Barkdoll (2008) published a similar method, based on the fractional formula of Wilcock and Crowe (2003). They define a log-normal distribution for the dimensionless shear stress θ and propose a slightly different calculation procedure in the stochastic sub-steps which should lead to less computing effort.

2.4 Variability of bedload transport

A first analysis of the herein used data showed strong irregularity between the measured discharges and sediment transport rates. For equal discharge values, the transport rate varied within up to four orders of magnitude even though the measurements of discharge were averaged and those of bedload transport integrated over 15 minutes time (Fig.2.1). Similar results were observed at other swiss plate geophone stations (Turowski & Rickenmann, 2010). Such inhomogeneities might occur due to turbulences

causing spatial variability in flow velocity and hence in bed shear stress (Cooper, 2012; Kleinhans & van Rijn, 2002; Einstein, 1950).

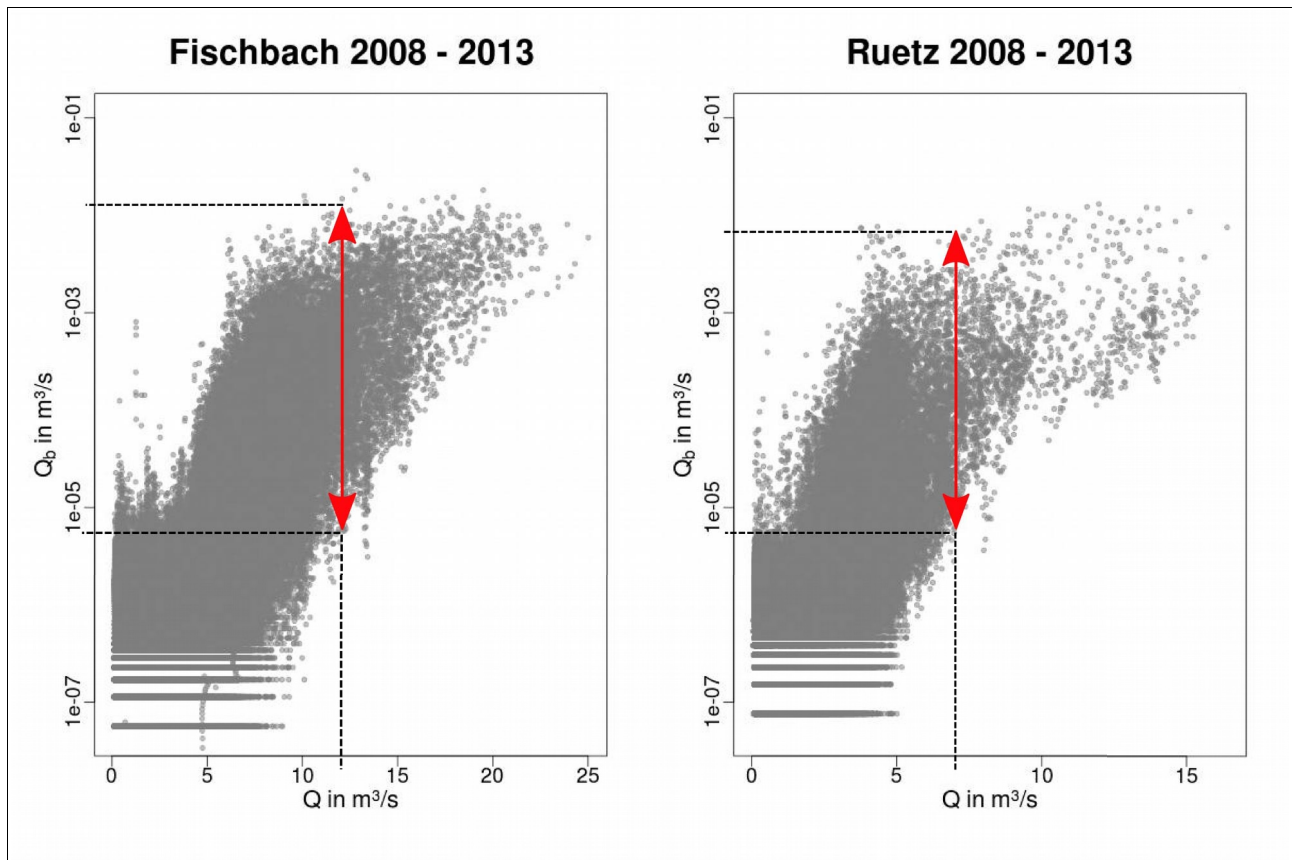


Fig. 2.1: q_b over q ; the red arrows illustrate the variability of bedload transport rate at a certain discharge.

As bedload transport is a very complex process, studies also deal with further influences like natural flow patterns (Ancey et al., 2006), composition of the stream bed (Church & Kellerhals, 1978; Recking, 2013), waiting time between two bedload motion events (Turowski, 2010; Heyman et al., 2013) or interactions between several forces (Fan et al., 2014). In all these publications, different probability distribution functions for the investigated elements were assessed.

Recking (2013) reflected about the variability in both bed and flow parameters which is lost during the width integration of measurements or in 1D-bedload-computations. Therein, he assessed probability distribution functions (later called pdfs) for dimensionless bed shear stress θ , sand fraction F_s , D_{50} and the ratio D_{84}/D_{50} . The pdfs were calibrated with extensive data from literature and further used to reproduce sets of input parameters. This process should implicate the spatial variability of these parameters over the stream width. Bedload transport rates were calculated fractional and for different flow stages (θ/θ_c).

Therefore, he used the equation of Wilcock & Crowe (2003) in a Monte Carlo simulation and averaged the results over all reruns. Comparison with measured rates led to several inferences about nonlinearity effects in bedload prediction. An important conclusion for this work is, however, that taking into account the variance terms may improve simulation outcomes. This statement is valid especially for low flow stages, but the results are still orders of magnitudes lower than the measurements. Herein, a similar approach will be investigated and, moreover, by the use of the equation of Cheng (2002), it might be possible to improve results for low flow stages. Furthermore, it will be investigated if it is possible to concentrate the variance in bed and flow properties within only one stochastic input parameter, θ_c . The acceptance of this hypothesis would simplify the calculations considerably.

By now, several investigations about the variability of θ_c were carried out, e.g. by Buffington & Montgomery (1997) or Bunte et al. (2013). They analyzed values for θ_c from literature, mainly gathered from flume experiments or sampler campaigns in different streams. All of them strictly interpreted θ_c as threshold for incipient motion. However, their results can only be seen as guidance values for the following computations because the starting moment of bedload transport can not be detected exactly in the 15-min-integrated geophone time series and, as a further contrast, the exponential Cheng-formula is used in this work.

Turowski et al., (2011) compared the flow conditions at the beginning of bedload transport events with those at the end of the previous event and found a strong correlation. Hence, also the younger history of the flow regime causes variations in the threshold for incipient motion. Moreover, most of the other mentioned publications conclude that the highest uncertainty is observable when the actual shear stress is in the range of the threshold. Again, this supports the idea that the threshold underlies a certain variability.

2.5 The modeling tool sedFlow

SedFlow is a software tool to simulate fractional bedload transport in mountain streams. It was developed and published in 2014 at the research institute WSL in Switzerland (Heimann et al., 2014b). Now it may be downloaded free and open-source under the terms of the GNU General Public License (Free Software Foundation, 2007) from the website www.wsl.ch/sedFlow.

The main goals of the developers were to create a fractional bedload transport simulation model which contains several state-of-the-art approaches for the specific processes in steep streams and which allows for shorter computing times than other published models. Achieving the latter should enable long-term simulations for entire catchments and channel networks with confluences. Further goals were flexibility in the model code as well as in data pre- and post-processing.

To keep calculation times short, some simplifying assumptions concerning the hydraulics were taken. The software is designed as 1D-model, i.e. flow parameters are integrated both over depth and width of the defined calculation sections. For the computation of the flow hydraulics three options are implemented: (i) an explicit and (ii) an implicit kinematic wave algorithm as well as (iii) a passing on of uniform discharge for the whole channel. The implicit kinematic wave is solved analytically by using an approach that omits time consuming iterations but requires the channel geometry to be strictly v-shaped or an infinitely deep rectangle (Liu & Todini, 2002). Accordingly, stream reaches in sedFlow are defined rectangular with fixed width. In contrast to the kinematic wave options, the use of the uniform discharge enables to deal with negative bed slopes by the virtual formation of pondages. Here, the gradient of hydraulic head can not decrease below a positive, close to zero threshold. Heimann et al. (2014b) discuss the effects of these simplifications more detailed.

As core options amongst others, there are two approaches for flow resistance and four for bedload transport implemented in sedFlow:

- flow resistance: fixed power law, basically after (Strickler, 1923); variable power law according to (Rickenmann & Recking, 2011)

- bedload transport: according to (Cheng, 2002), (Wilcock & Crowe, 2003), (Recking, 2010), or (Rickenmann, 2001).

All the bedload transport equations are modified for fractional transport. Considering the aim of this thesis, also the assignment of θ_c has to be mentioned. By now, the two possibilities are a user-defined constant value or the slope-dependent calculation according to Lamb et al. (2008).

To set up a sedFlow simulation, the channel network is subdivided into homogeneous reaches. For each of them, the following input data need to be provided: GSD of surface and subsurface bedload layers, representative cross section width, reach length, bed

slope, alluvium thickness, and bedrock roughness. At the upper end of every reach, time series of discharge and transported sediment may be provided, only for the topmost reaches, discharge input is mandatory. Input and output data are stored in standard formatted ascii-files (Heimann, 2014).

During the development phase, sedFlow was applied and tested at several Swiss mountain streams. Heimann et al. (2014a) described the application at the Kleine Emme and the Brenno where they carried out a proof-of-concept study with an extensive examination of most of the applicable options and the effects of their use. Additionally, a sensitivity analysis was executed regarding the uncertainties in input data like GSD, discharge or the constant threshold θ_c . In these two catchments, morphology data from cross section surveys with a time lag of five, respectively ten years were available. A sediment budget was assessed by interpreting the surveyed results together with estimations of bank erosion, lateral inputs and the sediment material transported out of the catchment. Subsequently, the accumulated bedload transport and the erosion, respectively deposition over the longitudinal course of the streams were used to calibrate the model. The input discharge was simulated by means of the rainfall-runoff-model PREVAH (Viviroli et al., 2009) based on observations near the study sites.

Finally, the authors concluded that the model is principally applicable for simulations in mountain streams and presented a detailed overview of the effects of different approaches as well as some tips for further use. Within this thesis, sedFlow was applied to examine the possibility to implement a stochastic module for θ_c in combination with the use of the Cheng-equation (Eq. 2.13). The latter was implemented after the previously described study and untested so far. Furthermore, the potential to reproduce temporally high-resoluted time series of bedload transport was appraised.

3 Data

3.1 Study area

The geophone stations which deliver the data for this work are installed in the beds of two mountain streams in Tyrol, Austria. To begin with, see a short overview of some geographic facts in table 3.1 and a regional map in figure 3.1.

Tab. 3.1: geographic facts

	Fischbach	Ruetz
Tributary of	Ötztaler Ache, Inn	Sill, Inn
Coordinates of the geophone station, WGS 1984	Long.: 11.010672° Lat.: 47.071929°	11.162924° 47.013629°
Altitude of the geophone station	1540 m	1684 m
Catchment area	71 km ²	28 km ²
Glaciated fraction of the catchment	17 %	22 %
Highest altitude in the catchment	3497 m (Schrankogel)	3474 m (Ruderhofspitze)

The catchments are located in the northern slopes of the alpine main ridge on crystalline rocks like gneiss and schist. The hydrological regime after Mader et al., (1996) may be termed as nivo-glacial (NIG 6) for both gauges (Fig. 3.2). However, the use of this

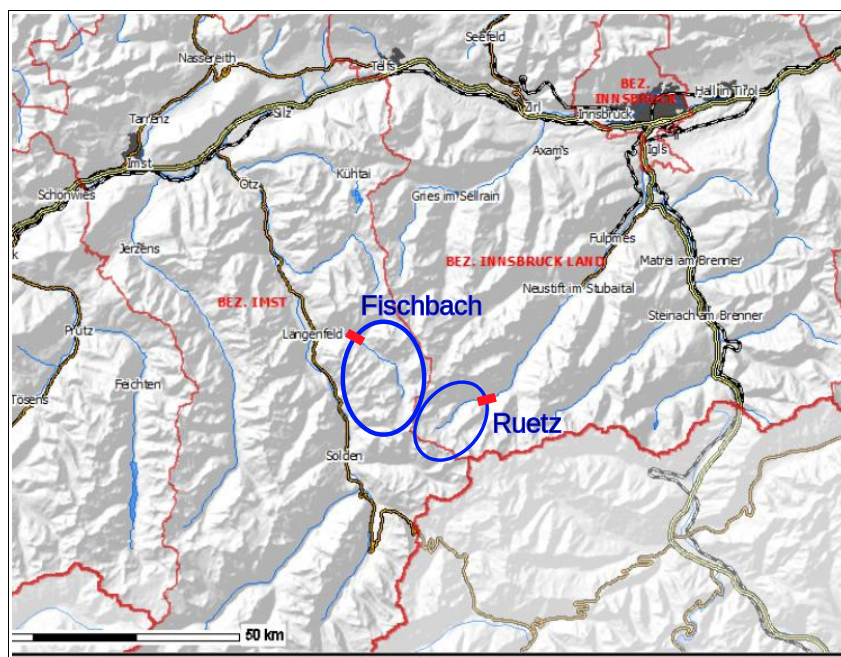


Fig. 3.1: map with catchments (roughly, blue) and geophone stations (red); scale invalid

classification is actually incorrect in this case, because it should be based on more than 10 years of discharge data, whereas only 6 years are available. Indeed, the categorization should simply illustrate the hydrological situation. Especially during high flow season discharge follows a distinct daily cycle.

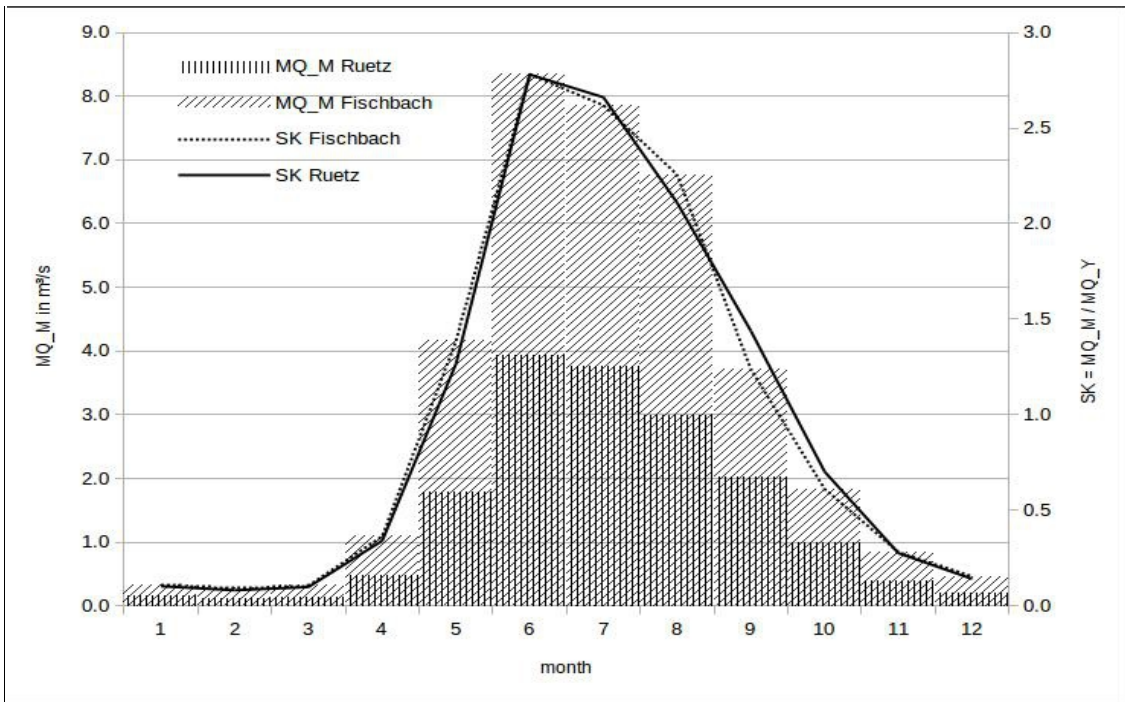


Fig. 3.2: assessment of hydrologic regimes, time series of monthly averages (MQ_M) and relative monthly averages (SK)

3.2 Field measurements

In fall 2013, a detailed survey was carried out in both catchments. To get an insight into the hydrological and morphological circumstances, the stream and its catchment were explored by field investigations. As holistic as possible, the torrent system was analyzed and the sediment balance was estimated by means of maps with orthophotos, a handheld GPS device and the educated eye. Additionally, photo points were fixed with the purpose to compare the situations of fall 2013 and 2014. The taken pictures cover the biggest part of the stream length.

As a conclusion, the stream reaches above the geophone stations are comparable in their system-morphological characteristics. Over the length of approximately one kilometer upstream of the geophone measuring site, the channels were considered as homogeneous with just slightly variable width and slope. A lack of tributaries, vegetation effects, remarkable side erosion sites as well as unlimited sediment supply from the bed consolidated this judgment. Hence, the geomorphological situation is ideal for the aims of this thesis because it may be assumed that bedload mobilization and redeposition happen almost exclusively in the stream bed. The integration and averaging of geometric parameters should not cause severe biases and misinterpretations. Accordingly, only

these reaches were the subjects of further analyses and are called homogeneous reaches (HORE) in the following parts.

Subsequently, further surveys were carried out in the HOREs to obtain robust input data for bedload prediction attempts. In the Fischbach, 18 cross sections within 220 meters upstream of the geophone were surveyed with a tachymeter and a lateral resolution of approximately 0.5 meters. In the Ruetz, a longitudinal section with a resolution of one up to two meters was taken. These surveys should deliver the mean slope and the standard deviation of the riverbed for calculations according to Yochum et al. (2012). The reason for measuring in different directions layed in the morphology of the HOREs. The Ruetz is a typical step-pool stream whereas the Fischbach has a homogeneous bed without any characteristic steps. Hence, it was assumed that this might be an appropriate way to indicate the variability in bed elevation which crucially influences the flow resistance. The value for variability, σ_z in equations 2.5a and 2.5b, is the averaged standard error of bed elevation referred to a linear trend in each surveyed profile. Equation 3.1 illustrates the exact calculation where x_i stands for the measured elevation, \hat{x}_i for the corresponding elevation on the regression line and n for the number of measured points..

$$\sigma_z = \sqrt{\frac{\sum (x_i - \hat{x}_i)^2}{n}} \quad (3.1)$$

Grain size distributions (GSD) of the bedload mixture in the investigated reaches were measured by means of line count analyses (LCA) in fall 2013. To account for the sediment fraction finer than two centimeters, a mathematical correction for surface bedload referring to Fehr (1987) was applied. In Fischbach four and in Ruetz three measurements were taken in the HORE. This is not a large number, but it was impossible to do more LCAs due to the flow regime even though they were taken in fall when the conditions are best for taking samples in the stream bed. The resulting GSDs differ from those which were presented in recent publications about these geophone stations (Rickenmann et al., 2014) (Rickenmann, 2014). The latter resulted from a combination of earlier LCA measurements and back-calculations based on the calibration of the gauge station using the flow resistance equation after Rickenmann and Recking (2011; Eq.2.3). For consistency reasons, these GSDs (Tab. 3.2) were used for all following analyses and computations.

Tab. 3.2: geometric parameters

	Fischbach	Ruetz
width B / m	8.5	8.5
slope S (HORE)	0.017	0.023
σ_z	0.17	0.59
D ₉₀ / m	0.40	0.65
D ₈₄ / m	0.32	0.53
D ₅₀ / m	0.13	0.20
D ₃₀ / m	0.07	0.10

3.3 Continuous bedload transport measurements

In both study streams, Fischbach and Ruetz, measuring stations with so-called Swiss Plate Geophones (SPG) were installed in spring 2008. The SPG is an indirect method to measure bedload transport continuously by recording vibrations during transport events. Therefore, the devices were bedded into an armored concrete sill with a U-shaped steel profile as figure 3.4 shows. The top surface of the construction is flush with the stream bed but laterally inclined with a slope of 5 %. This inclination should improve the stage-discharge relation for shallow flows.

The actual sensors are fixed inside of an aluminum housing on the bottom side of a 50x36x1.5 cm steel plate as visible in figure 3.3. This plate is screwed to a steel frame but separated by an elastomer layer which should absorb oscillations from the surroundings and the other plates. In the particular case, 16 plates are installed in each geophone station, but only every other one is equipped with a sensor. Figure 3.6 shows the structure schematically.

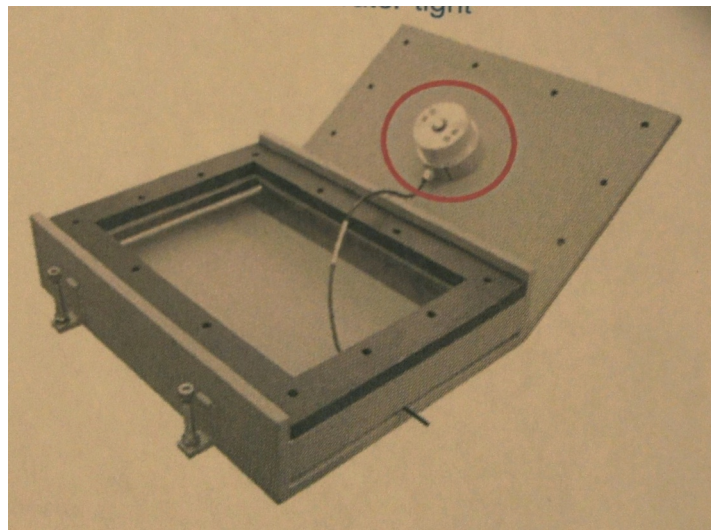


Fig. 3.3: schematic illustration of an open geophone unit, sensor case inside the red circle, ©WSL



Fig. 3.4: geophone station in the Ruetz, 1: concrete sill with geophon plates in steel profile, 2: pillar for calibration basket, 3: stairs with visual water gauge (=location of pressure gauge)

In the sensor case, a flexibly mounted magnetic core moves inside of a coil when a bedload particle hits the plate's surface whereby electrical flux is induced. The voltage is proportional to the speed of the magnet, and the kinetic energy, respectively, and sampled with a temporal resolution of 10 kHz. After a first operation period over 3 weeks, the raw signal was dampened by about 30% because the maximal amplitudes exceeded the measuring range of +/- 10V.

Due to limited storage capacity on the linked computers, only certain summary values are recorded in regular mode instead of the raw signal.

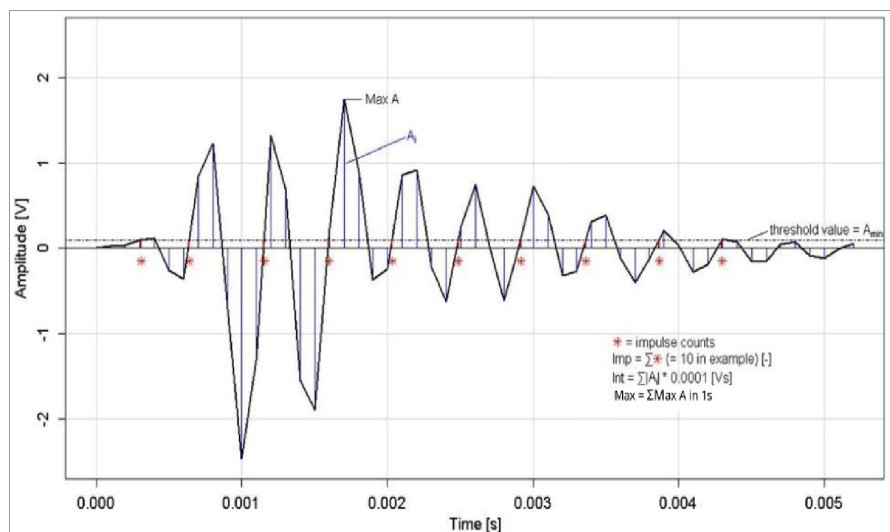


Fig. 3.5: measurement principle of geophones for "daily data", modified from (Rickenmann et al., 2014)

Hence, the default output interval is 15 minutes. Figure 3.5 illustrates the operating principle and the stored values are (i) the sum of exceedances of a positive threshold A_{min} (Imp in Fig.3.5, 0.07 V for the actual stations), (ii) the sum of maximal peaks in each second (Max) and (iii) the integrals of the absolute voltage amplitude (Int). Since 2010, the integrals of the square voltage values are recorded in the column for Int . Additionally, the sums of impulses higher than 17 gradual thresholds between 0.056 and 12 V are stored in a second file.

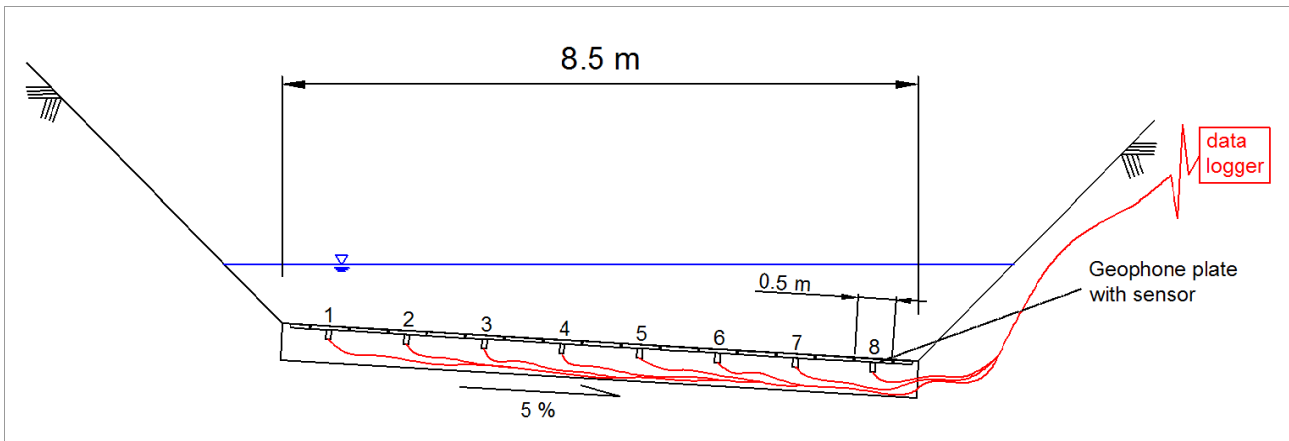


Fig. 3.6: schematic cross profile of the geophone station, the numbers 1-8 mark the plates which are equipped with a geophone sensor

The threshold of 0.07 V should assure the elimination of noise coming from water flow, electric noise etc. For this reason, only impacts from transported bedload with a grain size exceeding about 2 cm should be stored. Besides, the discharge is measured approximately four meters upstream of the geophones by an automatic pressure gauge.

The geophone sensors were calibrated during the last years to enable the direct converting of recorded impulses to bedload transport rates. For this purpose, a basket sampler was used to catch the bedload material transported over a SPG plate during a short period of time (up to 60 minutes), the mass was weighed and compared to the observed geophone summary values. An iron-coated pillar of armored concrete in the channel center carried the basket sampler (Fig. 3.4). Consequently, the calibration could only be performed for one plate in each stream. The regressions were carried out with each of the three above-mentioned summary values and the analyses of 28 (Fischbach) and 17 (Ruetz) calibration measurements yield a linear relationship without intercept between these two values. As an outcome, best results are expectable using the sum of impulses (Imp) in the equations 3.2a and 3.2b.

$$\text{Fischbach:} \quad M = 2 * 1.3 * 0.0517 * \text{Imp} \quad (3.2a)$$

$$\text{Ruetz:} \quad M = 2 * 1.37 * 0.0660 * \text{Imp} \quad (3.2b)$$

M stands for the transported bedload mass in kilogram. The factors 1.3 and 1.37, respectively, account for the sediment fraction smaller than two centimeters which is undetectable for the SPG. Additionally, the multiplication with 2 is necessary to obtain an integrated value for the whole channel width considering that only half of the effective width is equipped with sensors (Rickenmann et al., 2014; Rickenmann, 2014). Consequently, all transport rates analyzed in this thesis are computed by equations 3.2a and 3.2b and transformed to volumetric rates with an assessed density of 2650 kg/m³.

4 Methods

4.1 Plausibility check

A first view onto the stored data raise the impression of partly implausible measurements. Thus, to omit misinterpretations caused by obviously wrong data, a close investigation was started with a visual and subjective analysis of the time series focused on the sums of impulses. More precisely, implausible values were identified by scrolling through the “daily data” and detected in accordance to the following criteria: sudden increases of bedload transport over approximately two orders of magnitude while discharge stayed constantly low, inhomogeneities between single plates (again greater than approximately two orders of magnitude), known electrical problems like broken system parts and known special events like impact tests on the plates or maintenance works. Whenever plausibility problems occurred, all impulse values were set to NotANumber, what means that they were excluded from further analysis.

Additionally, some certain plots of the transport rates show interesting patterns. Figure 4.1 presents the relation between classified discharge and the respective sum of impulses, as well as the distribution of impulses in a boxplot. With decreasing discharge, bedload rates are not heading to zero, as they were supposed to, but stay on a nearly constant level. Furthermore, the plates at lower elevation measured higher transport rates than the plates at higher elevation when discharge was relatively high. This was expected, but in contrast, the measurements at low discharges recorded changed patterns (Fig. 4.2).

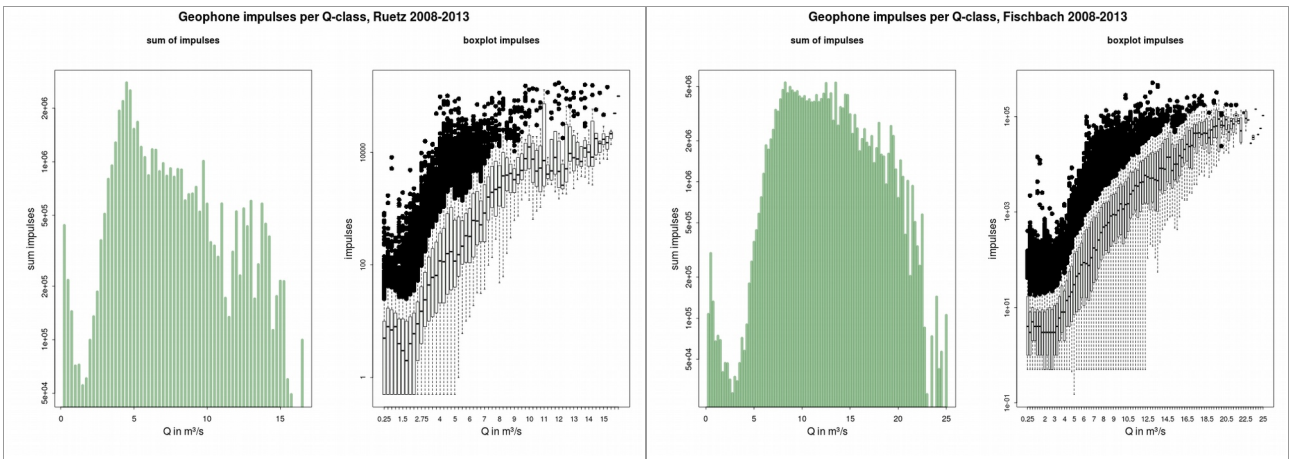


Fig. 4.1: geophone impulses per Q-class for Ruetz (left) and Fischbach (right); in each plot: left: sum of impulses, right: boxplot with distribution of impulses

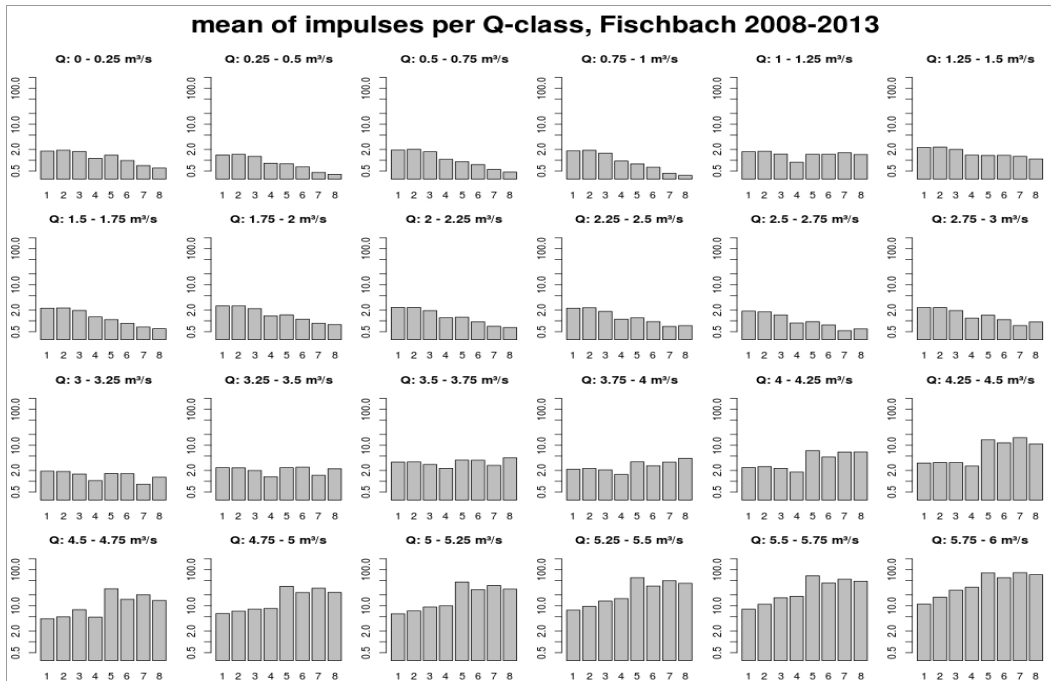


Fig. 4.2: mean of impulses for different Q-classes; number of geophone plate on the x-axis, 1 is the plate on the orographic right-hand side and has the highest elevation, 8 is on the orographic left-hand side with the lowest elevation

A possible interpretation of figure 4.1 is the incidence of a certain discharge threshold for considerable sediment transport. If it is exceeded, the stream bed breaks up and sediment mobilisation happens directly at the observed site. As long as discharge is lower, sediment particles are mobilized further upstream and transported through the observation section. Consequently, the phase when discharge is higher than a defined critical value will be called phase 2, when discharge is less, phase 1 according to Buffington & Montgomery (1997). The critical discharge is listed in Tab. 4.1.



Fig. 4.3: Fischbach, geophone site, right quarter out of flow area, 13.11.2014

Moreover, some potential sources of irregularities are recognizable at the sites in late fall or winter. First of all, the geophone stations are located close to streets with heavy traffic. Especially at the Ruetz, snow is removed extensively from the surrounding traffic areas into the streams, containing ice and grit. During this season, flow is very shallow and at both sites, the highest plates fall dry as a consequence of the lateral inclination of the



Fig. 4.4: Ruetz, geophone site from upstream, 14.11.2014

bottom sill. These circumstances are visible in figures 4.4 and 4.3. However, it is not yet clear how strongly they affect the measurements despite of the logging threshold (see 3.3), but the presence of an influence seems very likely.

Considering all these results, it was decided to eliminate the data of phase 1 before most of the following analyses. Only about 2-3 % of the total bedload transport will be excluded (Fig. 4.5). This value is marginal, especially if we keep in mind that the measured volumes here seem implausibly high. However, the aim of the current project is a modification of simulation models which still include uncertainties over orders of magnitudes, hence the elimination of phase 1 values will not influence the results considerably.

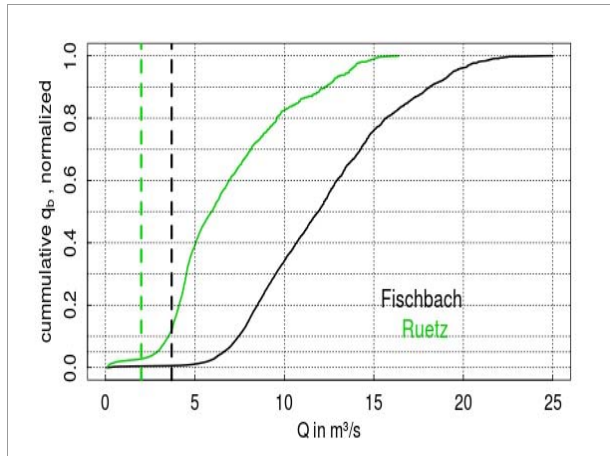


Fig. 4.5: normalized cumulative bedload transport in relation to discharge, dashed lines mark the cutoff value

Tab. 4.1: overview of data resources and their treatment (number of 15-min-timesteps)

	Fischbach	Ruetz
Start	27.05.08, 00:15	18.06.08, 10:00
End	28.10.13, 23:45	01.11.13, 00:00
Raw data	190 175	188 313
Gaps	6 801	2 374
Visually excluded	3 750	28
Excluded, Phase 1	112 947	128 663
Critical Q in m ³ /s	3.7	2.0
Data pairs for analysis	66 677	57 248

4.2 Search for patterns in critical shear stress

4.2.1 Determination of θ_c and basic concept

As Cheng (2002) transformed the MPM-equation into an exponential form (see 2.3), the dimensionless critical shear stress parameter θ_c has changed its characteristics. In contrast to the former meaning as strict threshold, now it may be interpreted as a reference value for the resistance of the stream bed. Herein, several attempts were made to find certain reproducible patterns in the temporal behavior and the variability of θ_c . For all the following calculations and analyses the free software environment R was used (R Core Team, 2013).

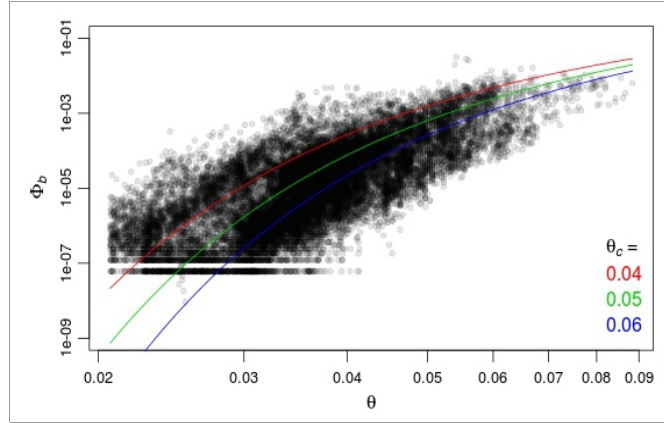


Fig. 4.6: Cheng-function, variable θ_c , data randomly excerpted from Fischbach

The first step is the determination of θ_c -values from the measured data pairs of q and q_b . Therefore, Φ_b was calculated from the q_b -measurements using equation 2.8 and θ' from the discharge values by use of the equations 2.1, 2.7, 2.11 and 2.12. The Cheng-function was fitted to the resulting data pairs by means of a non-linear-regression with θ_c as variable. Figure 4.6 shows the principle of this step schematically. Therefore, a time frame of user-defined length limited the data which was involved in the determination of one resulting θ_c -value. The time frame rolled along the time series with an advancing lag of one time step, what led to a new θ_c -time series of nearly the same length as the original. Herein, also the residuals may have been analyzed.

A second way to compute θ_c independently for each time step uses the rewritten Cheng-equation (Eq. 2.13) in the form:

$$\theta_c = -\theta^{1.5} \ln\left(\frac{\Phi_b}{5 \theta^{1.5}}\right) \quad (4.1).$$

The applicability of the second method was controlled by computing a moving average filter rolling along the yielded time series with the same time-frame-length as used for the non-linear-fit. The results for θ_c are identical.

4.2.2 Temporal variability of θ_c

Another simple temporal regularity of θ_c might lie in the seasonal cycle. The plots of θ_c over time in figures 4.7 and 4.8 show a triangular shape and higher variability from approximately mid of May to mid of July (week 23 to 30). As an exact parametrization and reproduction of this pattern in a statistically proper way is not trivial, it may be more practicable to consider it as an effect of the discharge regime as described later in 4.2.5. However, another kind of temporal variability might be observed in the

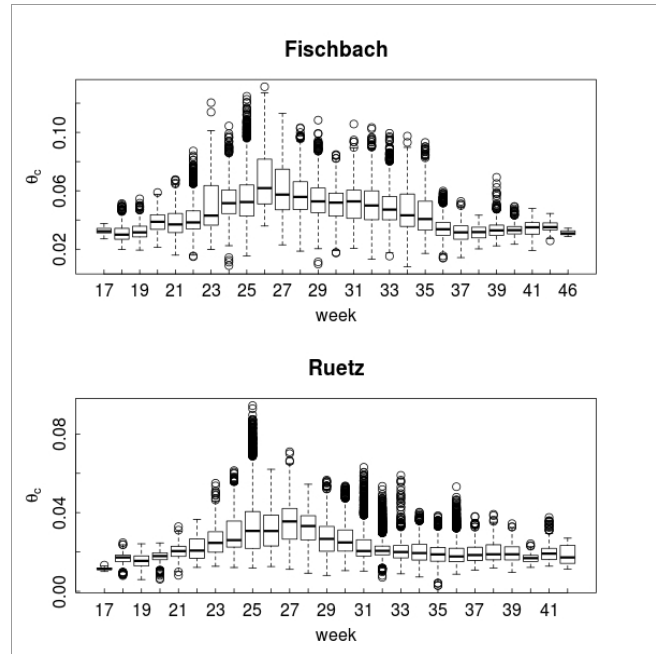


Fig. 4.7: θ_c over calendar weeks, 2008-2013

residuals inside the time frames for fitting θ_c . More precisely, we can look at the correlation coefficient R^2 and the residuals, respectively the standard deviation of the residuals, in each computation time frame (R Core Team, 2013). Plotting the results over θ' or q_b in figure 4.9 illustrates again the absence of significant patterns. Accordingly, also the goodness of fit does not change with increasing discharge or transport rate.

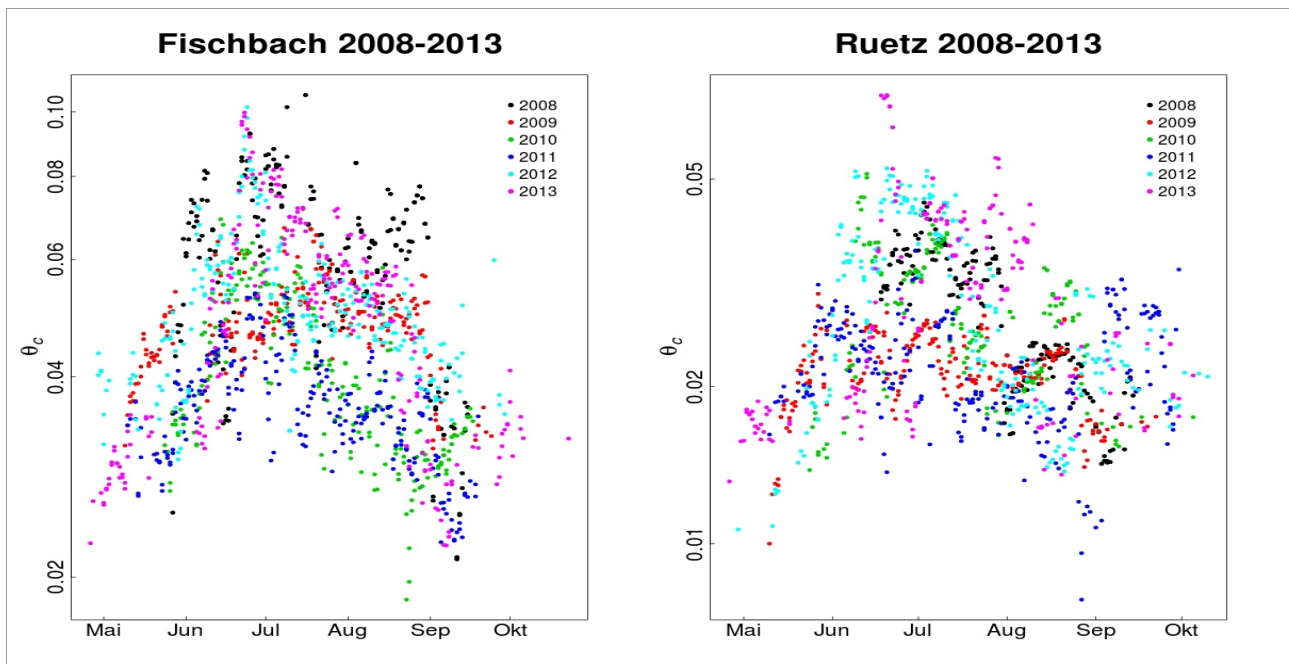


Fig. 4.8: time series of daily averages of θ_c , computed with non-linear fit, length of time frame = 1 d

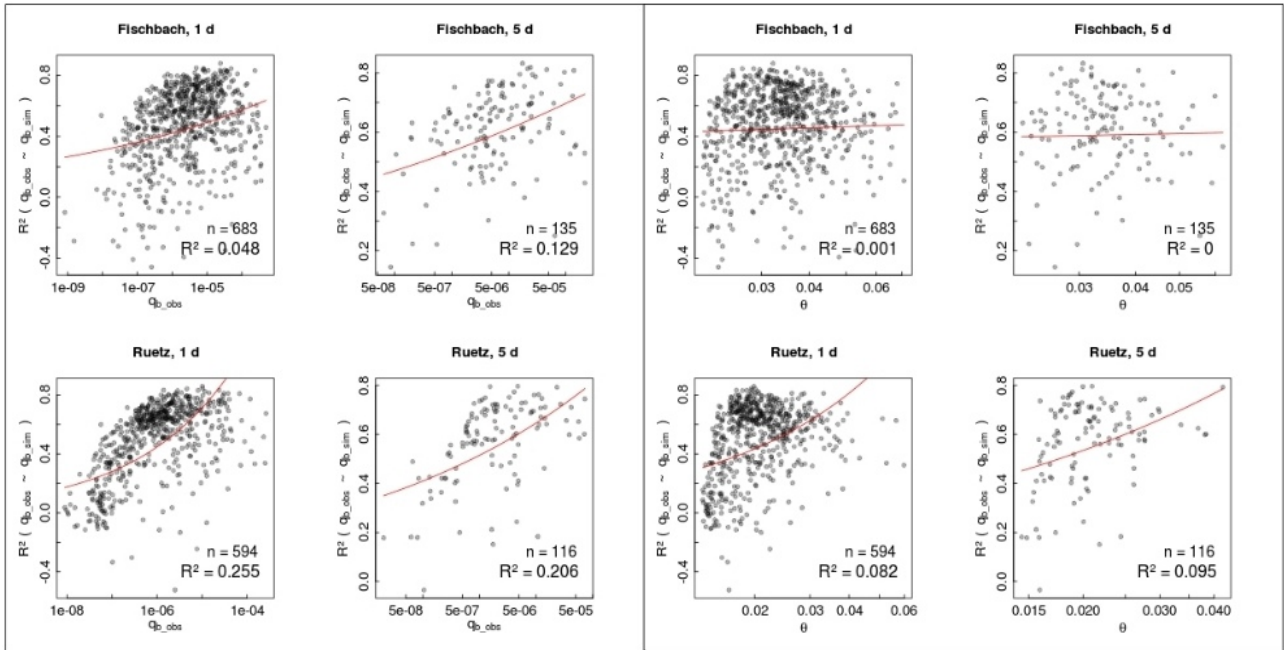


Fig. 4.9: correlation coefficients R^2 from non-linear-fits of the Cheng-equation ($\Psi_b \sim \theta$) over different time frames (length = 1 resp. 5 days), plotted over mean transport rate (left half) and mean dimensionless shear stress θ (right half), time frame shift = length of time frame,

4.2.3 Hysteresis and further relations

The SPG stores data in given time intervals independent from flow state. Hence, data pairs are collected during both rising and falling discharge periods. Many hydrological processes show a so-called hysteresis, i.e. a different behavior when discharge rises to when it falls. With the herein used data sets, also bedload transport rates may be examined for such effects. Especially the distinct diurnal fluctuations in the two glaciated catchments provide a good opportunity to look for hysteresis phenomena.

For this analysis, the whole data sets including phase-1- and phase-2-discharges were used. A data point was classified to the rising limb when the respective discharge increased in comparison to the previous time step and vice versa. As a consequence, the transport rates were plotted against the shear stress with additional information about the direction of the hydrograph. This approach does not directly deal with the threshold θ_c , but if there was a clear difference between the transport rates during rising and falling discharge, the respective back-calculated values for θ_c would have also diverged.

However, a detailed visual examination was possible only for several days in a row due to the large amount of data in the charts. To allow a clearer visualization and comparison over a longer period, it appeared promising to normalize each value of θ and Φ_b with the corresponding daily maximum.

Subsequently, no distinct and constant hysteresis effects were detectable in a visual analysis for several periods of variable length. Some examples for the yielded charts are provided in appendix B. As a representative summary, moreover, figure 4.10 shows the differences between the daily means of θ_c -values at the rising limb of the hydrograph and those at the falling limb together with a 30-days moving average.

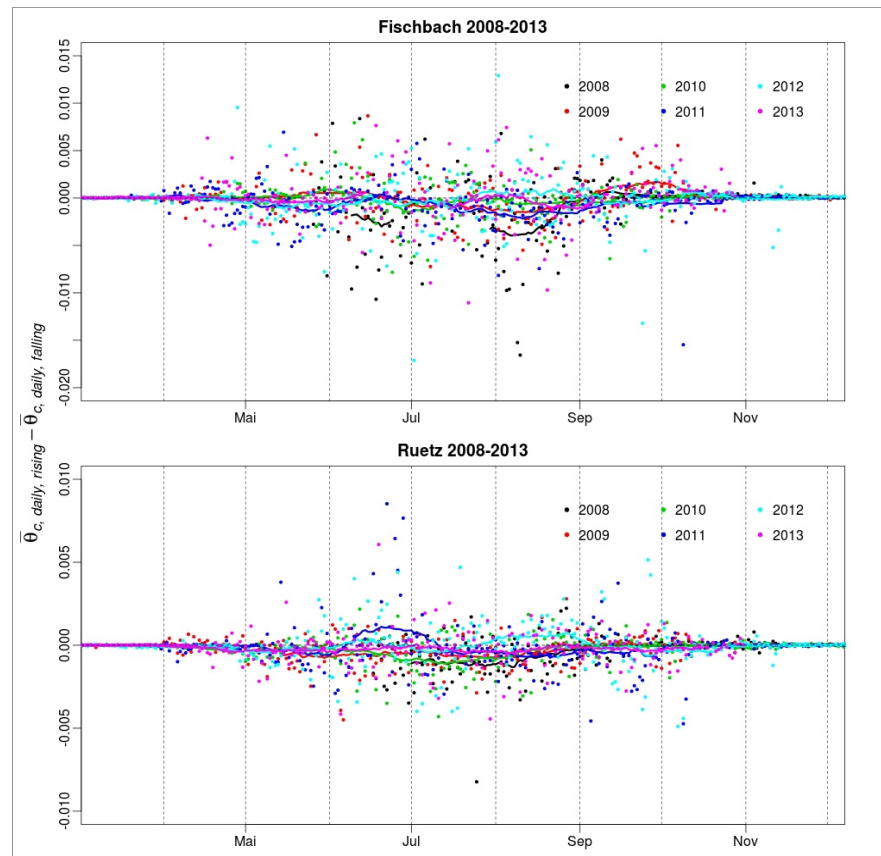


Fig. 4.10: daily means of $\theta_{c,rising}$ - daily means of $\theta_{c,falling}$; lines = 30-days moving average

In addition to the analyses which are explained in the main part of the thesis, several further ideas were tested. Some selected outcomes are illustrated in further charts which are listed and explained in appendix B as they are either leading to a different direction than the rest of the work, go too far into detail or are hardly interpretable. Nevertheless, they might include or provoke some interesting thoughts for further research.

4.2.4 Selected regressions with θ_c

The back-calculated θ_c data were also analyzed as a collective, not ordered in time. Eventual relationships between θ_c and other parameters were examined using regression analysis. Therefore, the data need to be stationary and independent. At the study sites, steady-state may be assumed because the time frame of six years is in fact too short to

detect any significant hydrological trend. Accordingly, a trend elimination based on too short time series might be misleading as the results of this work should at its best improve long-term simulations. However, for the six years of measurements, there are no severe man-made impacts or catastrophic events known, which could have changed the hydrological characteristics of the streams considerably (verbal communication with local people, 2013 and 2014).

Nevertheless, the time series are not independent. The back-calculated θ_c values show strong autocorrelation (Fig. 4.11). As the amount of data is large enough, the simplest way to get rid of the dependency is to draw data pairs randomly, either one per a defined time period or a certain number from the whole data set. Repeating multiple times gives a larger data set of independent θ_c values which may be used for statistically more proper analyses. A further way to avoid dependence and potential trend effects is to differentiate the time series and examine the differences $\Delta\theta_{c,t} = \theta_{c,t} - \theta_{c,t-1}$.

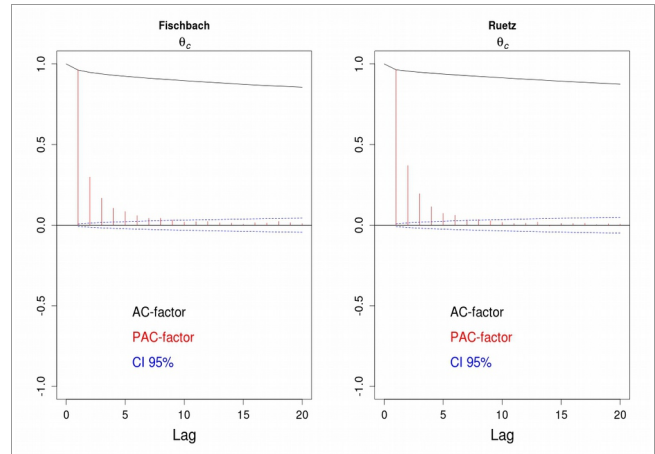


Fig. 4.11: autocorrelation functions of θ_c -time series

As already mentioned before, also the presence of a relation between θ_c and the discharge seems possible. Figures 4.12 and 4.13 show the regression of θ_c dependent on q , or θ respectively, resulting from both a linear and a power-law fit. The correlation coefficients, R^2 , are round 0.4 for the Fischbach and 0.6 for the Ruetz respectively. Hence, the dependence may be called rather weak.

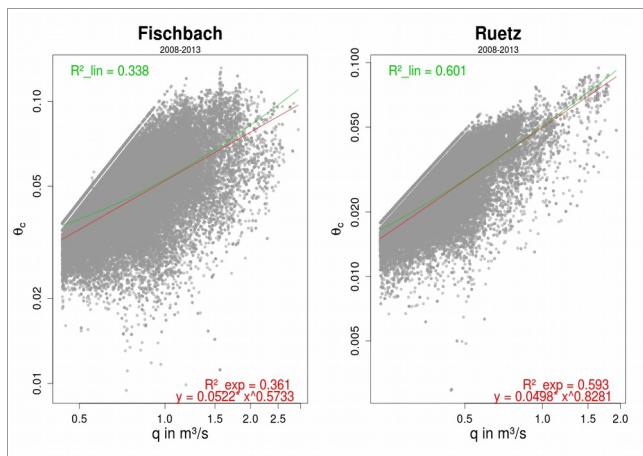


Fig. 4.12: regression of θ_c over q

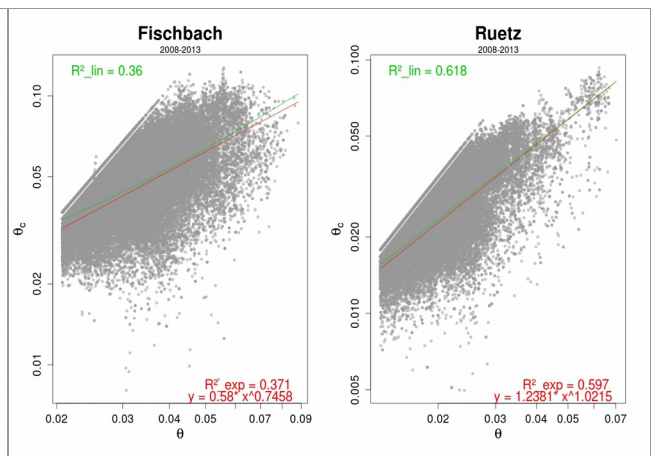


Fig. 4.13: regression of θ_c over θ

4.2.5 Stochastic considerations

In this thesis, four basic approaches were tested to implement a stochastic determination of θ_c in the established bedload transport computation procedure. The calculations were carried out for one core variant and one additional alternative. Generally, theoretical probability functions were fitted to a certain data set. All these distribution fits were evaluated by means of the Anderson-Darling-Test (Anderson & Darling, 1952). As a result, the hypothesis that the pdf adequately represent the data had to be rejected on a significance level of 0.05 for each fit. Nevertheless, the relatively best fits were passed on because alternatives, like the use of non-parametric distributions, would have entailed a model complexity beyond the scopes of this work.

To begin with, a possibility (later called S1 in table 4.2) is the fit of a probability function to the θ_c data and the subsequent generation of random values for each time step. In the original time series, θ_c is auto-correlated over long time lags (Fig. 4.11) which should be represented in the simulation. Moreover, also the partial auto-correlation coefficients are significantly different from zero over several time lags (Fig. 4.11).

Hence, it is difficult to find an adequately simple way to represent the effect in a basic simulation attempt. For the first computations, the autocorrelation was neglected and θ_c values were generated randomly for each time step. This might give at least an

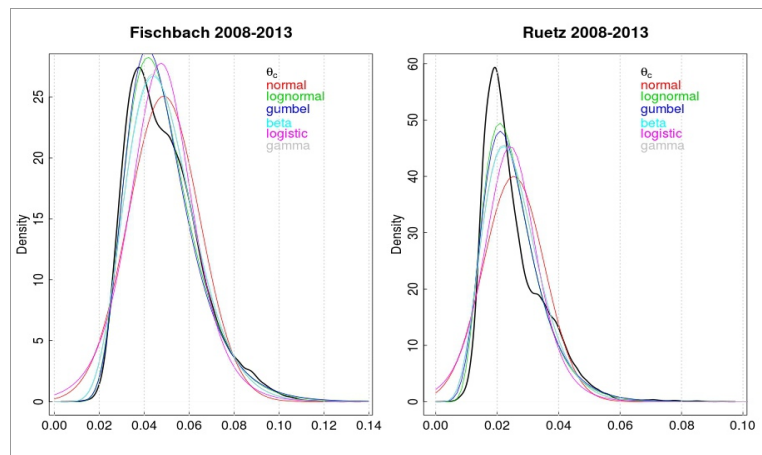


Fig. 4.14: pdf fitting to θ_c

idea about the applicability of this approach in an order-of-magnitude scale. Anyhow, as it would have been the simplest way to implement stochastics in the following simulations, it was described further even though the other strategies promised better results. In figure 4.14, the empirical probability distribution function of θ_c and the examined theoretical pdfs were plotted together. Visually, the gamma and the log-normal distribution were assessed as most appropriate.

Another idea (S2) is to consider the regression of θ_c over θ , or q respectively (Fig. 4.12 and Fig. 4.13). The correlation coefficients are between 0.4 and 0.6, i.e. not impressively high, so it might be statistically improper to use the gained parameters further. Nevertheless, it is an intuitive idea that eliminating the influence of θ might especially eliminate some hidden periodic patterns in θ_c which are linked to the diurnal or also seasonal cycles of the discharge. Especially considering figure 4.8 and the explanations in chapter 4.2.3, it might be an appropriate workaround. From another point of view, this procedure may eliminate the influence of the discharge in equation 4.1. Accordingly, the pure variability might be left to be analyzed. In detail, a pdf is fitted to a collective of drawn residuals resulting from the power-law-fit in figure 4.13 (Fig. 4.15). Subsequently, random values are generated from the assessed pdf and added to the regression function, what delivers again a row of simulated values for θ_c . Moreover, the regression coefficients from figure 4.13 may be used to modify the Cheng-equation as follows:

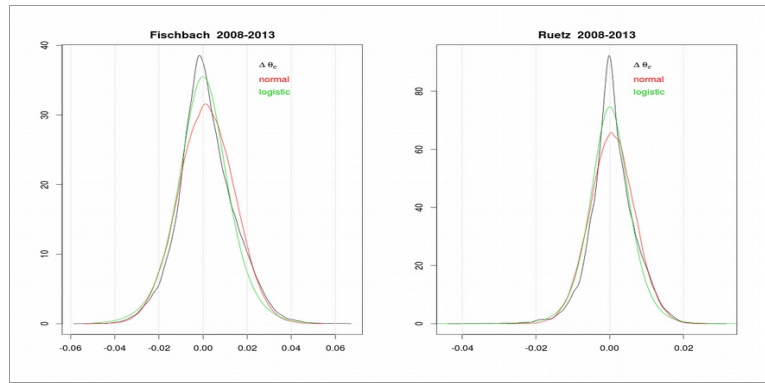


Fig. 4.15: pdf to residuals of fit $\theta_c \sim \theta$

$$\text{Fischbach: } \Phi_b = 5 * \theta^{1.5} * e^{\left(\frac{-0.58}{\theta^{0.75}}\right)} \quad (4.2a)$$

$$\text{Ruetz: } \Phi_b = 5 * \theta^{1.5} * e^{\left(\frac{-1.24}{\theta^{0.48}}\right)} \quad (4.2b)$$

The third implementation (S3) of stochastics is based on an analysis of the differences $\Delta\theta_c$. As the differences are still auto-correlated, the further used values are again randomly drawn. They seem symmetrically distributed with zero as a mean (Fig. 4.16). As

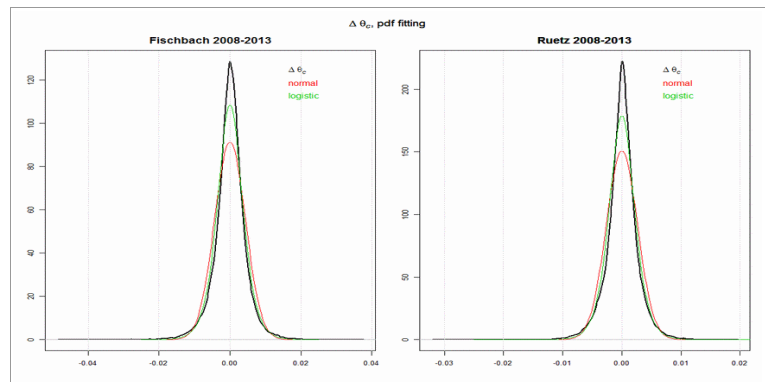


Fig. 4.16: pdf to $\Delta\theta_c$

variant 1 a normal distribution and a logistic distribution as variant 2 are fitted and used to reproduce a row of random differences. The new θ_c time series starts with the mean of θ_c over the calibration period as θ_c -value for the first time step. For each new time step, a computed $\Delta\theta_c$ -value is added to the previous θ_c .

Based on the latter, a fourth approach (S4) used an established and more sophisticated method which combines some of the already mentioned thoughts and is termed as ARIMA- or SARIMA-model (Maniak, 2010). To set up such a model, the given time series is analyzed for significant auto-regressive (AR) and moving average (MA) effects. The corresponding terms account for dependence, each in a slightly different way. If the data are non-stationary, also differentiation (I for the subsequently necessary integration) may be applied. All of these three parts are applicable in several orders which define how many time steps are considered for the parametrization. In the annotation, the orders are listed in brackets after the abbreviation for the model type. Accordingly, an ARIMA(1,1,1)-model accounts for auto-regressive and moving average dependence over one time step after a single differentiation of the input time series.

Precisely, for the generation of new time series, random values are drawn from a certain distribution for each time step and the actual output value is calculated as a weighted average by applying slightly different algorithms for both AR- and MA-terms. Therein, random values are included from as many time steps as are defined by the certain orders. The used weights as well as the parameters of the distribution are determined in advance as model parameters. If the integrative term (I) is non-zero, this determination is applied to the differentiated original time series and the sub-result of the ARIMA-model generation is integrated to yield the actually demanded time series.

This method is implemented in the statistics software R (R Core Team, 2013). It enables the automatic estimation of orders and parameters and the subsequent simulation of time series. Such an automated analysis suggested an ARIMA(5,1,0)-model for optimal reproduction of the θ_c time series. To restrict the complexity of the model, auto-regression was considered only for two time steps. This is also common practice in hydrology (Nachtnebel, 2009) and including more than two time steps might be designated as over-parametrization. Hence, the parameters of an ARIMA(2,1,0)-model and subsequently the θ_c time series were computed. The second variant for comparison included also a seasonal effect. After some variations of the seasonal part, a SARIMA(2,1,0)x(2,1,0)-model provided best intermediate results and was implemented as variant 2.

4.3 Punctual bedload simulations for the control sections

In simulation projects, calibration and validation should be carried out (Nachtnebel, 2009). Herein, the data of 2 years, 2012 and 2013, were reserved for validation and comparison of the different methods and their results. The parameters for the different modeling attempts were determined by analyzing the data from 2008 to 2011. The ratio 2:1 for calibration to validation data and the remaining four years for calibration are not optimal, but it was subjectively decided that at least two years should be dedicated for calibration. Further application of this concept with data from longer measurements will balance the drawbacks and lead to more proper results.

Punctual, width-integrated and non-fractional bedload transport simulations were computed for the control sections at the geophone sites. Therefore, geometric and grain size input values were assigned as listed in table 3.2. Each of the stochastic analyses described in 4.2.5 provided certain parameters which were used for the subsequent computation of θ_c time series. To balance implausible results or outliers, the generation was done a certain number of times (n) following a Monte-Carlo-approach. That gave n θ_c values for each time step and the mean of these was passed on to the further computation of bedload transport rates. As non-stochastic status quo alternative, also the mean of the back-calculated θ_c -values over the calibration time and θ_c calculated with the equation after Lamb et al. (2008) were used for simulation runs.

The above-mentioned equation of Yochum et al. (2002) yielded very poor results, orders of magnitude too high to be plausible, and was consequently not used further. The reason for the deviation might be a wrongly chosen method for the determination of σ_z . However, as this approach is not implemented in sedFlow, neglecting it does not endanger the goals of this thesis. As a summary, table 4.2 gives an compact overview of the used simulation setups.

Tab. 4.2: simulation procedures, overview

abbr.	explanation
	Flow resistance
	approach after Rickenmann and Recking (2011), Eq. 2.3 and 2.4
	Bedload transport
	approach after Cheng (2002)
	Calculation of θ_c
S0	<p>Non-stochastic, Var.1: θ_c = mean of θ_c over calibration period; Var.2: θ_c after Lamb et al. (2008), Eq. 2.9; herein used values for Var.1 determined by drawing from calibration time series, mean over 50 draws with each 1000 values: Fischbach: $\theta_c = \mathbf{0.0475}$ (± 0.0001), Ruetz: $\theta_c = \mathbf{0.0239}$ (± 0.0001); Var.2: $\theta_c = 0.15 * S^{0.25} \rightarrow$ Fischbach: $S = 0.017$, $\theta_c = \mathbf{0.054}$, Ruetz: $S = 0.023$, $\theta_c = \mathbf{0.058}$ (for Var.2, no correction of the slope after eq. 2.11)</p>
S1	<p><u>Calibration:</u> 1000 randomly drawn values out of back-calculated θ_c-time series, integration of 50 draws, visually choose pdf in Fig. 4.14 -> Var.1: gamma, Var.2: lognormal distribution <u>Simulation:</u> generation of θ_c for each time step, θ_c = mean out of 50 runs</p>
S2	<p><u>Calibration:</u> power-law-regression of $\theta_c \sim \theta$ (Fig. 4.13), Var.1: approximate pdf to residuals, normal distribution (Fig. 4.15); Var.2: no residuals, θ_c from regression line <u>Simulation:</u> generation of θ_c for each time step, θ_c = mean out of 50 runs</p>
S3	<p><u>Calibration:</u> differentiation of θ_c time series ($\Rightarrow \Delta\theta_c$), approximate symmetric pdfs (Fig. 4.16), Var.1: normal distribution; Var.2: logistic distribution</p>

	<p><u>Simulation:</u> generation of $\Delta\theta_c$ from pdfs, $\theta_{c,1}$ = mean θ_c of calibration period, add $\Delta\theta_{c,t}$ to previous $\theta_{c,t-1}$, mean out of 50 runs</p>
S4	<p><u>Calibration:</u> automatically fit ARIMA(2,1,0)- and SARIMA(2,1,0)x(2,1,0)-model as Var.1 and Var.2</p> <p><u>Simulation:</u> automatically create θ_c-time series using the appropriate functions in R</p>

4.4 Bedload simulations with sedFlow

A very simple model setup was used for first sedFlow simulations and to compare the results with those from the punctual simulations in chapter 4.3. Precisely, two successive reaches with the parameters from table 3.2 were placed upstream of one reach with no active layer. The latter represents the geophone station with its solid, unerodible bed. Before, a test had shown that the use of short reach lengths, less than approximately 20 meters, lead to erroneous results like oscillations which are most likely occurring due to numerical instability. Accordingly, a reach length of 500m was chosen for the two active reaches to secure stable and sound results.

To optimize comparability, the GSDs of surface and subsurface layers were assessed identical and the options in sedFlow were set with the intent to apply a calculation procedure which corresponds to the R-simulations. At the topmost reach, discharge time series for pure water and sediment need to be assigned. Here, the continuously measured discharge at the gauge right above the geophone was taken as pure water input. The simulations were computed without sediment input because it was assumed that mobilization takes place only in the stream bed. Additionally, the long channel reaches shall assure unlimited availability of bedload material to be moved by the simulated forces. The artificial equilibrium of transport capacity and bedload transport should be balanced after the first reach.

4.5 Model skill estimation

To compare the results of different bedload transport calculation approaches, an appropriate method needed to be developed. The easiest technique to obtain a first qualitative impression is to plot the time series and interpret them visually, while for quantitative evaluation, many test statistics are known from literature. Zambrano-Bigiarini (2014) presented an extensive collection of such routines and facilitated the calculation in the R statistical software environment. These methods compare two time series, usually an observed and a simulated one and as a result, one single value expresses the goodness of the model, i.e. the similarity of the two time series.

Generally, such test statistics are particularly sensitive to differences at certain parts of the time series, mostly at the peaks, the mean or the variability. For long-term bedload transport simulations on catchment scale and with focus on the sediment budget, the most important outcome is the accumulated bedload transport (ABT) over a certain period. Accordingly, the first value to assess the model skill is the ratio of the simulated ABT to the measured ABT.

In addition, the Kling-Gupta efficiency (KGE) after Gupta et al. (2009) and Kling et al. (2012) was taken into account. This statistic is based on the mean square error (MSE) and its normalization, the Nash-Sutcliffe efficiency (NSE), which are widely used for hydrological model evaluation. Gupta et al. (2009) advanced the latter to avoid certain potential mathematical problems and further facilitate a separate analysis of the different components which build up the result, namely a correlation, a bias and a variability term. They state furthermore that the correlation term, representing the regression of observed against simulated values, very likely is the major factor therein, which means that the KGE is sensitive at the most frequent (thus low) bedload transport stages. Hence, it is an optimal compliment to the ABT-ratio which is primarily determined by high transport rates. The KGE possibly ranges from 1 to negative infinity, the optimal value is 1. Moreover, several other statistics in the package of Zambrano-Bigiarini (2014) were tested during the work for this thesis but yield very similar results to one of the above-mentioned values. Consequently, only the two previously described were used to keep the analyses easily interpretable.

5 Results

5.1 Punctual bedload simulations

The presented bedload transport simulations were applied for each year separately and the efficiency criteria for every variant and year are given in tables 5.1 and 5.2. Therein, the row name stands for the experimental setup according to table 4.2. Furthermore, figures 5.1 and 5.2 show a visualization of the ratio between simulated and observed bedload transport rates, classified by the observed transport stage θ/θ_c together with information about the corresponding mass distributions of transported and simulated bedload. These charts especially allow a view on the tendency for over- or underestimation in dependence of the transport stage. Additionally, the simulation results were plotted as scatter plots both yearly and over the whole study period. The complete series of charts is listed and explained in appendix A.

Caused by the stochastic computation sub-step, there are small differences between the results of multiple simulation reruns with identical inputs. The values for the ABT-ratio and the KGE vary in the second or third decimal. Thus, the accuracy in tables 5.1 and 5.2 is set to two decimals as further decimals should not be considered in this summarizing comparison. However, method S3 is an exception where the results are diverging over several orders of magnitude. This might be caused by an erroneous algorithm or basic concept, respectively the insufficient goodness of the distribution fit. As method S4 also includes differentiation, hence accounts for the same basic thoughts, and the error in S3 was not detectable after deep examination, no further effort was spent to improve the algorithm. Consequently, this method was excluded from the evaluation.

Tab. 5.1: results model skill estimation, Fischbach

var.		ratio ABT							KGE						
		2008	2009	2010	2011	2012	2013	mean	2008	2009	2010	2011	2012	2013	mean
S0	1	2.20	0.95	0.63	0.19	2.30	2.10	1.40	-0.95	0.72	0.32	-0.22	-0.40	-0.29	-0.14
	2	1.60	0.46	0.37	0.07	1.40	1.30	0.87	0.18	0.21	0.03	-0.36	0.52	0.54	0.19
S1	1	2.70	0.98	0.65	0.20	2.30	2.10	1.49	-1.00	0.72	0.33	0.22	-0.46	-0.34	-0.09
	2	2.70	0.99	0.64	0.20	2.30	2.10	1.49	-1.00	0.73	0.34	-0.21	-0.46	-0.33	-0.16
S2	1	0.81	0.56	0.22	0.16	0.72	0.58	0.51	0.29	0.12	-0.23	-0.31	0.21	0.16	0.04
	2	0.80	0.54	0.21	0.15	0.71	0.58	0.50	0.29	0.11	-0.23	-0.31	0.20	0.17	0.04
S4	1	2.50	0.83	0.57	0.17	2.10	1.90	1.35	-0.70	0.63	0.26	-0.25	-0.19	-0.09	-0.06
	2	2.50	0.83	0.57	0.17	2.10	1.90	1.35	-0.70	0.64	0.26	-0.25	-0.19	-0.09	-0.06

Tab. 5.2: results model skill estimation, Ruetz

var.		ratio ABT							KGE						
		2008	2009	2010	2011	2012	2013	mean	2008	2009	2010	2011	2012	2013	mean
S0	1	1.90	0.63	2.70	0.60	3.90	15.00	4.12	-0.08	0.38	-0.92	0.41	-2.40	-19.00	-3.60
	2	0.00	0.00	0.06	0.01	0.12	1.00	0.20	-0.52	-0.45	-0.36	-0.47	-0.20	0.29	-0.29
S1	1	2.00	0.64	2.70	0.62	3.90	15.00	4.14	-0.11	0.38	-0.91	0.43	-2.40	-19.00	-3.60
	2	2.00	0.65	2.70	0.61	3.90	15.00	4.14	-0.13	0.42	-0.97	0.42	-2.40	-19.00	-3.61
S2	1	0.55	0.36	0.43	0.14	0.51	1.60	0.60	-0.08	-0.14	-0.08	-0.31	0.05	0.27	-0.05
	2	0.54	0.34	0.43	0.14	0.50	1.60	0.59	-0.09	-0.15	-0.08	-0.31	0.05	0.29	-0.05
S4	1	1.50	0.45	2.20	0.49	3.30	13.00	3.49	0.30	0.18	-0.43	0.29	-1.80	-17.00	-3.08
	2	1.50	0.45	2.20	0.49	3.30	13.00	3.49	0.30	0.18	-0.44	0.29	-1.80	-17.00	-3.08

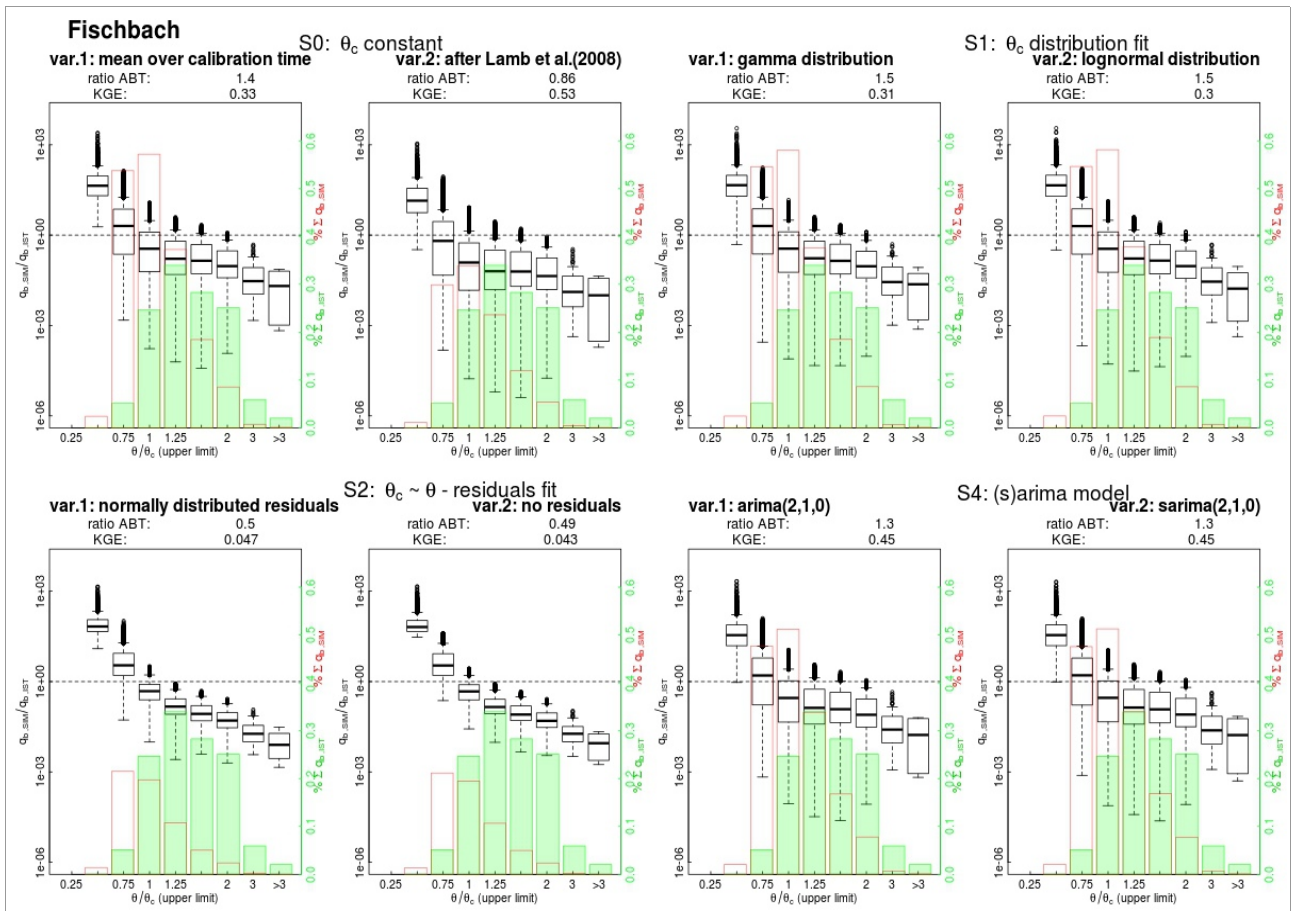


Fig. 5.1: boxplots showing the results of simulations for the Fischbach, classified by flow stage (θ/θ_c), barplots showing the corresponding distribution of transported bedload mass for observed and simulated time series

All these outcomes may be interpreted with the conclusion that all methods deliver simulation results which are unsatisfactory in comparison with typical hydrological methods (e.g. Pechlivanidis et al. 2014) but, however, in a typical range for bedload issues. As

variant S0_1, the calculation of a constant value for θ_c after Lamb et al. (2008), is widely used as default procedure (e.g. in sedFlow), a comparison with this method is practically important. Thus, the results of the Ruetz show a strong advantage of all other methods over S0_1 whereas at the Fischbach, S0_1 performs rather good. This might be an indication for higher vulnerability to differences in the catchment characteristics. Furthermore, all variants except S2 and S0_1 deliver very similar outcomes. Considering also the variability shown in the boxplots above, variant S2 might be assigned as most stable and promising although it underestimates transport at high stages stronger than the other variants.

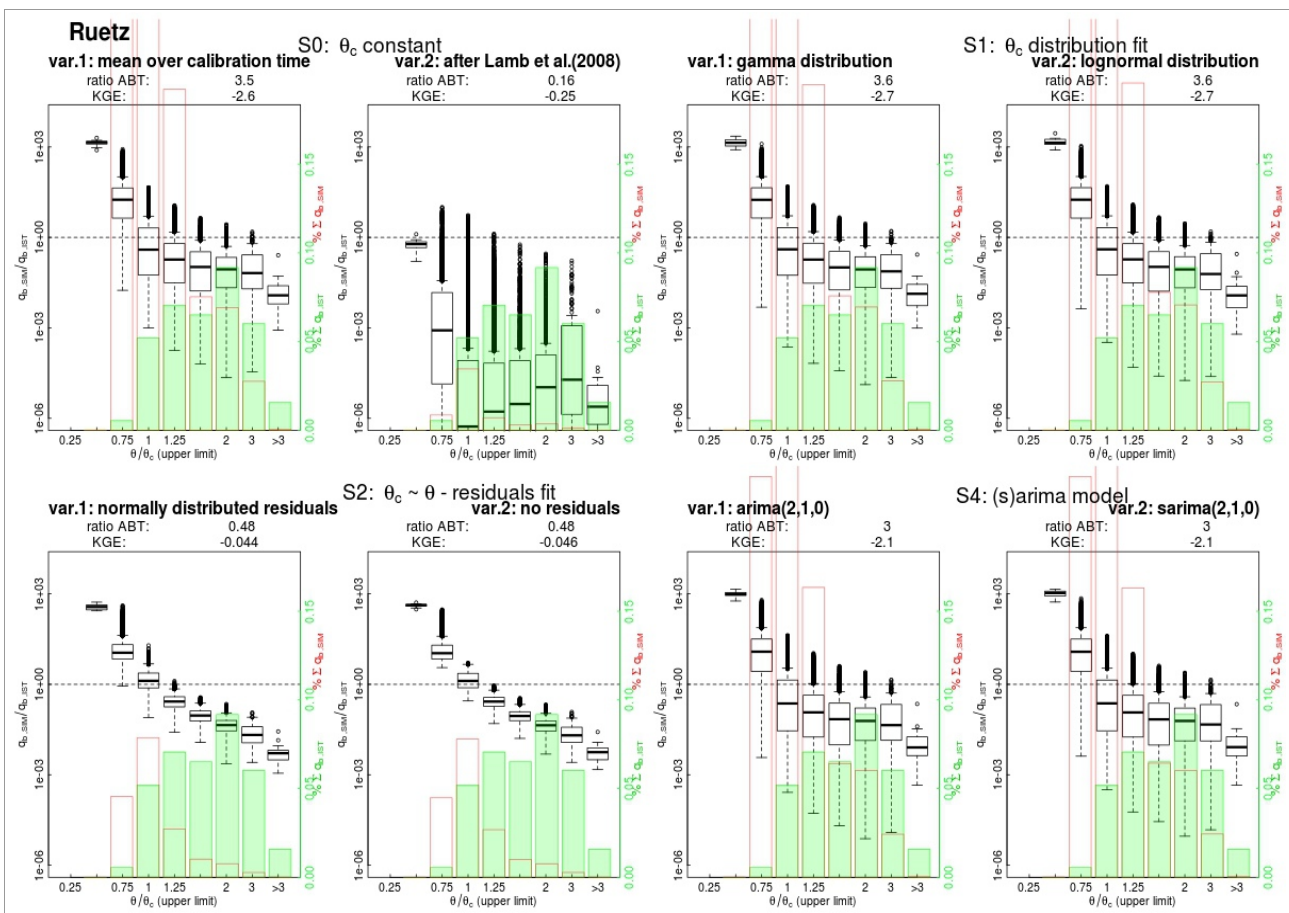


Fig. 5.2: boxplots showing the results of simulations for the Ruetz, classified by flow stage (θ/θ_c), barplots showing the corresponding distribution of transported bedload mass for observed and simulated time series

5.2 sedFlow simulations

Simulations with the bedload equation of Rickenmann (2001, Eq. 2.10) for comparing intents yielded a high similarity between the results of sedFlow- and punctual simulations. As a conclusion, this confirms the concept to validate one method by means of the other. By contrast, it was not possible to obtain comparable results with the equation of Cheng (2002). An intensive search for the reason of this error ended in the finding that the equation is implemented erroneously to the sedFlow code. More precisely, the transformation from the basic form (Eq. 9) to a fractional form like published in the Appendix of Heimann et al., (2014b) causes too high transport rates. Figures 5.3 and 5.4 show the comparison of the two equation types computed in R for the same control section as the punctual simulations. As a result, the yearly accumulated bedload transport calculated by use of the fractional approach exceeds the non-fractional outcomes by a factor of up to 15 at the Fischbach and even up to 100 at the Ruetz.

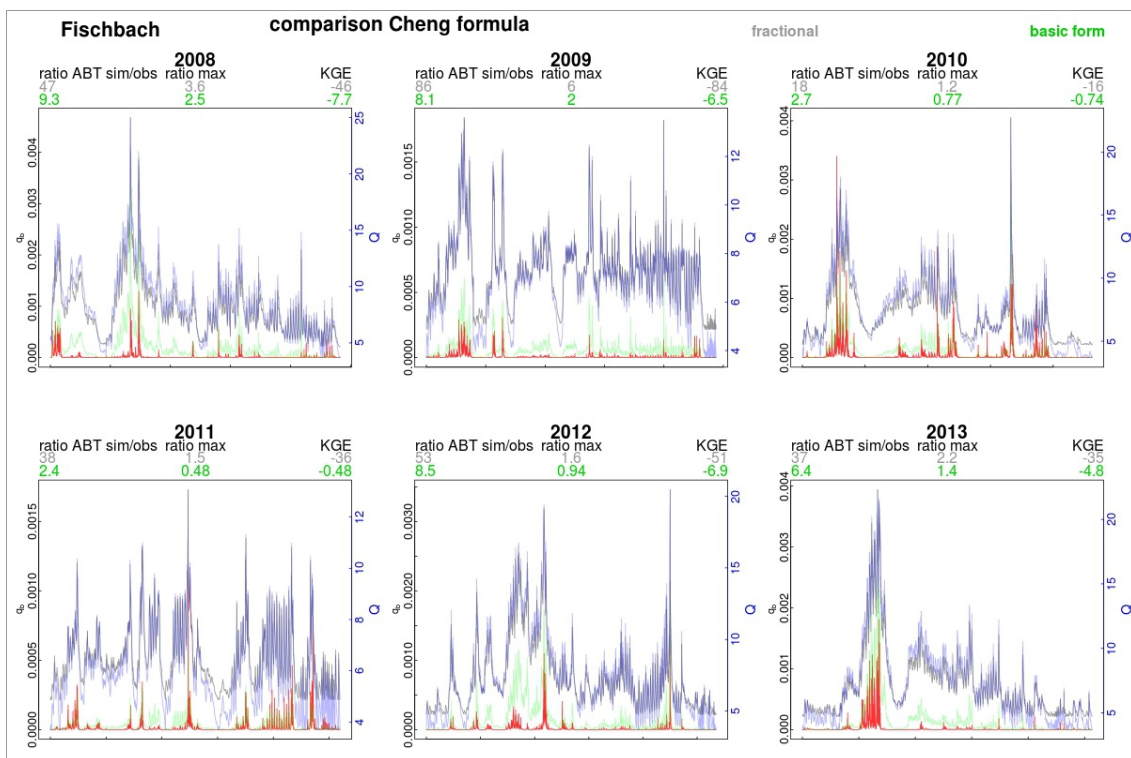


Fig. 5.3: comparison of the two forms of Cheng-equation, green: basic form, grey: fractional form, blue: Q in m^3/s ; Fischbach

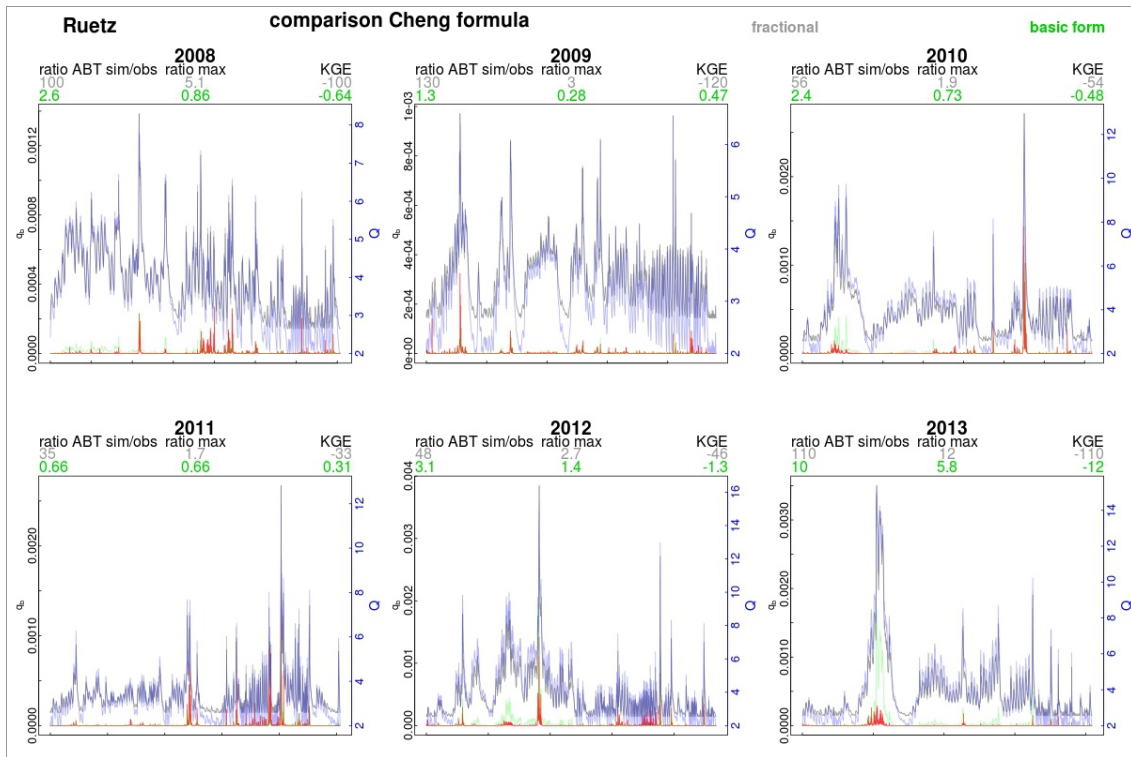


Fig. 5.4: comparison of the two forms of Cheng-equation, green: basic form, grey: fractional form, blue: Q in m^3/s ; Ruetz

Unfortunately, it was not yet possible to find a correct fractional formulation for the Cheng-equation to implement. As sedFlow is designed for fractional transport simulations, this bedload transport equation could not be used for further calculations. Accordingly, one main intention of this thesis, the development of an implementable stochastic extension for the Cheng-equation in sedFlow, failed due to external circumstances.

6 Discussion

The initial situation for this project was promising. Some certain circumstances like the hydro-morphological situation, the long-term high-resolution geophone data or the highly developed methodology, especially with sedFlow, should have allowed representative and robust analyses. During the work on this thesis, some drawbacks arose. First of all, the plausibility control showed that the logged bedload transport data during low flow periods are implausible and should be excluded from further analyses. By now, it was impossible to clearly ascertain the reasons for the irregularities but this is still topic of further research at the WSL.

Furthermore, the default logging frequency of the Swiss Plate Geophones, 15 minutes, was initially chosen with the main intention to measure the summarized bedload transport over long periods, i.e. years and decades. Accordingly, the data are well suitable for analyses of long-term sediment dynamics but not optimal for investigating the initiation of bedload motion, which is a temporally highly variable and frequent process (e.g. Heyman et al., 2013). A higher temporal resolution of the measurements would probably offer a better opportunity to analyze the physical background of bedload transport and especially bedload mobilization. Nevertheless, one goal of this thesis was to adapt a certain calculation procedure for long-term simulations where the used time steps are usually longer than 15 minutes. Hence, a temporally more detailed analysis might have led to less usable input parameters or complexer models.

Another possible source of uncertainties is an inhomogeneity in the stream bed right upstream of the geophone station. The solid sill interrupts the natural bed over the whole width and causes an artificial morphology. Precisely, a reach of approximately 20 m length upstream of the station is now planar with no slope, the active bedload layer is very homogeneous and finer than further above in the undisturbed bed. Especially in the Ruetz, where the natural bed is steeper and rougher, this alteration is conspicuous. Consequently, it is not a priori clear which geometric parameters represent the reality adequately. Herein, the inputs were assessed by means of measurements and calculations as described in 3.2.

By now, such drawbacks and similar problems are immanent in research on bedload transport. It is a very complex issue where numerous impacts, forces and happenings affect the feasibility of observing and interpreting high-quality data. Considering all this, there were several simplifications knowingly applied in the thesis to reach the principal goals. Moreover, as only a very little part of the wide range of hydrological methodology was touched, no global statement about the correlation of model complexity and goodness of results may be established. Rather, this underlines the characteristics of this thesis as a concept study dealing with a certain branch of possible utilizations for geophone data.

Interpreting the gained outcomes, nevertheless, it might be stated that the presented approaches are practicable, deliver plausible results and fulfill the requirement of short calculation time. Especially variant S2 promises possibilities to further improvements, for example by adapting the factor a_1 in the Cheng-equation (Eq. 2.13) or finding a better regression function (Fig. 4.13).

7 Conclusions

At the beginning of the work, the research question was not defined strictly. The intentions were to examine the given data extensively and find some patterns which might be easily reproducible in future simulation approaches. Moreover, it was a priori hardly possible to make concrete assumptions, neither about these patterns' characteristics nor their orders of magnitude. During the work, there emerged numerous ideas, provisional results or initial thoughts for further specific research. Following all them would have forced all hope for finishing the thesis to vanish.

However, the most important results are not those gained at the end by comparing the different stochastic simulation procedures. Rather, they appeared through the whole creation process, particularly in the plausibility check, the testing of sedFlow or the statistical analyses. In the end, the used methods might look quite dilettantish for the hydrologist's educated eye. That was, to some extent, accepted in advance and results from looking for a compromise with respect to accuracy, computation effort, simplicity, or the desire to examine several different approaches. Nevertheless, this thesis illustrates once more the complexity of the issue bedload transport and shows that there are many influences which affect the usability of an apparently good data and methodology basis.

If one of the presented methods is applied to other alpine streams, the estimation of parameters will be a challenging task. In this thesis, a large data set was usable to determine the parameters of the fitted probability distribution functions. For other streams worldwide, there are hardly ever data pairs of discharge and bedload transport rates available. Hence, for the presented methodology there will be at least two parameters to estimate and calibrate in addition to those needed for the basic model. Furthermore, the stochastic calculations deal with very small values without any obvious relation to detectable phenomena in nature. It might be possible, anyhow, to find a sound method to estimate these parameters from certain stream characteristics after continuative research including data from further, different catchments. Again, it will be an important task for the user to balance model complexity with expectable improvements in the resulting simulation accuracy.

Moreover, even though the data basis for this thesis is comparably vast, the temporal and spatial coverage is still low. Applying the developed concept to additional alpine

streams would yield a considerably better basis for universal statements. Besides, further research may also aim for testing other interesting stochastic methods, e.g. like presented in Duan & Barkdoll (2008) or Schmelter et al., (2011) using high-resolution geophone data.

8 Acknowledgements

I am very thankful to Dieter Rickenmann for sharing the project idea and his impressive knowledge about the processes in alpine streams as well as for his patient and constructive supervision. Many thanks, furthermore, to Hannes Hübl for his supervision and for allowing the cooperation with the external partners.

The responsible institution heads at WSL, Manfred Stähli and Alexandre Badoux deserve my appreciation for their administrative support. All of them made it possible for me to do part of my work in Switzerland which was a very educational and enjoyable experience. Special thanks go to the Dean of Studies at the BOKU, the federal aid institution for students Austria (Studienbeihilfenbehörde) and the Siegfried-Ludwig-Fonds for their financial support to cover the travel and living costs for the stays in Switzerland and at the sites in the Tyrol.

Furthermore, I'm very grateful to my officemates at the WSL, Florian Heimann, Martin Böckli and Alexander Beer, for empathetically supporting my first steps and giving interesting insights to the life and work of young scientists. Last but not least, I appreciate very much the efforts of the Open Source Community which eased my work considerably.

9 Literature

- Ancey, C., Böhm, T., Jodeau, M., & Frey, P. (2006). Statistical description of sediment transport experiments. *Physical Review E*, 74(1).
<http://doi.org/10.1103/PhysRevE.74.011302>
- Anderson, T. W., & Darling, D. A. (1952). Asymptotic Theory of Certain “Goodness of Fit” Criteria Based on Stochastic Processes. *The Annals of Mathematical Statistics*, 23(2), 193–212. <http://doi.org/10.1214/aoms/1177729437>
- Badoux, A., Andres, N., & Turowski, J. M. (2014). Damage costs due to bedload transport processes in Switzerland. *Nat. Hazards Earth Syst. Sci.*, 14(2), 279–294.
<http://doi.org/10.5194/nhess-14-279-2014>
- Bathurst, J. C., Graf, & Cao. (1987). Bed load discharge equations for steep mountain rivers. In *Sediment transport in gravel bed rivers*, Thorne et al. (eds.) (pp. 453–477). Chichester: Wiley.
- Bollrich, G., Martin, H., & Preißler, G. (2013). *Technische Hydromechanik. 1, 1*. Berlin: Verl. für Bauwesen.
- Buffington, J. M., & Montgomery, D. R. (1997). A systematic analysis of eight decades of incipient motion studies, with special reference to gravel-bedded rivers. *Water Resources Research*, 33(8), 1993–2029. <http://doi.org/10.1029/96WR03190>
- Bunte, K., Abt, S. R., Swingle, K. W., Cenderelli, D. A., & Schneider, J. M. (2013). Critical Shields values in coarse-bedded steep streams: Shields Values in Mountain Streams. *Water Resources Research*, 49(11), 7427–7447.
<http://doi.org/10.1002/2012WR012672>
- Cheng, N.-S. (2002). Exponential Formula for Bedload Transport. *Journal of Hydraulic Engineering*, 128(10), 942–946. [http://doi.org/10.1061/\(ASCE\)0733-9429\(2002\)128:10\(942\)](http://doi.org/10.1061/(ASCE)0733-9429(2002)128:10(942))
- Church, M., & Kellerhals, R. (1978). On the statistics of grain size variation along a gravel river. *Canadian Journal of Earth Sciences*, 15(7), 1151–1160.
<http://doi.org/10.1139/e78-121>
- Cooper, J. R. (2012). Does flow variance affect bedload flux when the bed is dominated by grain roughness? *Geomorphology*, 141-142, 160–169.
<http://doi.org/10.1016/j.geomorph.2011.12.039>
- Duan, J. G., & Barkdoll, B. D. (2008). Surface-Based Fractional Transport Predictor: Deterministic or Stochastic. *Journal of Hydraulic Engineering*, 134(3), 350–353.
[http://doi.org/10.1061/\(ASCE\)0733-9429\(2008\)134:3\(350\)](http://doi.org/10.1061/(ASCE)0733-9429(2008)134:3(350))
- Einstein, H.-A. (1950). *The bed-load function for sediment transportation in open channel flows* (Vol. 1026). Washington DC.
- Einstein, Hans Albert. (1936). Der Geschiebetrieb als Wahrscheinlichkeitsproblem.

<http://doi.org/10.3929/ethz-a-000092036>

- Fan, N., Zhong, D., Wu, B., Fofoula-Georgiou, E., & Guala, M. (2014). A mechanistic-stochastic formulation of bed load particle motions: From individual particle forces to the Fokker-Planck equation under low transport rates: stochastic bed load motion. *Journal of Geophysical Research: Earth Surface*, *119*(3), 464–482. <http://doi.org/10.1002/2013JF002823>
- Fehr, R. (1987). Einfache Bestimmung der Korngrößenverteilung von Geschiebematerial mit Hilfe der Linienzahlanalyse. *Schweizer Ingenieur Und Architekt*, *105*(38), 1104–1109.
- Ferguson, R. (2007). Flow resistance equations for gravel- and boulder-bed streams: FLOW RESISTANCE EQUATIONS FOR GRAVEL- AND BOULDER-BED STREAMS. *Water Resources Research*, *43*(5), n/a–n/a. <http://doi.org/10.1029/2006WR005422>
- Free Software Foundation. (2007). GNU GPL. Retrieved June 12, 2014, from <http://www.gnu.org/licenses/gpl-3.0.html>
- Gupta, H. V., Kling, H., Yilmaz, K. K., & Martinez, G. F. (2009). Decomposition of the mean squared error and NSE performance criteria: Implications for improving hydrological modelling. *Journal of Hydrology*, *377*(1-2), 80–91. <http://doi.org/10.1016/j.jhydrol.2009.08.003>
- Hassanzadeh, Y. (2012). *Hydraulics of Sediment Transport*. INTECH Open Access Publisher.
- Heimann, F. U. M. (2014). sedFlow User manual. WSL. Retrieved from http://www.wsl.ch/fe/gebirgshydrologie/wildbaeche/projekte/sedFlow/download/index_EN
- Heimann, F. U. M., Rickenmann, D., Böckli, M., Badoux, A., Turowski, J. M., & Kirchner, J. W. (2014). Recalculation of bedload transport observations in Swiss mountain rivers using the model sedFlow. *Earth Surface Dynamics Discussions*, *2*(2), 773–822. <http://doi.org/10.5194/esurfd-2-773-2014>
- Heimann, F. U. M., Rickenmann, D., Turowski, J. M., & Kirchner, J. W. (2014). sedFlow - an efficient tool for simulating bedload transport, bed roughness, and longitudinal profile evolution in mountain streams. *Earth Surface Dynamics Discussions*, *2*(2), 733–772. <http://doi.org/10.5194/esurfd-2-733-2014>
- Heyman, J., Mettra, F., Ma, H. B., & Ancey, C. (2013). Statistics of bedload transport over steep slopes: Separation of time scales and collective motion: BEDLOAD, TIME SCALES, AND COLLECTIVE MOTION. *Geophysical Research Letters*, *40*(1), 128–133. <http://doi.org/10.1029/2012GL054280>
- Hunziker, R. P., & Jäggi, M. N. R. (2002). Grain sorting processes. *Journal of Hydraulic Engineering*, *128*(12), 1060–1068.

- Jackson, J. A. (1997). *Glossary of geology*. (R. L. Bates & American Geological Institute, Eds.) (4th ed). Alexandria, Va: American Geological Institute.
- Kleinhans, M. G., & van Rijn, L. C. (2002). Stochastic Prediction of Sediment Transport in Sand-Gravel Bed Rivers. *Journal of Hydraulic Engineering*, 128(4), 412–425. [http://doi.org/10.1061/\(ASCE\)0733-9429\(2002\)128:4\(412\)](http://doi.org/10.1061/(ASCE)0733-9429(2002)128:4(412))
- Kling, H., Fuchs, M., & Paulin, M. (2012). Runoff conditions in the upper Danube basin under an ensemble of climate change scenarios. *Journal of Hydrology*, 424-425, 264–277. <http://doi.org/10.1016/j.jhydrol.2012.01.011>
- Lamb, M. P., Dietrich, W. E., & Venditti, J. G. (2008). Is the critical Shields stress for incipient sediment motion dependent on channel-bed slope? *Journal of Geophysical Research*, 113(F2). <http://doi.org/10.1029/2007JF000831>
- Liu, Z., & Todini, E. (2002). Towards a comprehensive physically-based rainfall-runoff model. *Hydrology and Earth System Sciences*, 6(5), 859–881. <http://doi.org/10.5194/hess-6-859-2002>
- Mader, H., Steidl, T., & Wimmer, R. (1996). *Abflussregime österreichischer Fliessgewässer: Beitrag zu einer bundesweiten Fliessgewässertypologie*. Wien: Umweltbundesamt.
- Maniak, U. (2010). *Hydrologie und Wasserwirtschaft Eine Einführung für Ingenieure*. Berlin, Heidelberg: Springer-Verlag Berlin Heidelberg. Retrieved from <http://dx.doi.org/10.1007/978-3-642-05396-2>
- Meyer-Peter, E., & Müller, R. (1949). *Eine Formel zur Berechnung des Geschiebetriebs* (Vol. 16). Zürich: Leemann.
- Nachtnebel, H.-P. (2009). *Studienblätter Hydrologie und Wasserwirtschaftliche Planung*. Wien: IWHW, BOKU.
- Pechlivanidis, I. G., Jackson, B., McMillan, H., & Gupta, H. (2014). Use of an entropy-based metric in multiobjective calibration to improve model performance. *Water Resources Research*, 50(10), 8066–8083. <http://doi.org/10.1002/2013WR014537>
- R Core Team. (2013). *R: A language and environment for statistical computing*. Vienna, Austria: R Foundation for Statistical Computing. Retrieved from www.r-project.org
- Recking, A. (2010). A comparison between flume and field bed load transport data and consequences for surface-based bed load transport prediction: FLUME AND FIELD BED LOAD TRANSPORT. *Water Resources Research*, 46(3), n/a–n/a. <http://doi.org/10.1029/2009WR008007>
- Recking, A. (2013). An analysis of nonlinearity effects on bed load transport prediction: NONLINEARITY AND BED LOAD PREDICTION. *Journal of Geophysical Research: Earth Surface*, 118(3), 1264–1281. <http://doi.org/10.1002/jgrf.20090>
- Rickenmann, D. (1990). *Bedload transport capacity of slurry flows at steep slopes* (Vol. 103). Zürich: ETH Zürich.

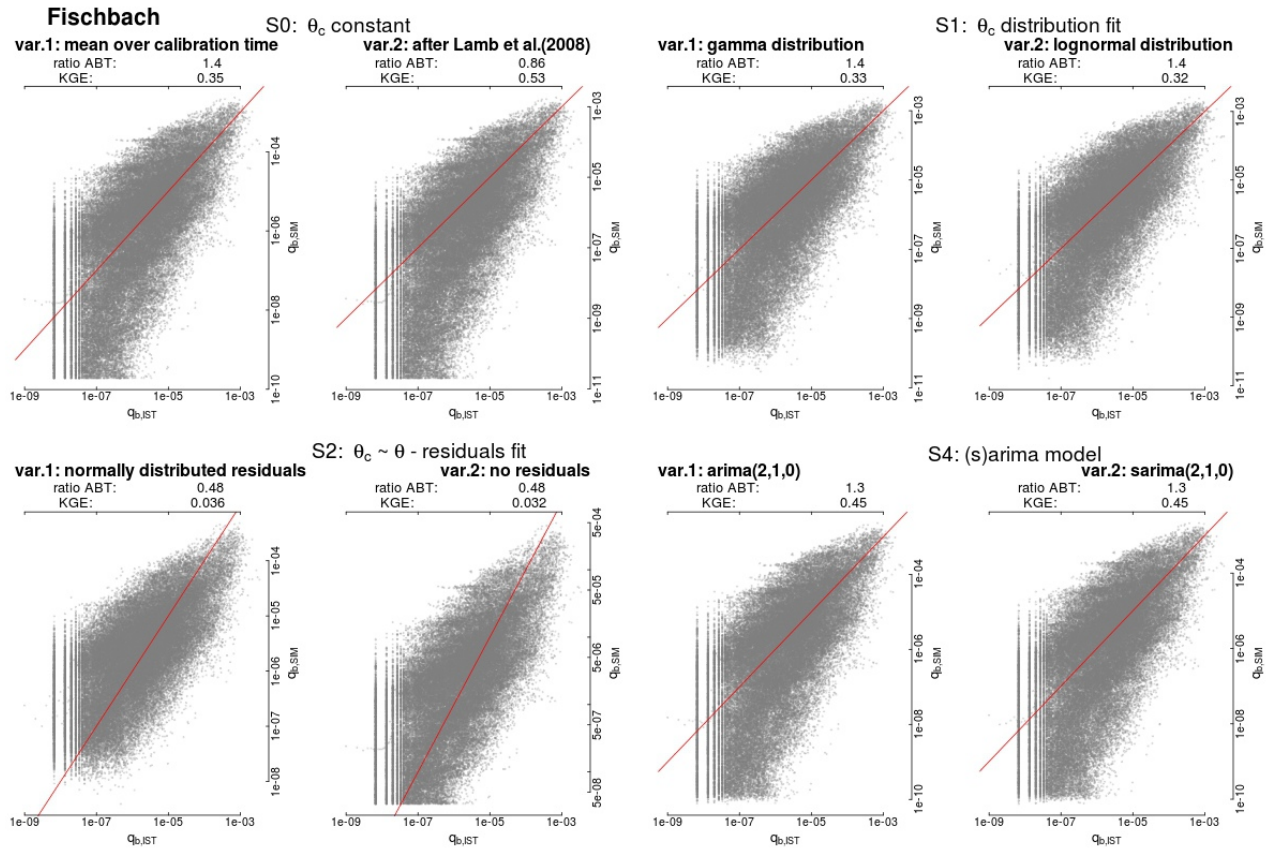
- Rickenmann, D. (1991). Hyperconcentrated Flow and Sediment Transport at Steep Slopes. *Journal of Hydraulic Engineering*, 117(11), 1419–1439.
[http://doi.org/10.1061/\(ASCE\)0733-9429\(1991\)117:11\(1419\)](http://doi.org/10.1061/(ASCE)0733-9429(1991)117:11(1419))
- Rickenmann, D. (1996). Fließgeschwindigkeit in Wildbächen und Gebirgsflüssen, 88(11/12), 298–304.
- Rickenmann, D. (2001). Comparison of bed load transport in torrents and gravel bed streams. *Water Resources Research*, 37(12), 3295–3305.
<http://doi.org/10.1029/2001WR000319>
- Rickenmann, D. (2013). *Methoden zur quantitativen Beurteilung von Gerinneprozessen in Wildbächen* (Vol. 9). Birmensdorf: WSL. Retrieved from www.wsl.ch/publikationen/pdf/13549.pdf
- Rickenmann, D. (2014, July 7). Geophon-Eichmessungen der TIWAG für die Periode 2008 - 2013: Analyse der Eichmessungen und Berechnungen zum Geschiebetransport. unpublished.
- Rickenmann, D., & Recking, A. (2011). Evaluation of flow resistance in gravel-bed rivers through a large field data set: EVALUATION OF FLOW RESISTANCE EQUATIONS. *Water Resources Research*, 47(7), n/a–n/a.
<http://doi.org/10.1029/2010WR009793>
- Rickenmann, D., Turowski, J. M., Fritschi, B., Wyss, C., Laronne, J., Barzilai, R., ... Habersack, H. (2014). Bedload transport measurements with impact plate geophones: comparison of sensor calibration in different gravel-bed streams. *Earth Surface Processes and Landforms*, n/a–n/a. <http://doi.org/10.1002/esp.3499>
- Schmelter, M. L., Hooten, M. B., & Stevens, D. K. (2011). Bayesian sediment transport model for unisize bed load: UNISIZE BAYESIAN SEDIMENT TRANSPORT MODEL. *Water Resources Research*, 47(11), n/a–n/a.
<http://doi.org/10.1029/2011WR010754>
- Shields, A. F. (1936). Anwendung der Ähnlichkeitsmechanik und der Turbulenzforschung auf die Geschiebebewegung. *Mitteilungen Der Preussischen Versuchsanstalt Für Wasserbau Und Schiffbau*, 26.
- Smart, G. M., & Jäggi, M. N. R. (1983). *Sedimenttransport in steilen Gerinnen* (Vol. 64). Zürich: ETH Zürich.
- Strickler, A. (1923). *Beiträge zur Frage der Geschwindigkeitsformel und der Rauheitszahlen für Ströme, Kanäle und geschlossene Leitungen* (No. 16). Bern: Sekretariat des Eidg. Amtes für Wasserwirtschaft.
- Turowski, J. M. (2010). Probability distributions of bed load transport rates: A new derivation and comparison with field data: PROBABILITY DISTRIBUTIONS OF BEDLOAD TRANSPORT. *Water Resources Research*, 46(8), n/a–n/a.
<http://doi.org/10.1029/2009WR008488>

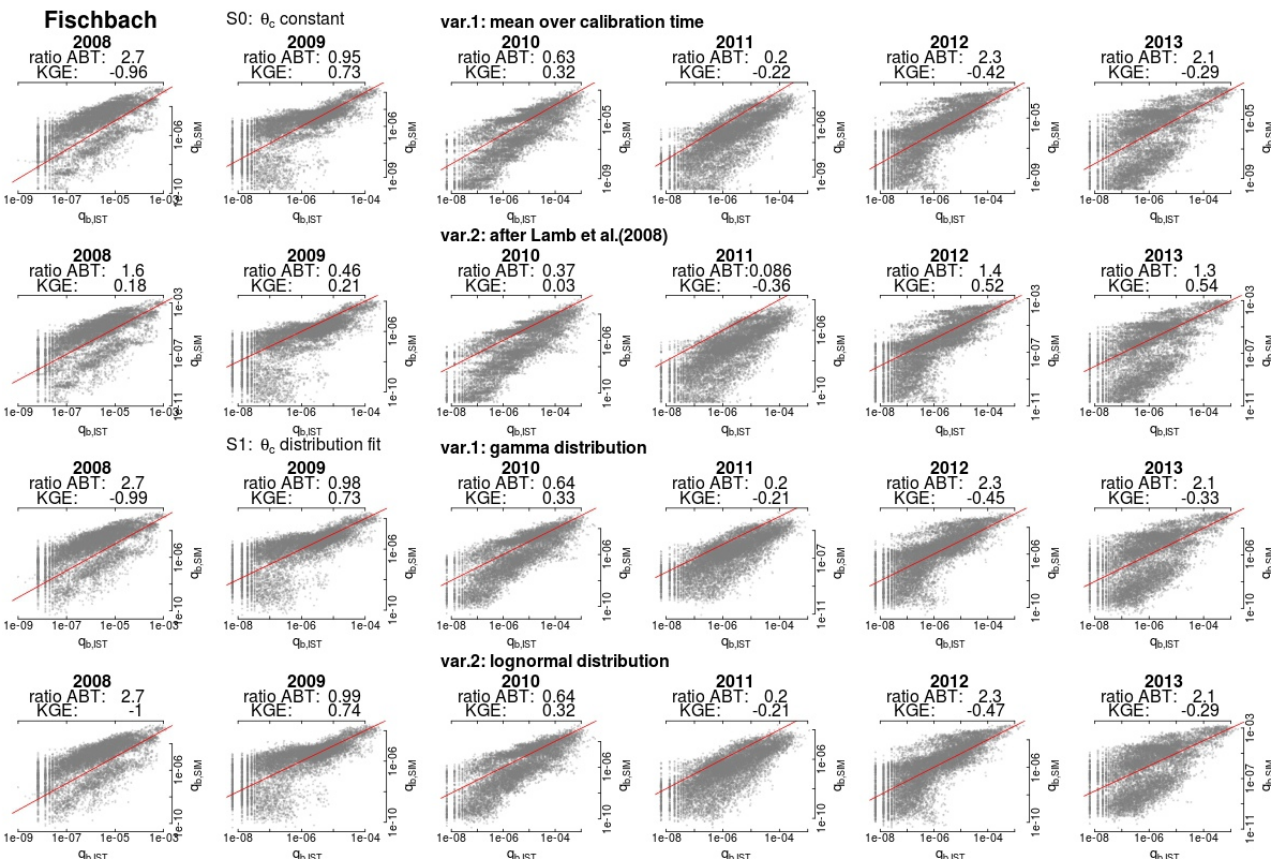
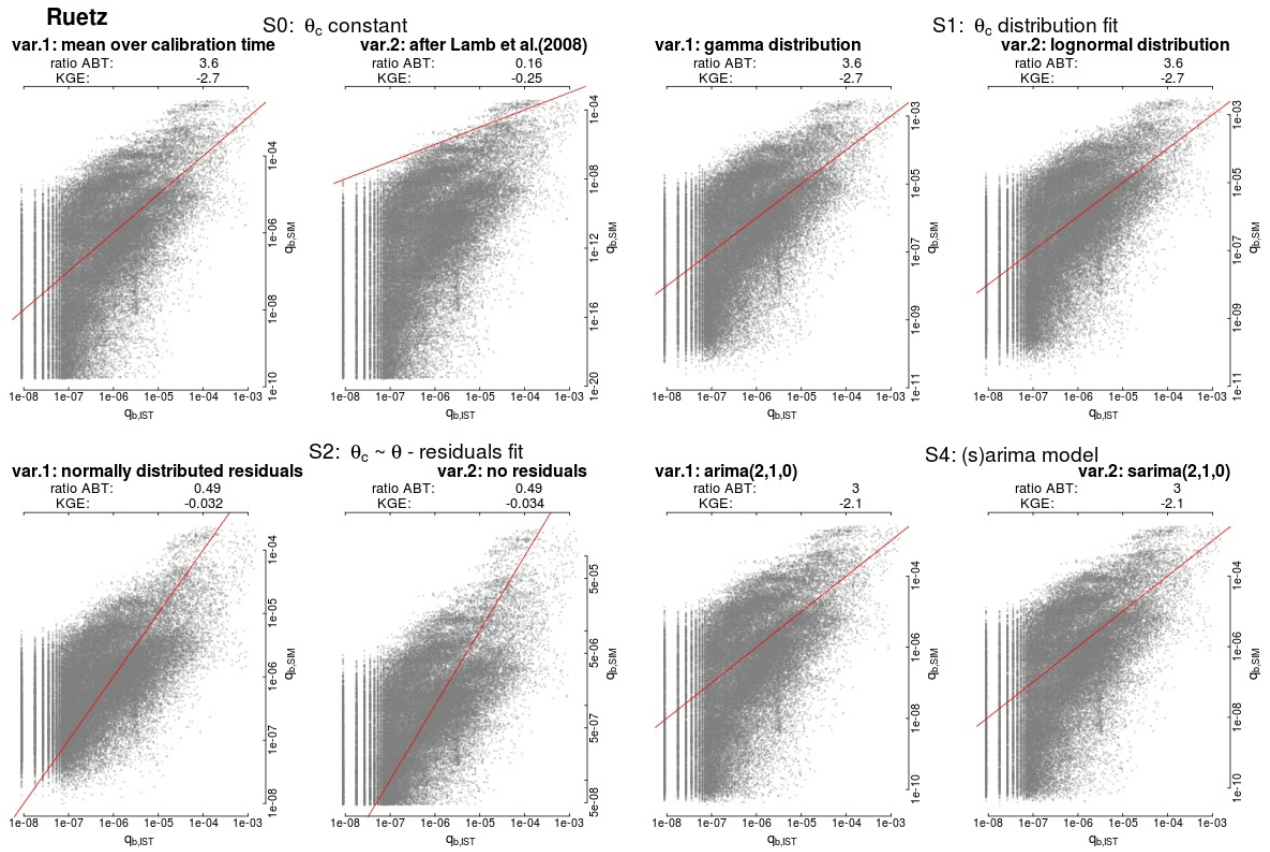
- Turowski, J. M., Badoux, A., & Rickenmann, D. (2011). Start and end of bedload transport in gravel-bed streams: START AND END OF BEDLOAD TRANSPORT. *Geophysical Research Letters*, 38(4), n/a–n/a.
<http://doi.org/10.1029/2010GL046558>
- Turowski, J. M., & Rickenmann, D. (2010). Measuring the Statistics of Bed-Load Transport Using Indirect Sensors. *Journal of Hydraulic Engineering*, 137(1), 116–121.
- Viollet, P.-L. (2012). *Water Engineering in Ancient Civilizations: 5,000 Years of History (IAHR Monographs)*. Boca Raton, USA: CRC Press.
- Viviroli, D., Zappa, M., Gurtz, J., & Weingartner, R. (2009). An introduction to the hydrological modelling system PREVAH and its pre- and post-processing-tools. *Environmental Modelling & Software*, 24(10), 1209–1222.
<http://doi.org/10.1016/j.envsoft.2009.04.001>
- Wilcock, P. R., & Crowe, J. C. (2003). Surface-based Transport Model for Mixed-Size Sediment. *Journal of Hydraulic Engineering*, 129(2), 120–128.
[http://doi.org/10.1061/\(ASCE\)0733-9429\(2003\)129:2\(120\)](http://doi.org/10.1061/(ASCE)0733-9429(2003)129:2(120))
- Wong, M., & Parker, G. (2006). Reanalysis and Correction of Bed-Load Relation of Meyer-Peter and Müller Using Their Own Database. *Journal of Hydraulic Engineering*, 132(11), 1159–1168. [http://doi.org/10.1061/\(ASCE\)0733-9429\(2006\)132:11\(1159\)](http://doi.org/10.1061/(ASCE)0733-9429(2006)132:11(1159))
- Yochum, S. E., Bledsoe, B. P., David, G. C. L., & Wohl, E. (2012). Velocity prediction in high-gradient channels. *Journal of Hydrology*, 424-425, 84–98.
<http://doi.org/10.1016/j.jhydrol.2011.12.031>
- Zambrano-Bigiarini, M. (2014). hydroGOF: Goodness-of-fit functions for comparison of simulated and observed hydrological time series. R package version 0.3-8.

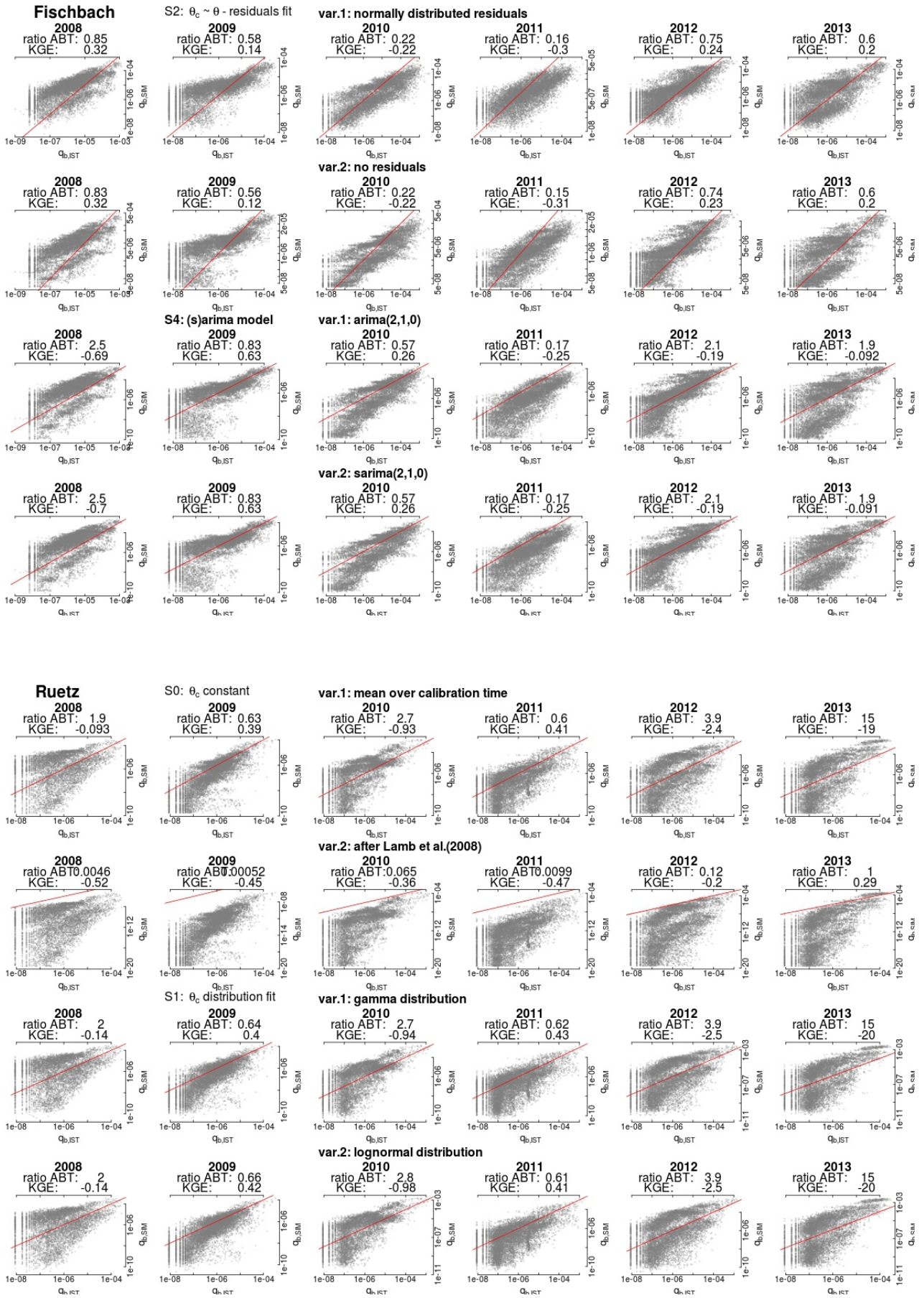
Appendix A

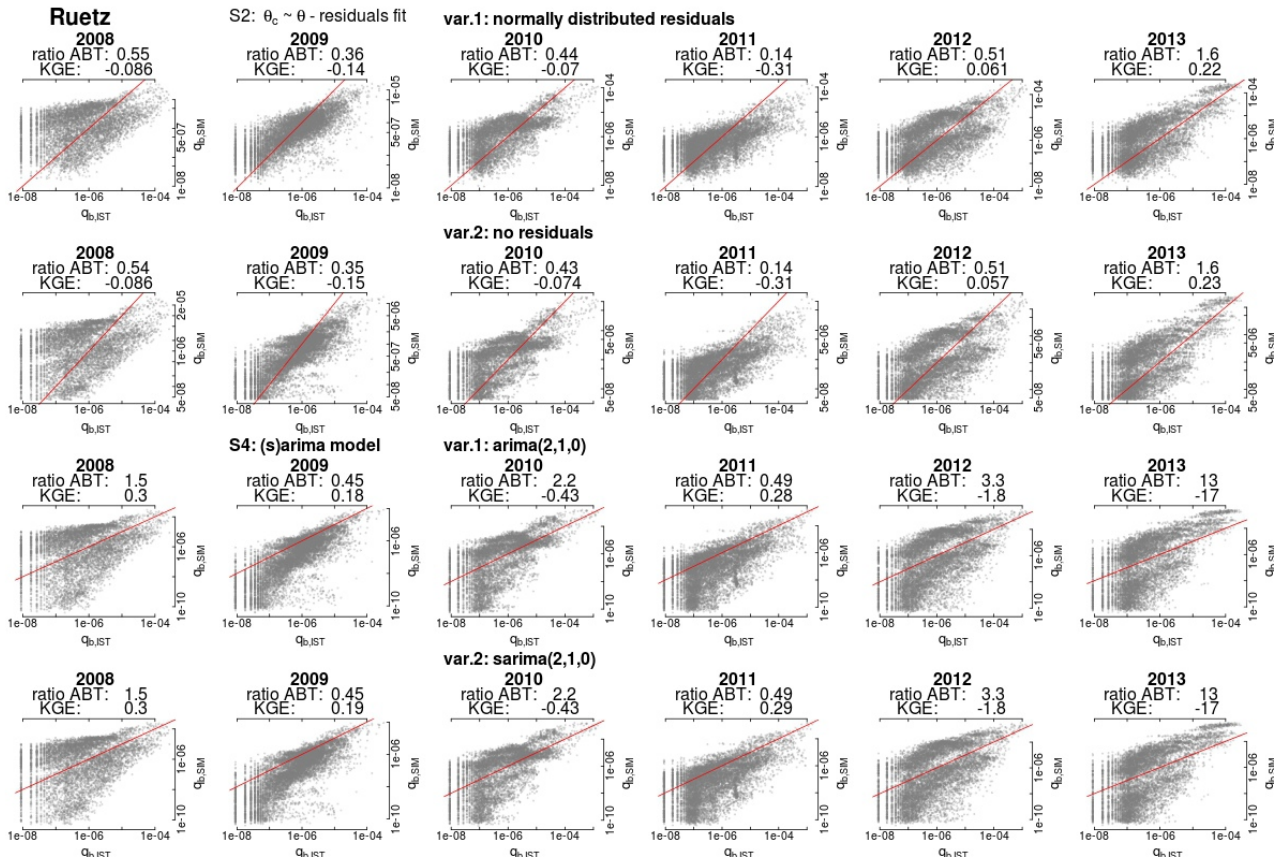
1 Scatter plots

The following charts show a comparison of simulated bedload transport rates with their corresponding observed values in scatter plots. To begin with, all computed data pairs are given for each variant and stream. Further below, the same visualization is can be found for each year.



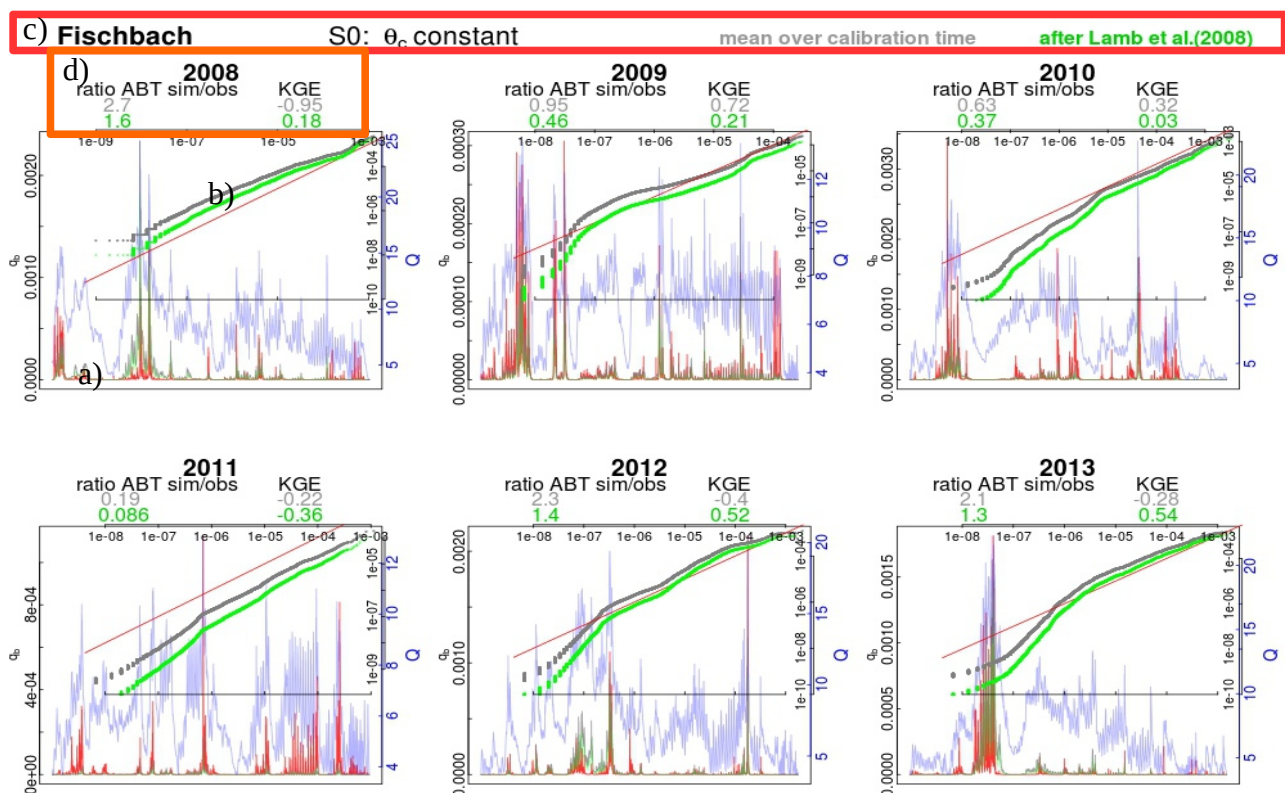






2 Time series and qq-plots

On the following pages, the results of the punctual bedload transport simulation (described in 4.2.4) are visualized. Therein, a separate plot for each year is included which contains the time series of discharge, observed as well as simulated bedload transport in two variants. In the overall headline of the composed chart, the simulation setups are notated shortly while every yearly window is titled by the year and the two evaluated efficiency criteria. The x-axis of the time series plots is not labeled because only the time steps of phase 2 are contained. Hence, the time lines are incomplete. Generally, they start somewhere in the end of April or begin of May and are nearly continuous until October.



a) Time series:

- red observed bedload transport
- gray, green ... simulated BT, var1 u 2
- blue observed Discharge

b) qq-plots:

- gray, green ... simulated BT, var1 u 2
- red ... 1:1 line (=perfect match)

c) overall head line: notation of used simulation setups

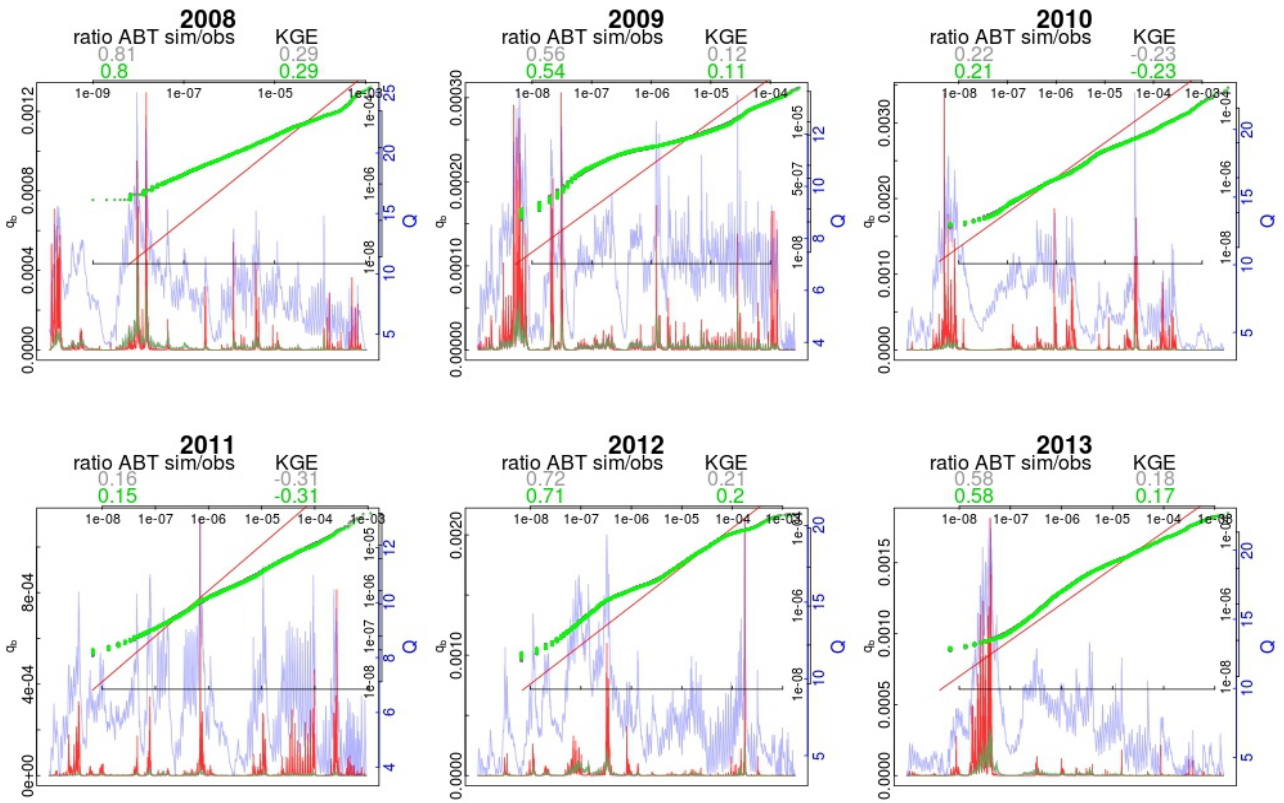
d) head lines of yearly windows: efficiency criteria, colors corresponding to above

Fischbach

S2: $\theta_c \sim \theta$ - residuals fit

normally distributed residuals

no residuals

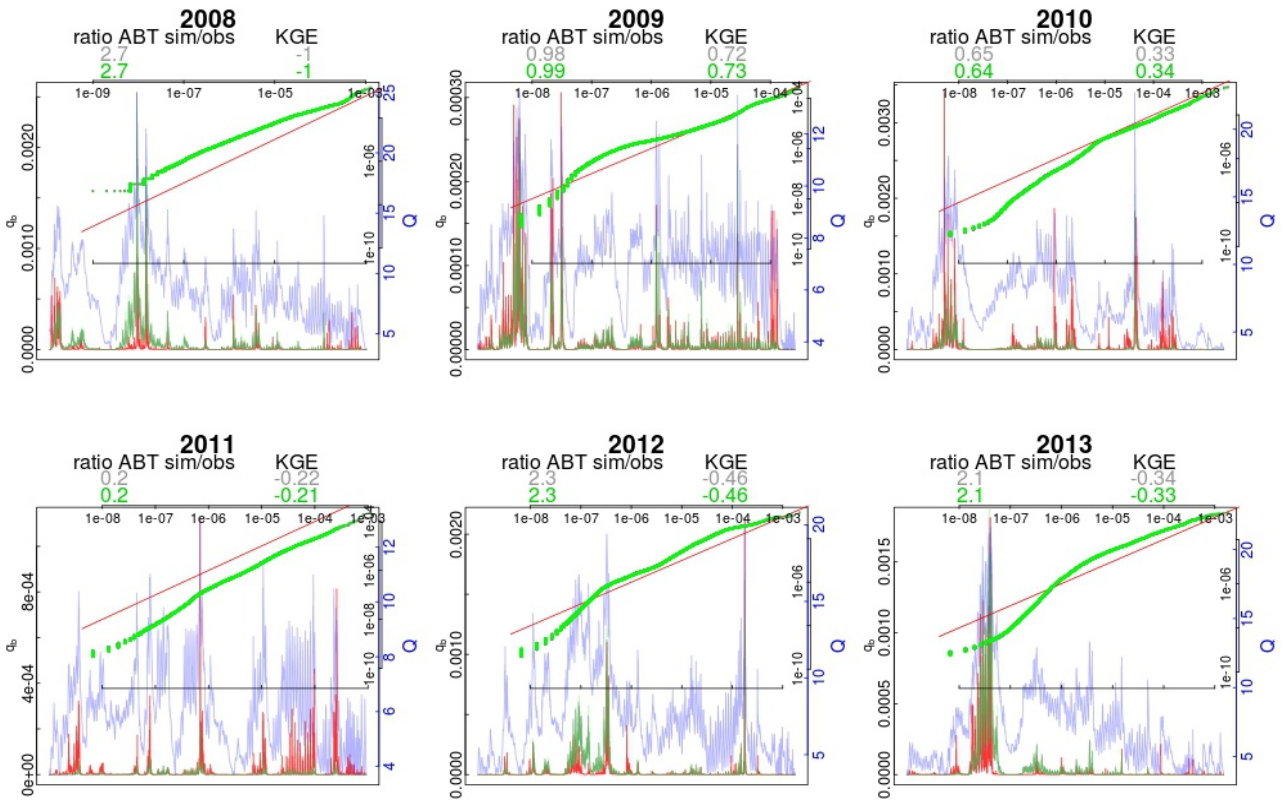


Fischbach

S1: θ_c distribution fit

gamma distribution

lognormal distribution

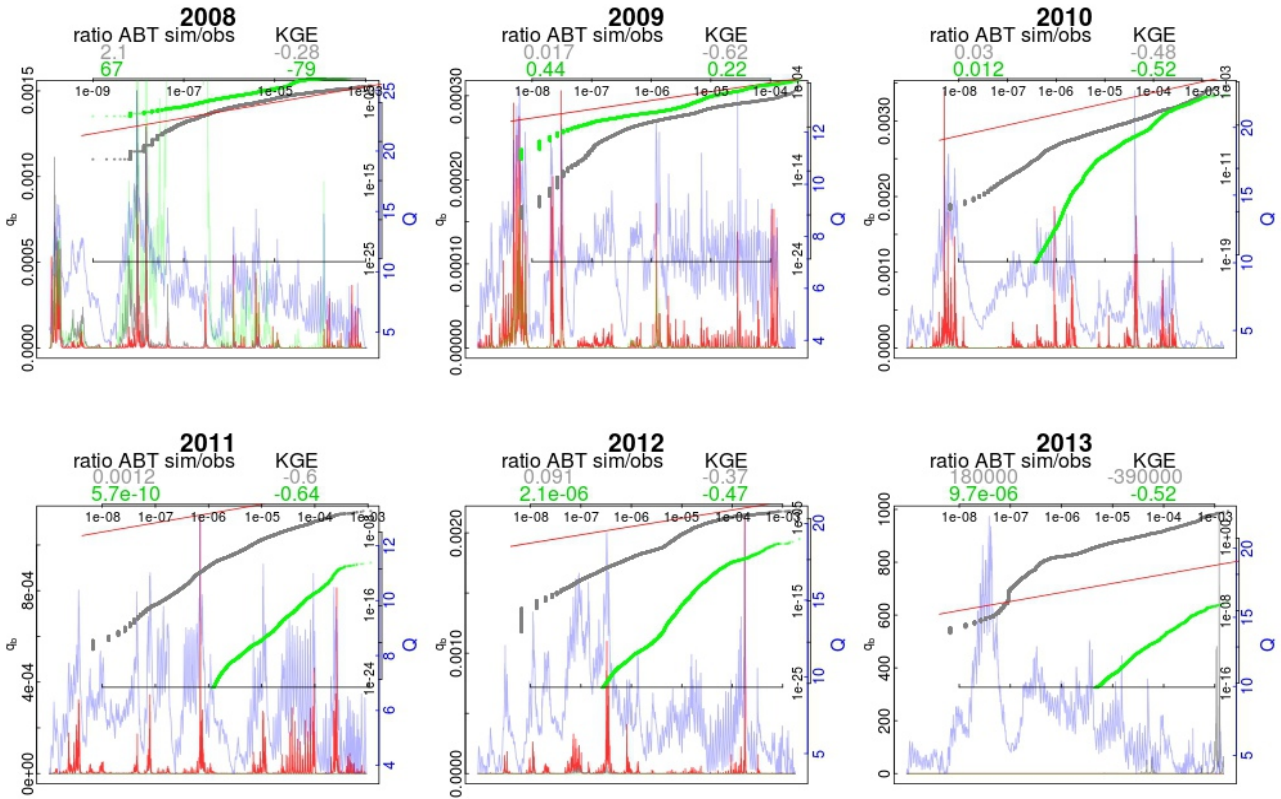


Fischbach

S3: θ_c differences fit

normally distributed differences

logistic distribution

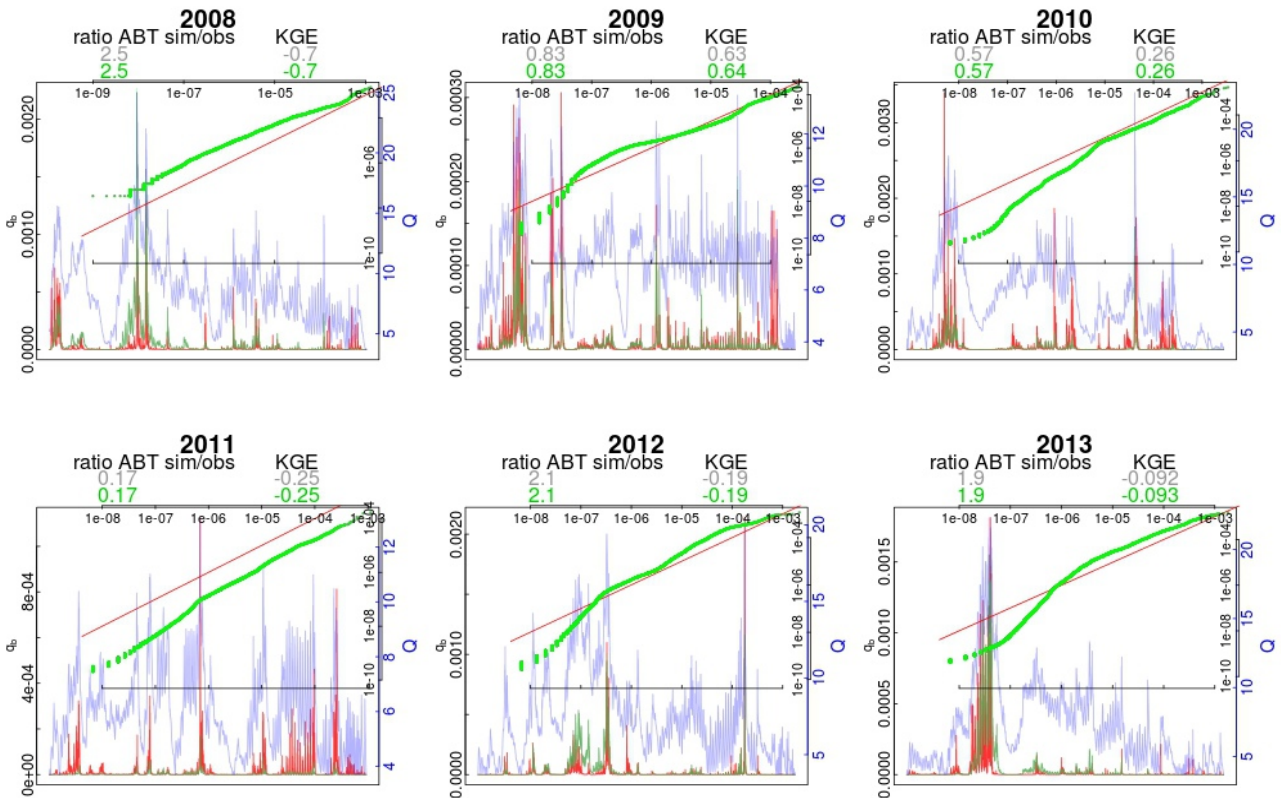


Fischbach

S4: (s)arima model

arima(2,1,0)

sarima(2,1,0)

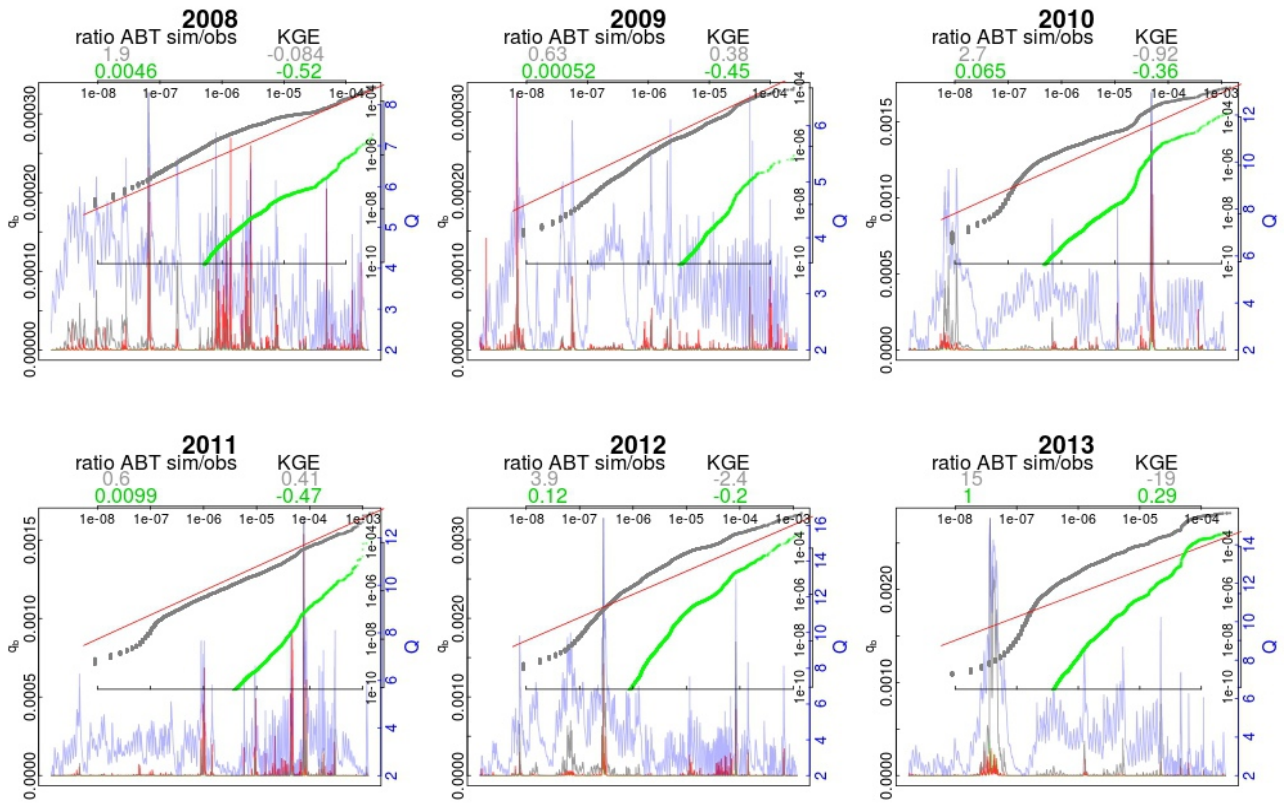


Ruetz

S0: θ_c constant

mean over calibration time

after Lamb et al.(2008)

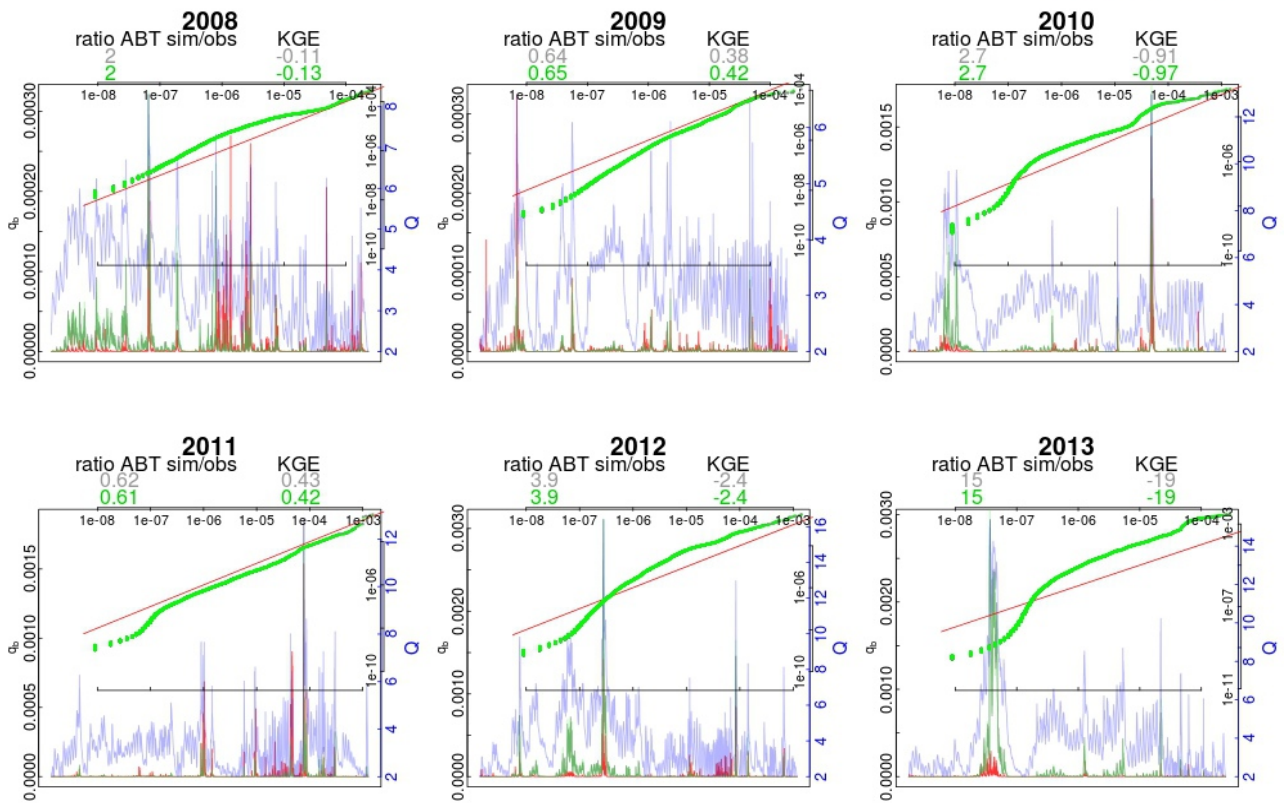


Ruetz

S1: θ_c distribution fit

gamma distribution

lognormal distribution

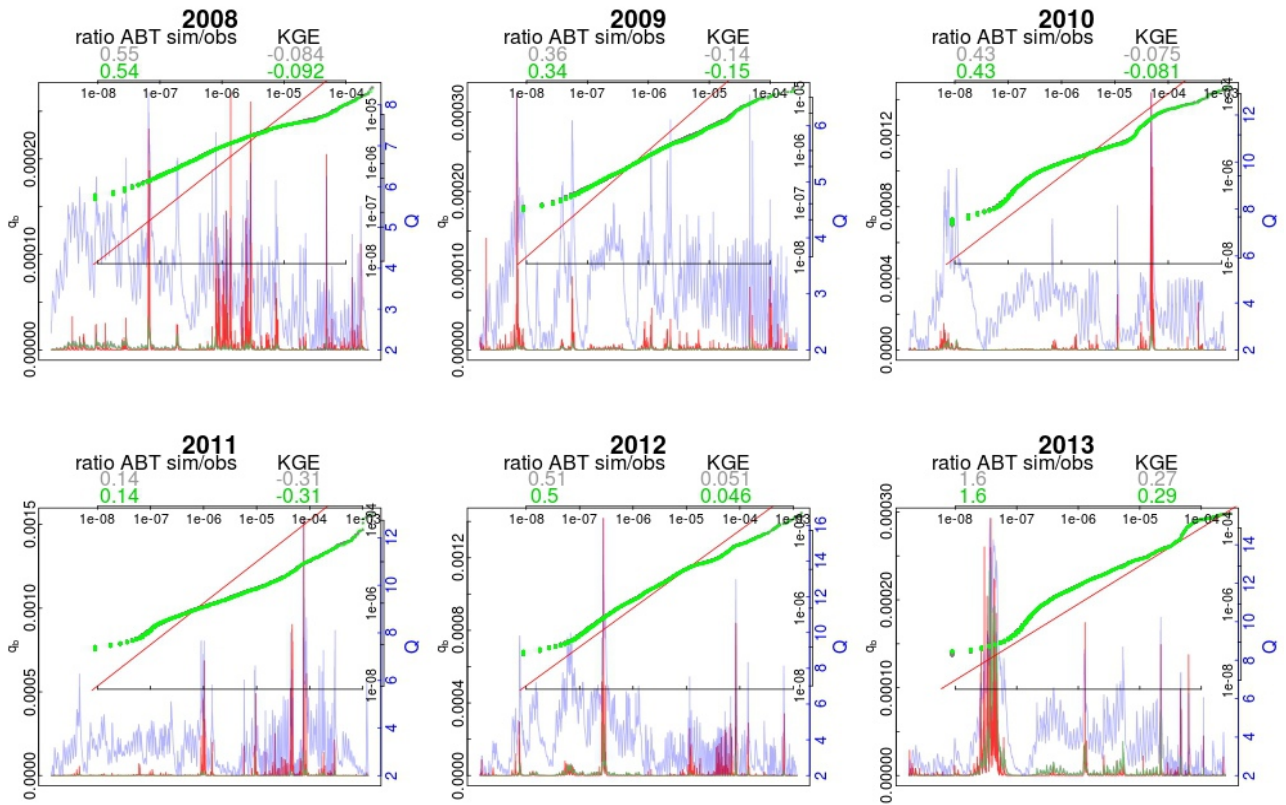


Ruetz

S2: $\theta_c \sim \theta$ - residuals fit

normally distributed residuals

no residuals

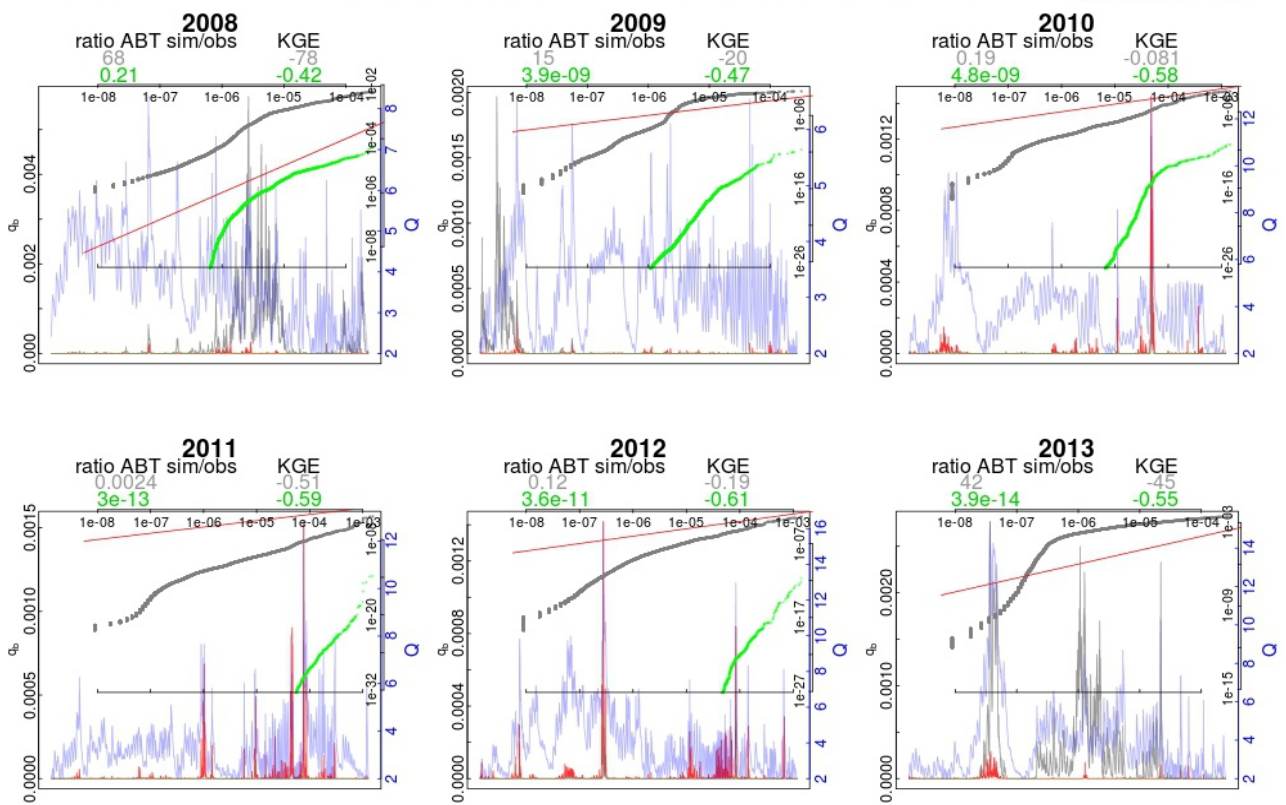


Ruetz

S3: θ_c differences fit

normally distributed differences

logistic distribution

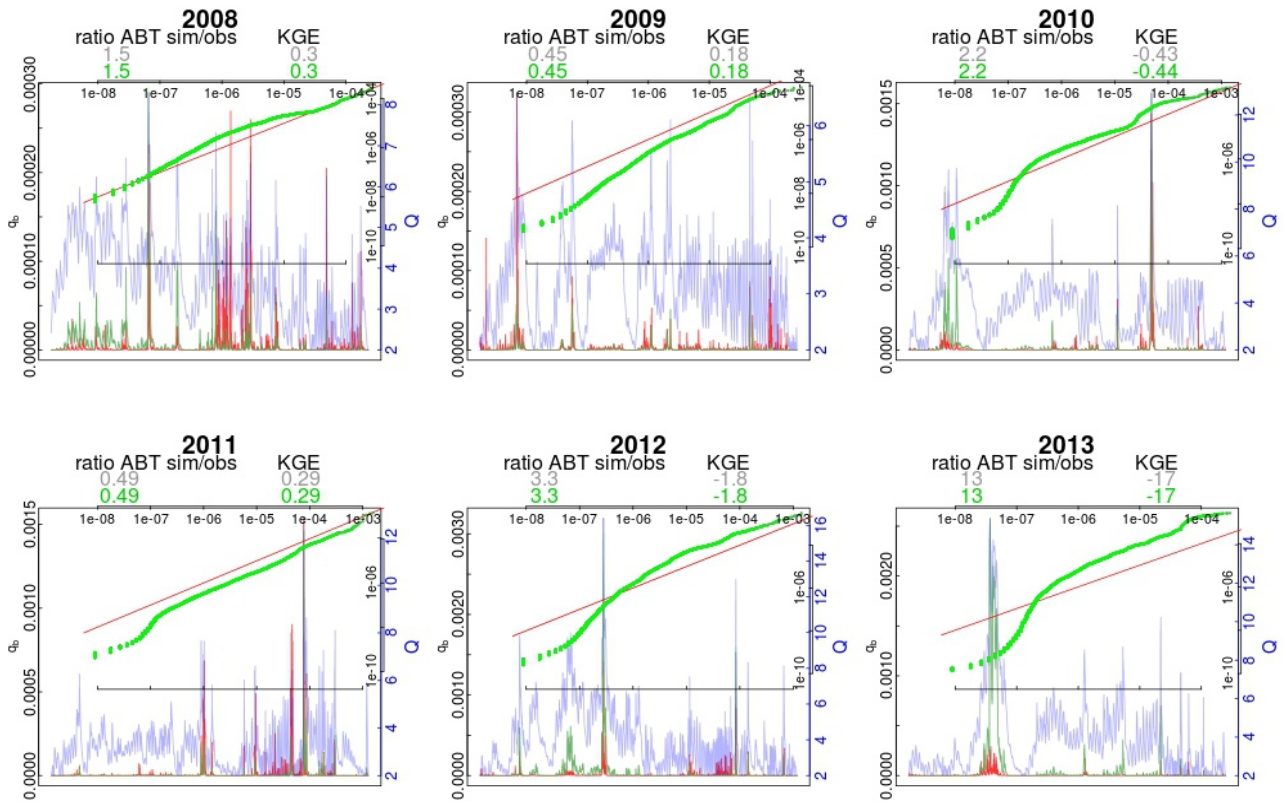


Ruetz

S4: (s)arima model

arima(2,1,0)

sarima(2,1,0)



Appendix B

1 Hysteresis

The following visualizations about hysteresis effects show the dimensionless bedload transport rate Φ_b plotted against dimensionless shear stress θ . Values taken while discharge rises are given in red, while discharge falls in black. In the figures B1 to B4, the lines result from a fit of the cheng-equation with variable θ_c for each day and hydrograph direction separately. The line type varies with the date, the dates are chosen randomly without any intent.

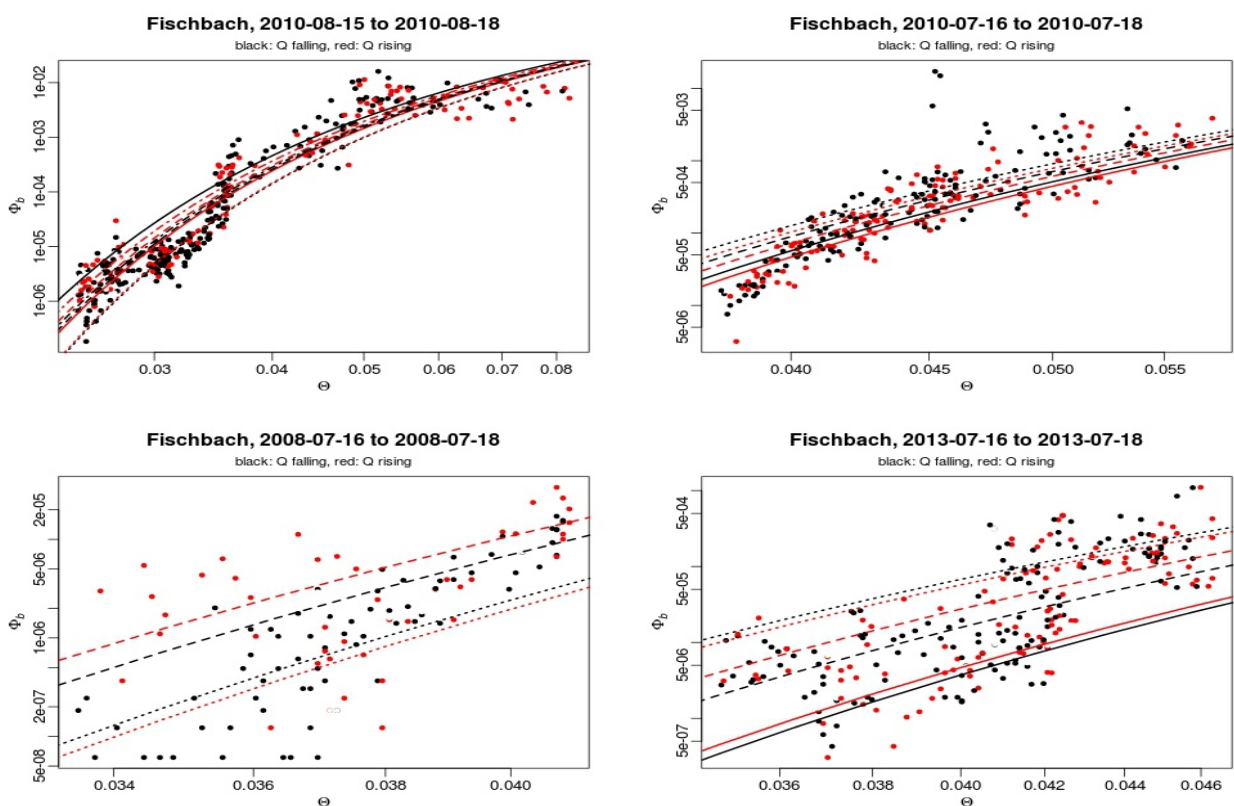


Fig. B1

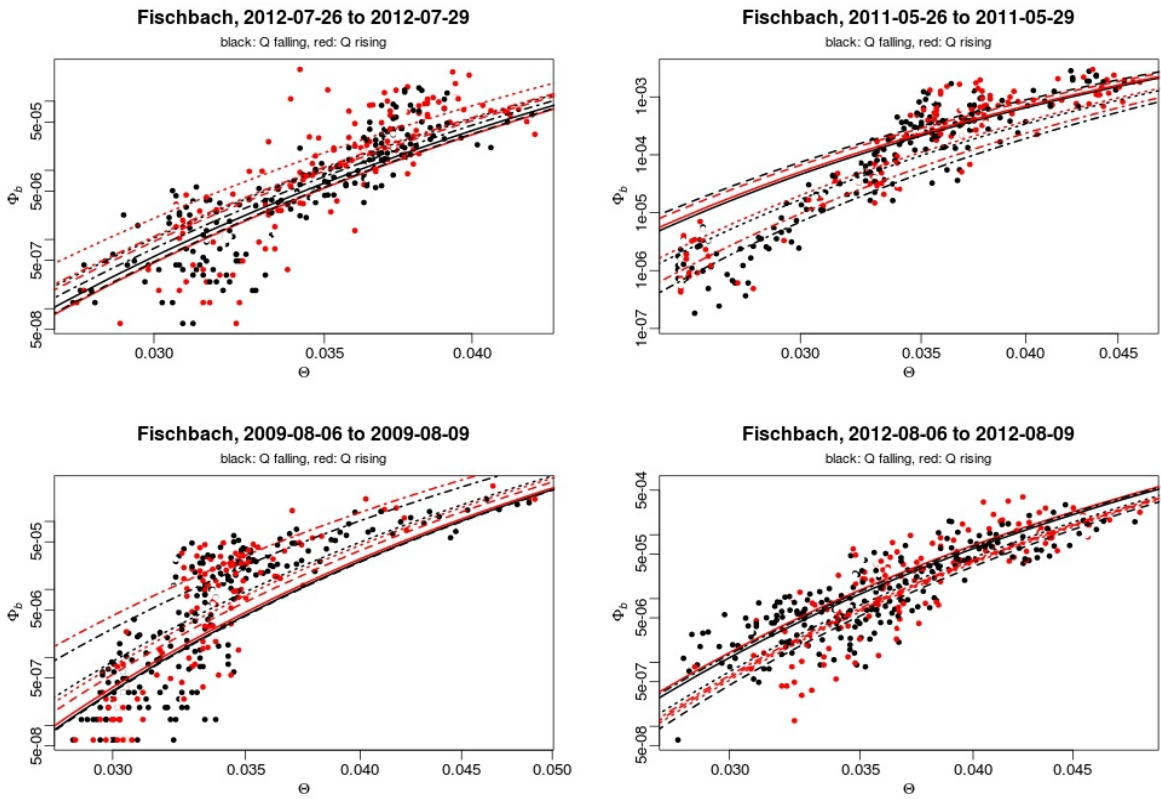


Fig. B2

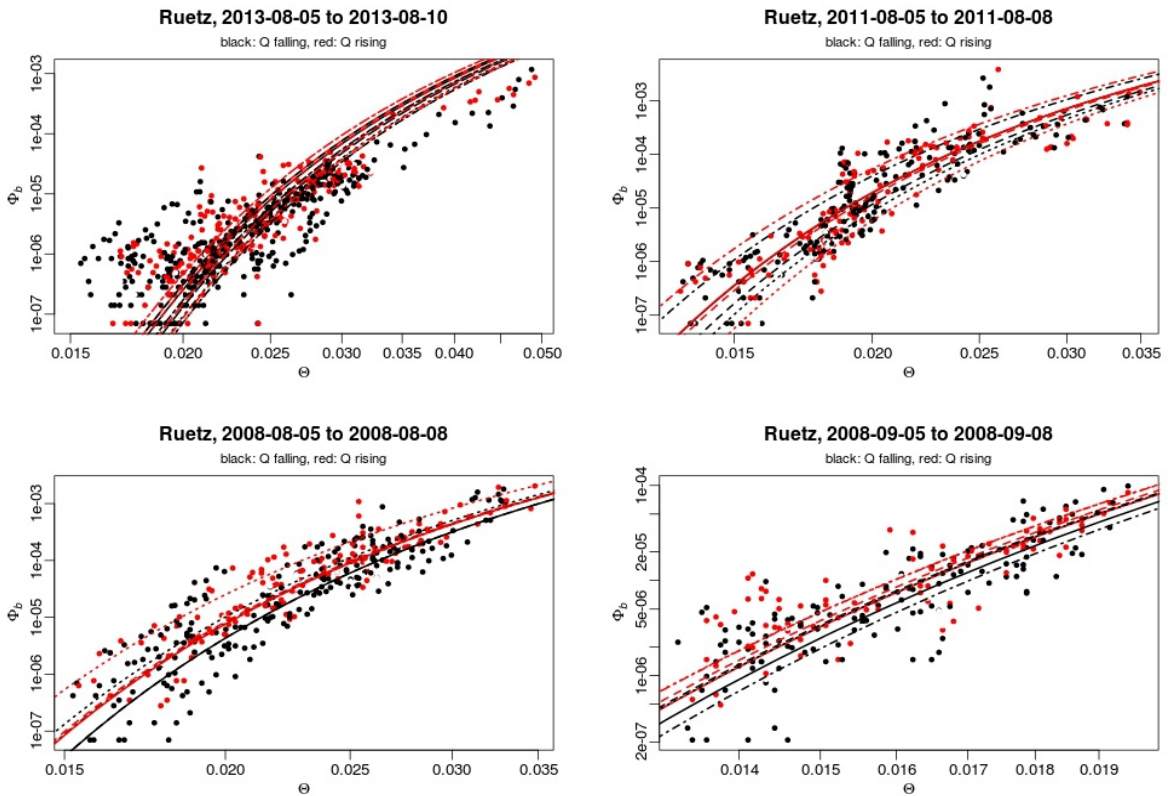


Fig. B3

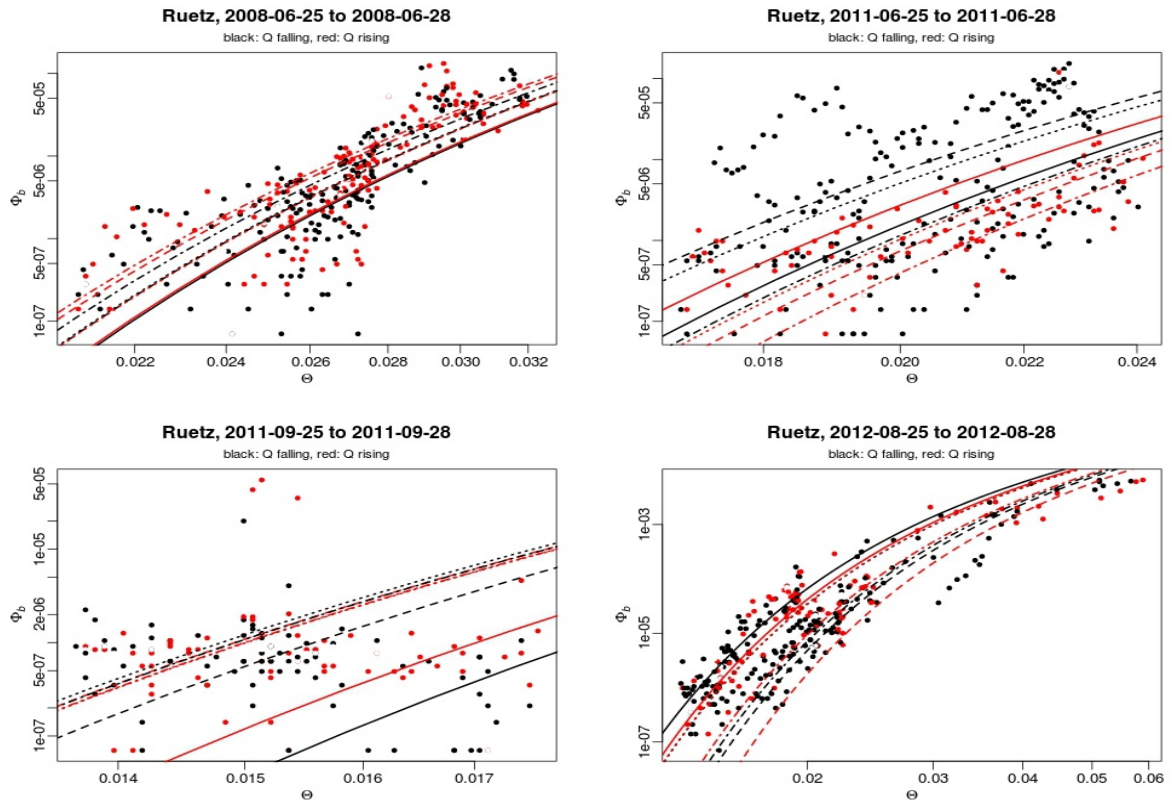


Fig. B4

For the following figures B5 – B8 the values of Φ_b and θ were normalized by their particular daily maximum. Thus, the values should be better comparable over a longer time period than before as they all head to 1 as the maximum. The bold, solid line results from a regression in the form $\log(y) \sim x$ for each hydrograph limb, the finer, dotted lines represent the 95%-prediction intervals. That means, 95% of future observations will be inside of this range.

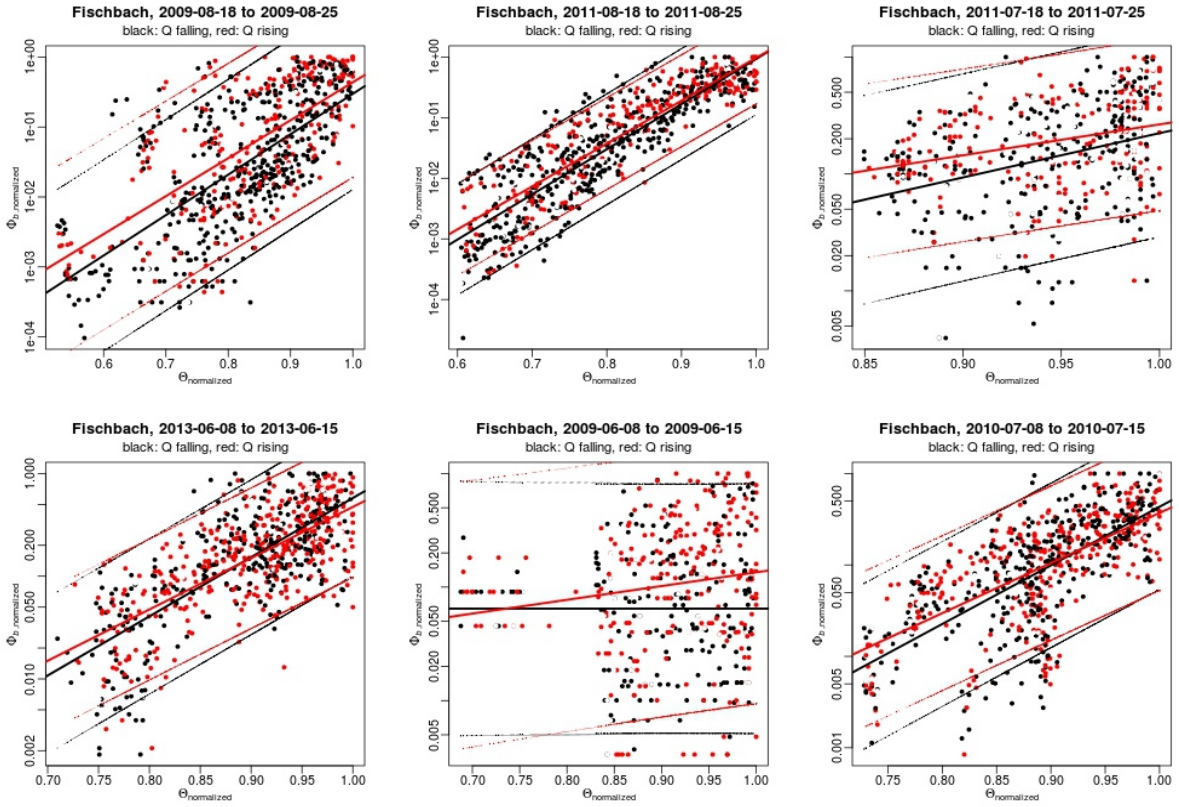


Fig. B5

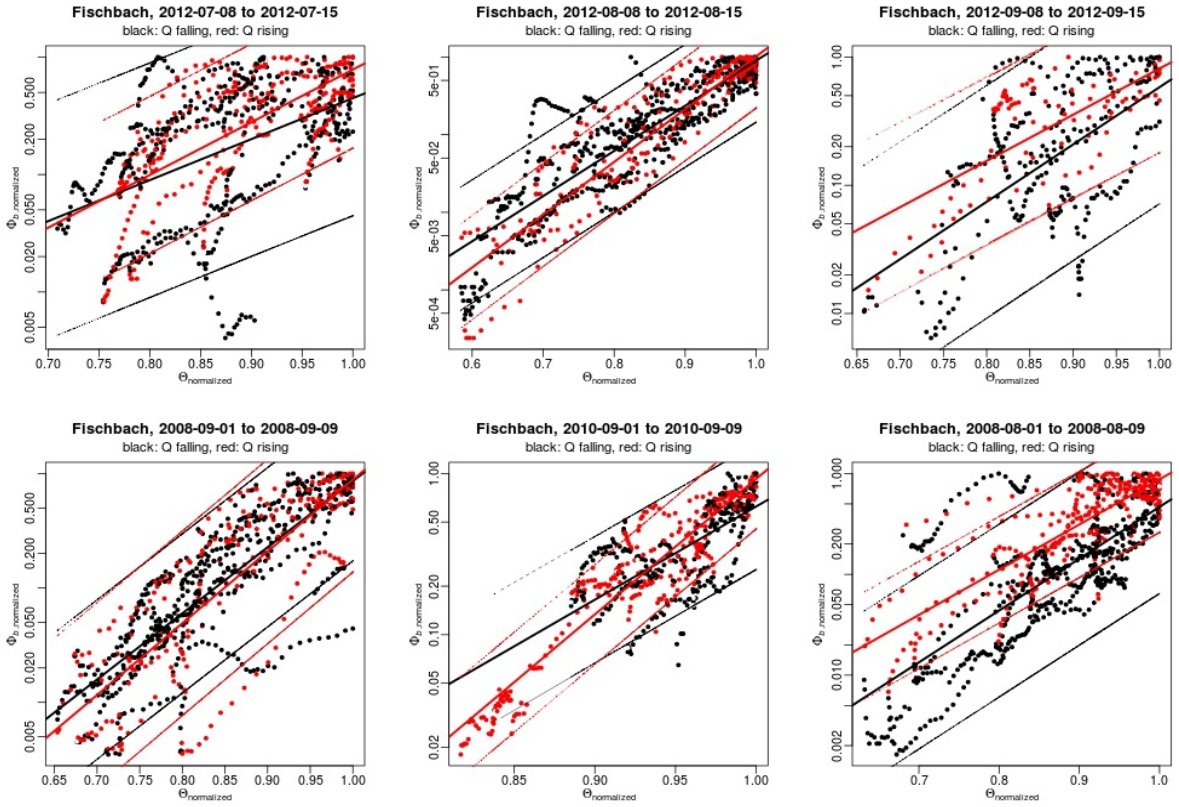


Fig. B6

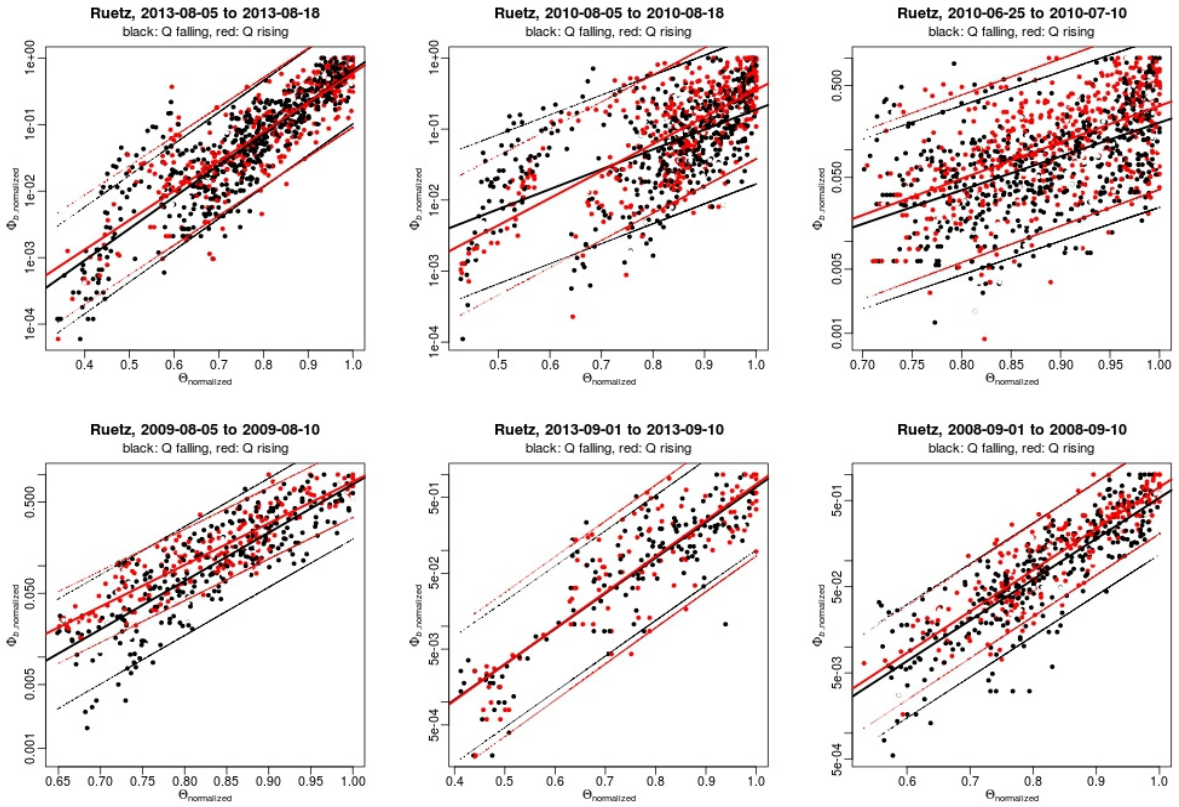


Fig. B7

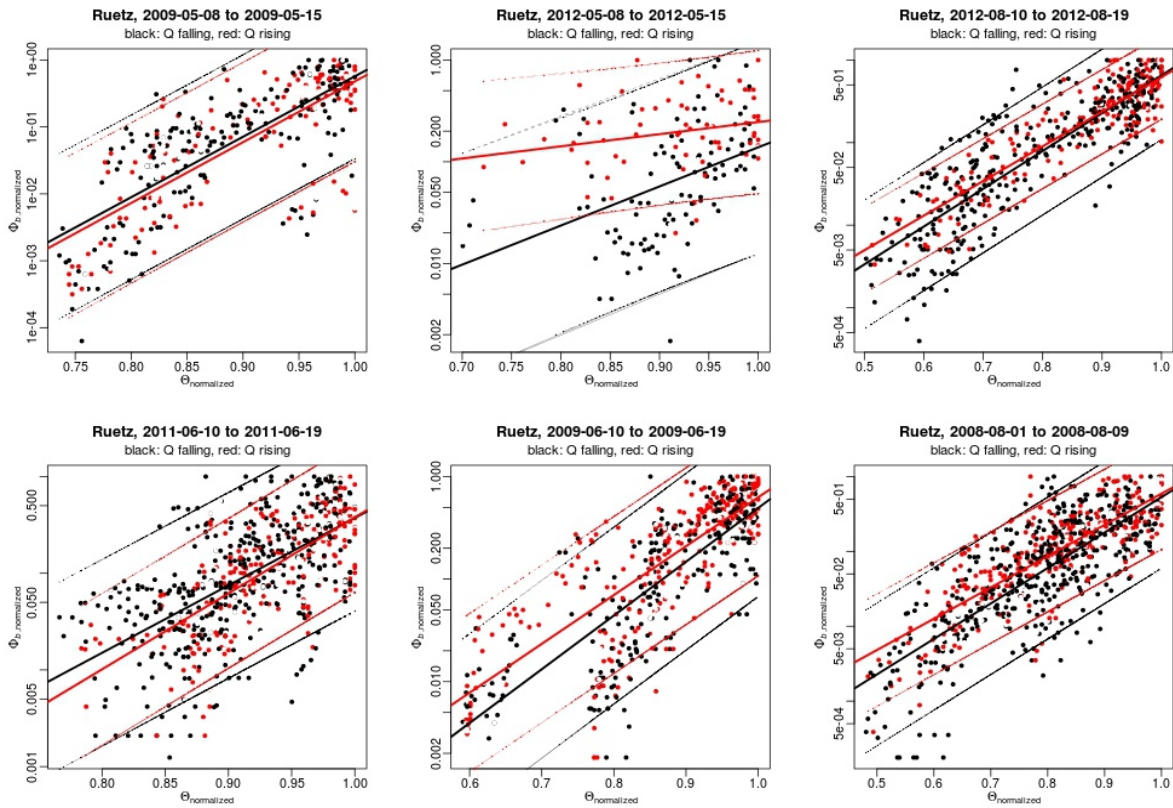


Fig. B8

2 Selected visualizations of time series

Here, the back-calculated θ -values for each time step are presented together with the time series for discharge Q and bedload transport rate q_b . Again, the time frames are chosen randomly.

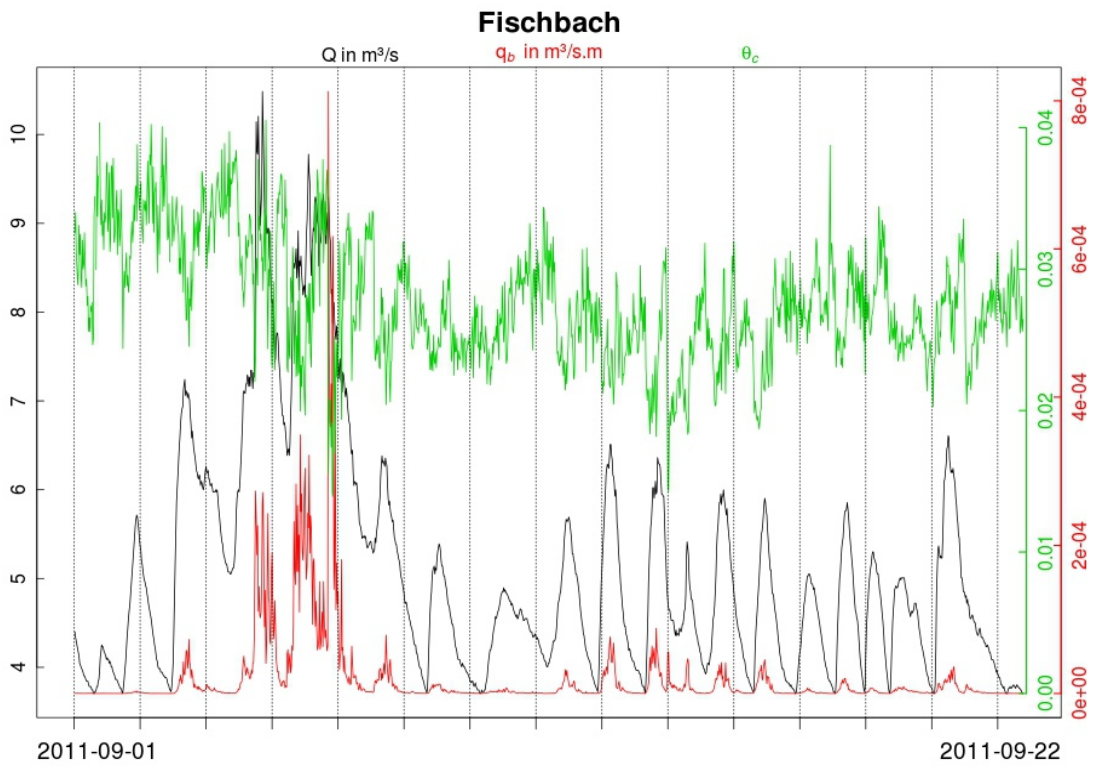


Fig. B9

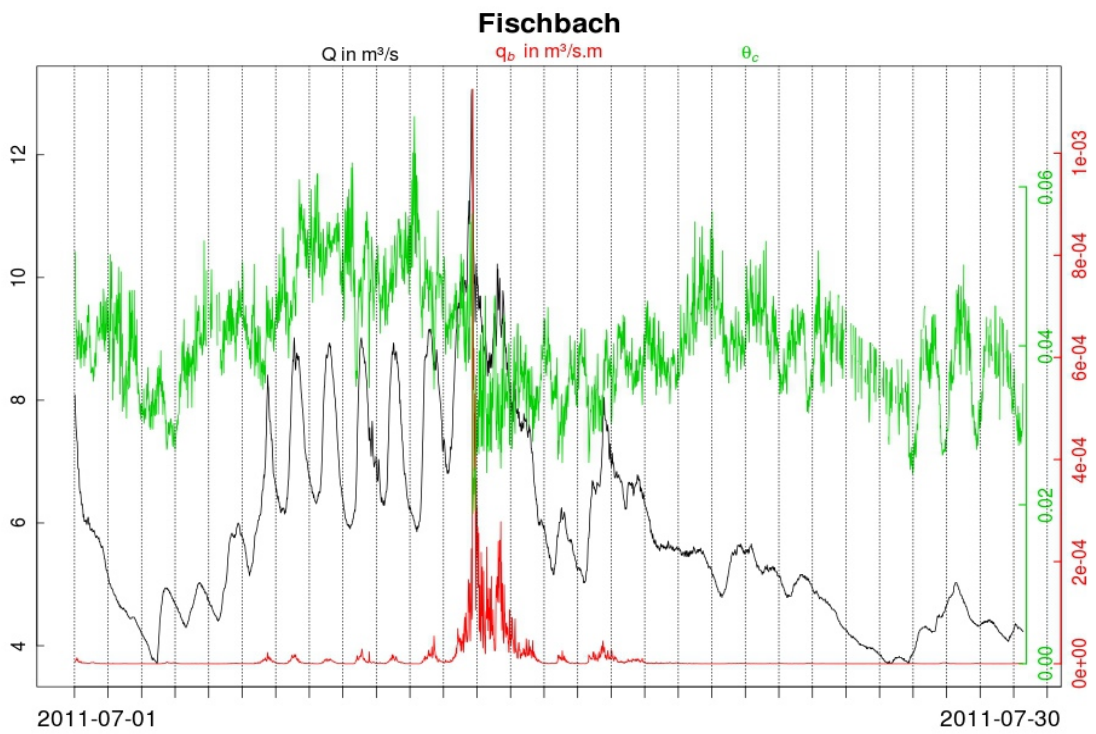


Fig. B10

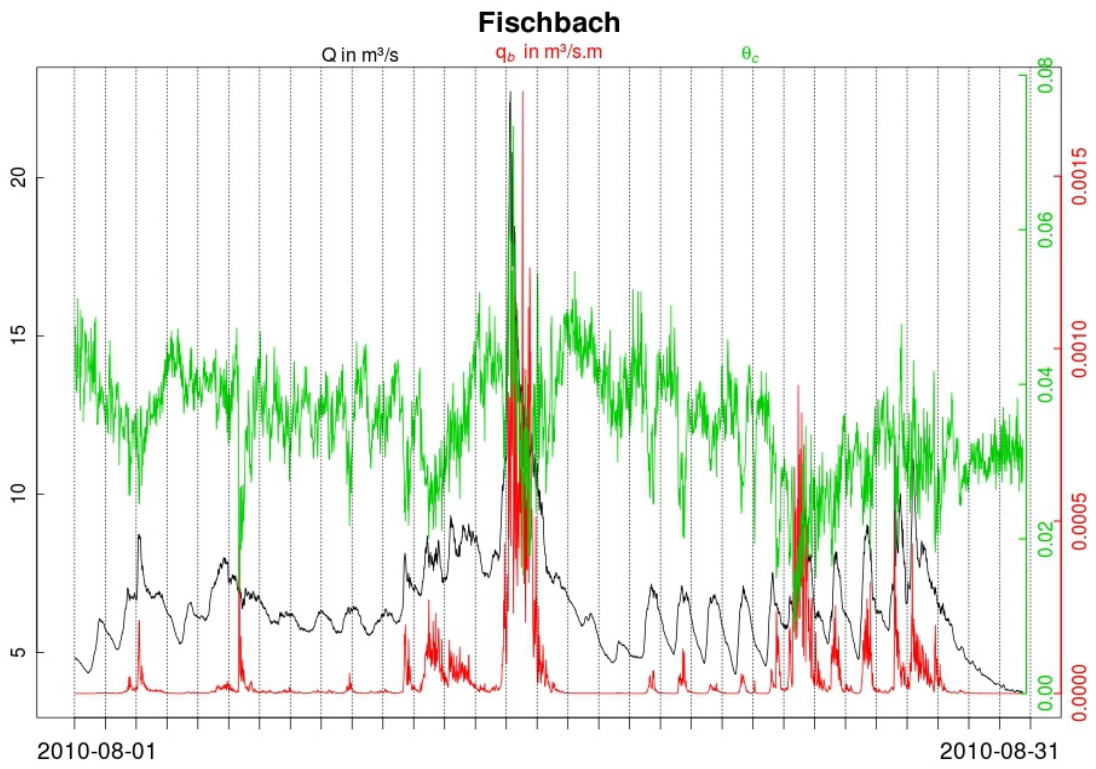


Fig. B11

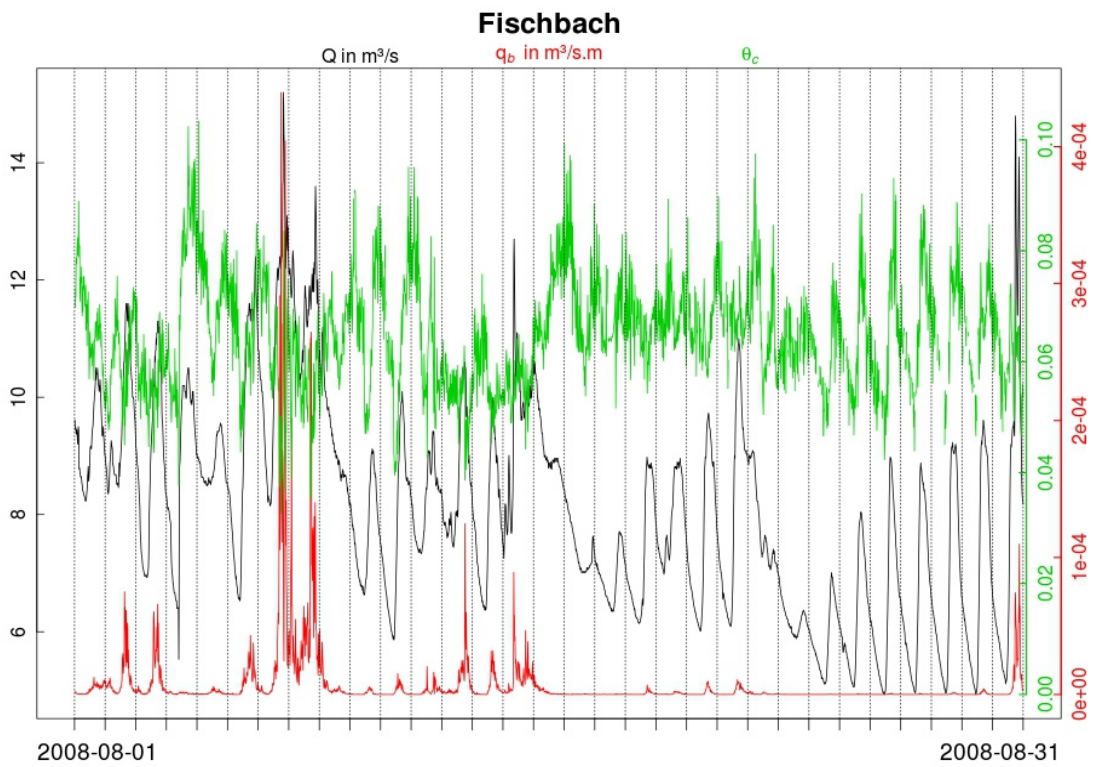


Fig. B12

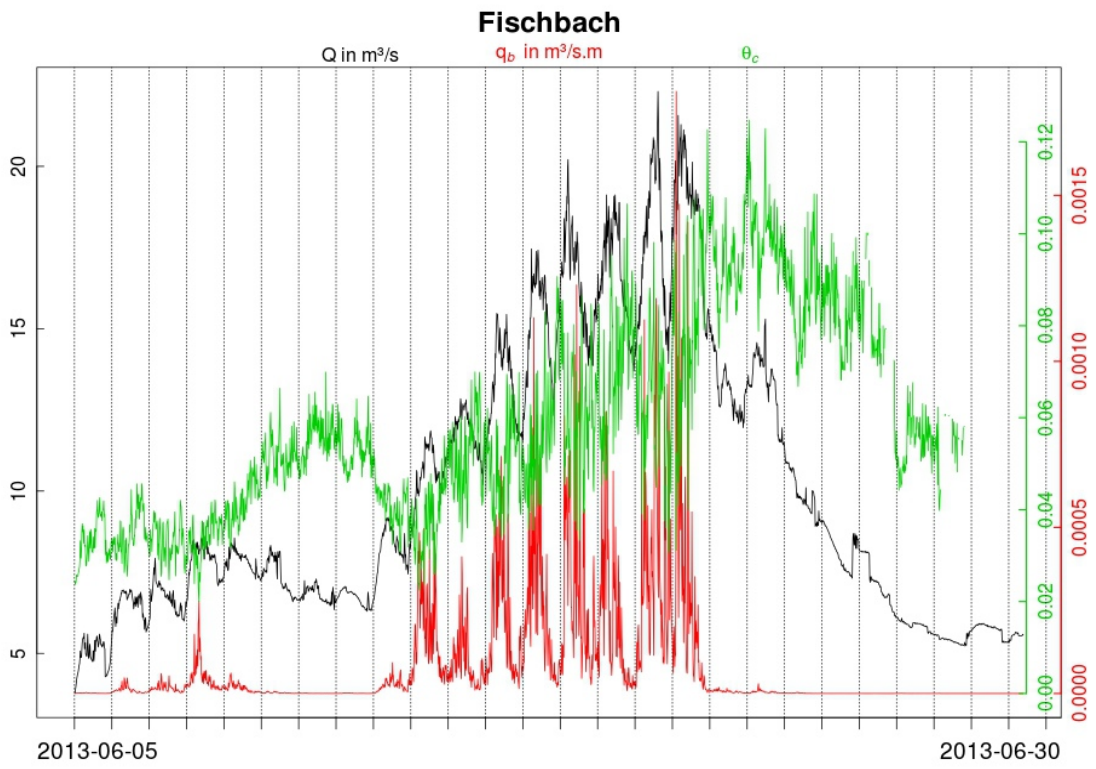


Fig. B13

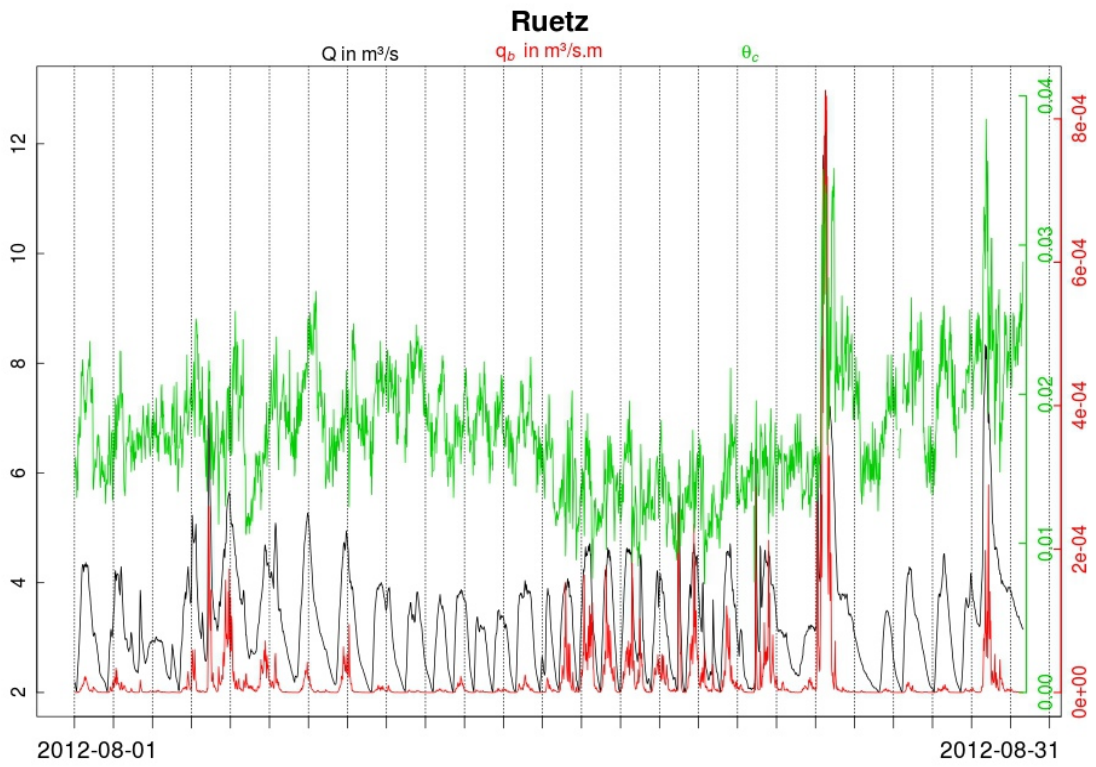


Fig. B14

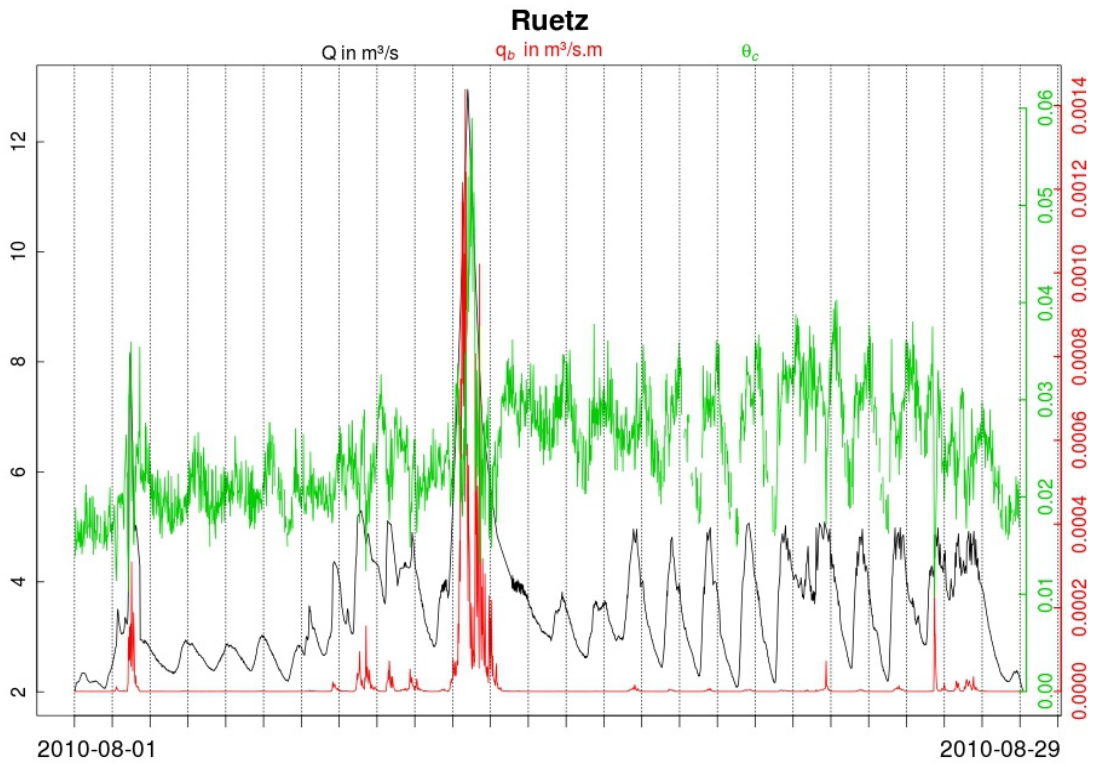


Fig. B15

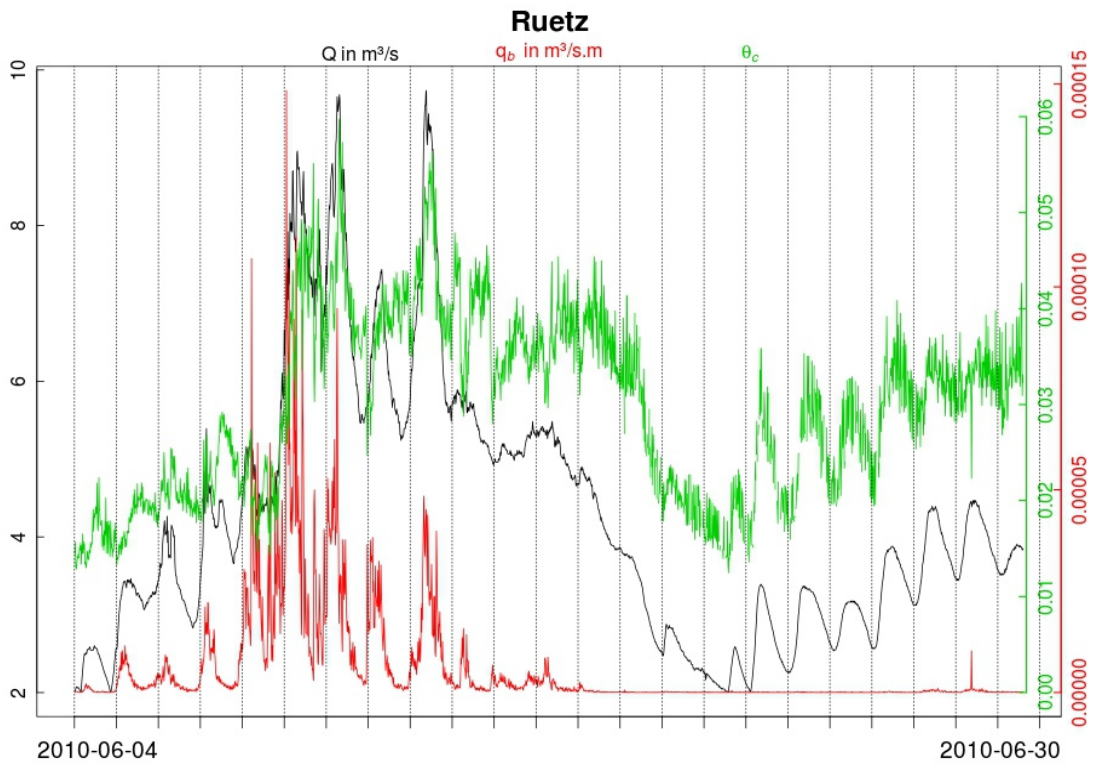


Fig. B16

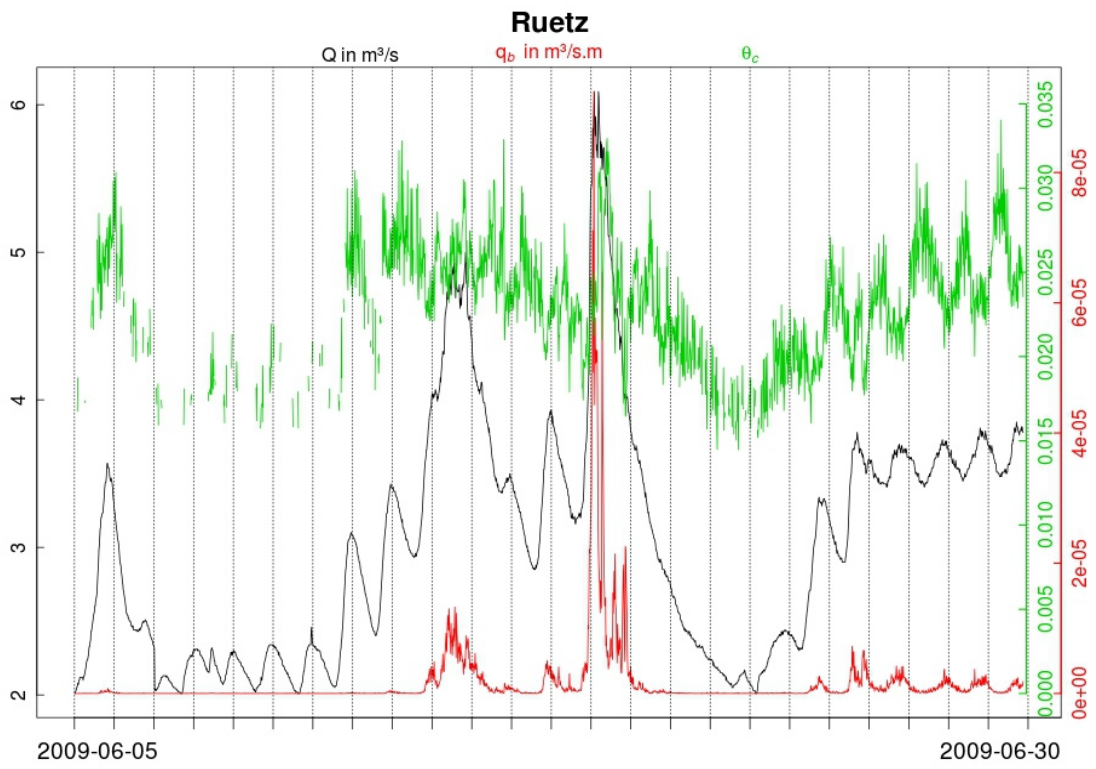


Fig. B17

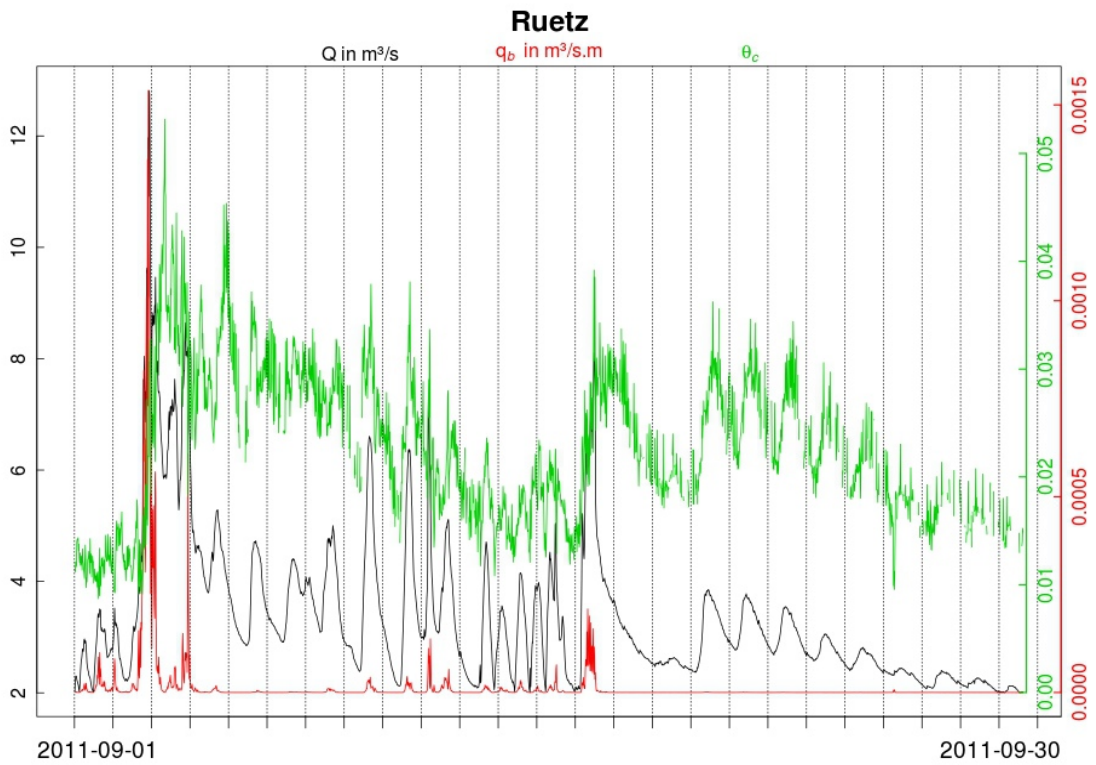


Fig. B18

3 Auto-correlations

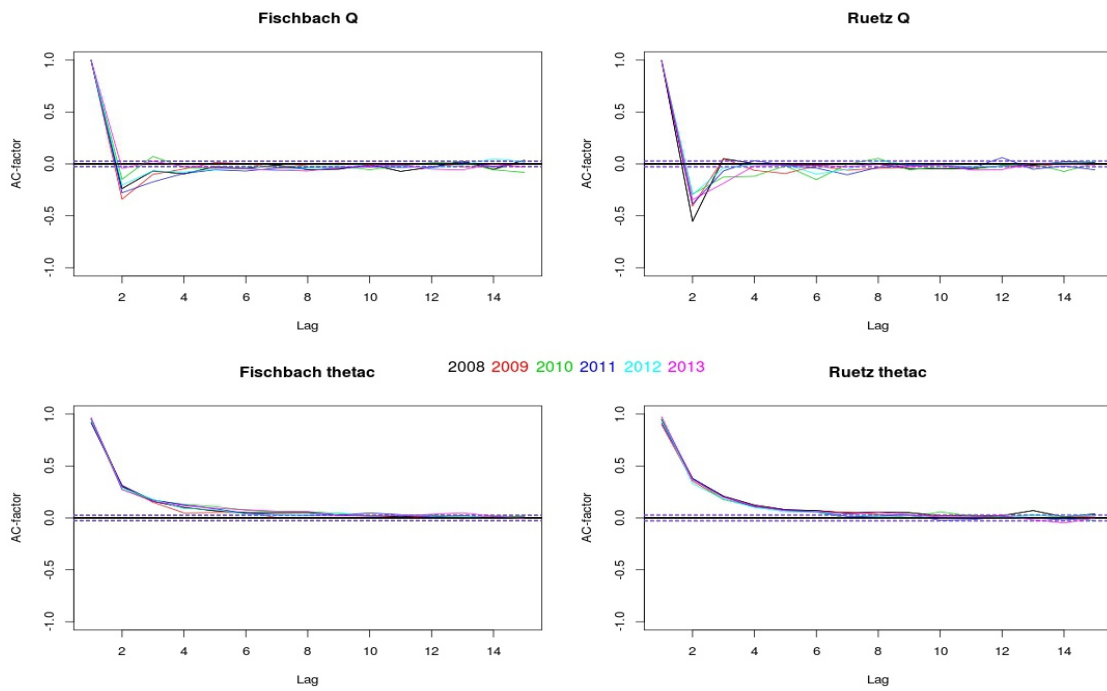


Fig. B19: partial auto-correlation diagrams

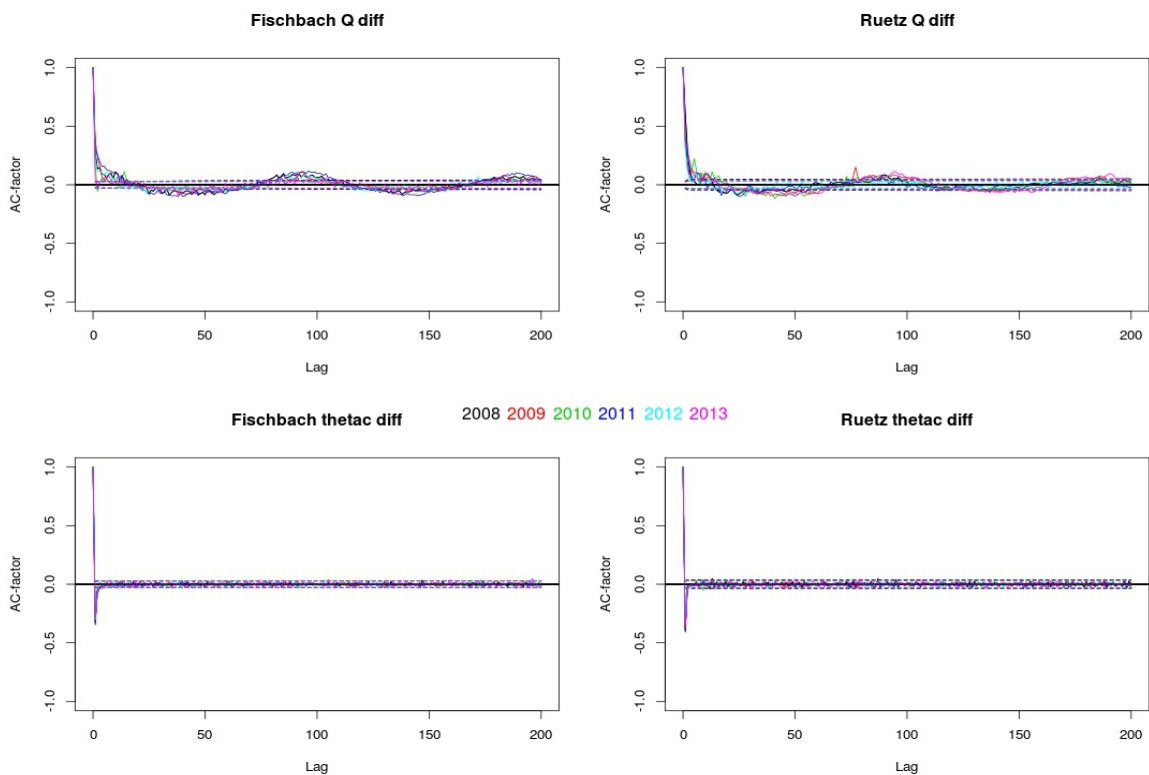


Fig. B20: auto-correlation of differentiated Q and θ_c time series

4 Lunar phases

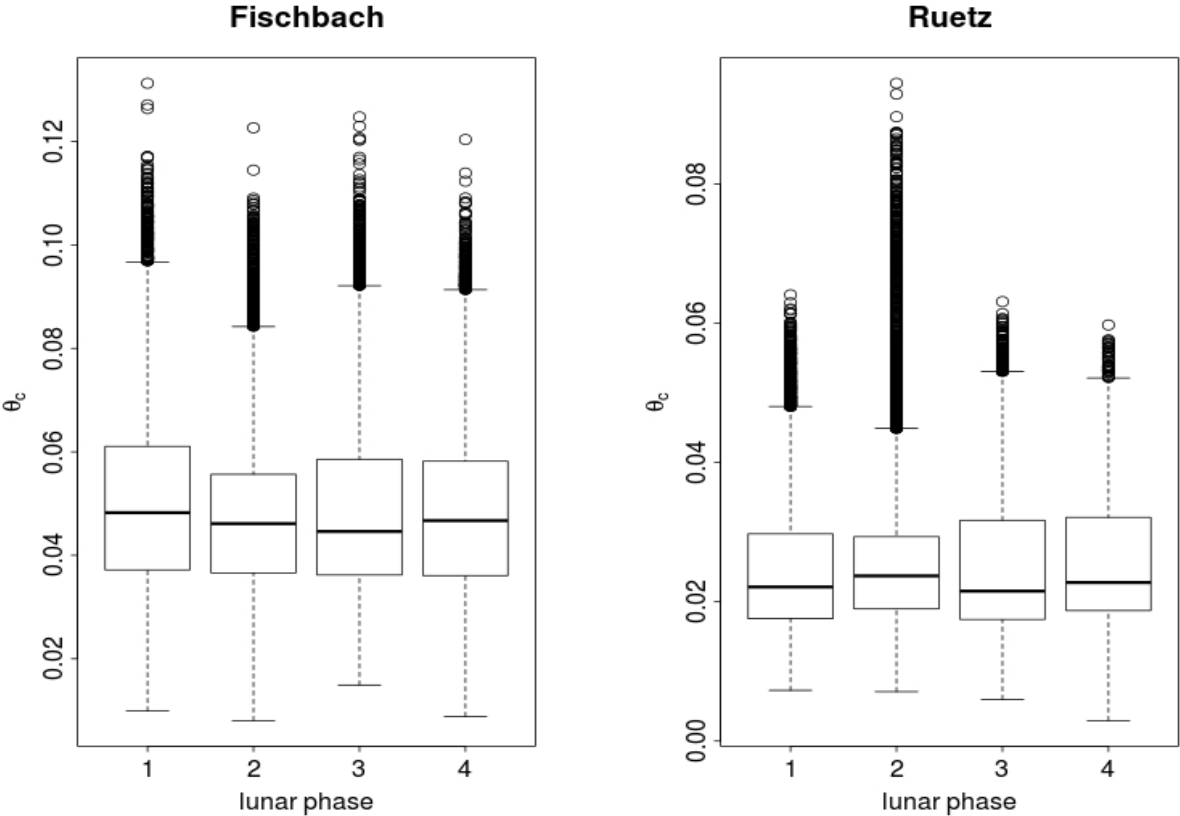


Fig. B21: boxplot of θ_c , grouped by lunar phases, 1=new moon -> half moon, 2=half moon -> full moon, and so on